Determining the quality and quantity of heat produced by proton exchange membrane fuel cells with application to air-cooled stacks for combined heat and power

by

Thomas Schmeister
B.Sc., University of Colorado, 1991
M.Sc., University of Colorado, 1993

A Thesis Submitted in Partial Fulfillment
of the Requirements for the Degree of

DOCTOR OF PHILOSOPHY

in the Department of Mechanical Engineering

Supervisory Committee

Determining the quality and quantity of heat produced by proton exchange membrane fuel cells with application to air-cooled stacks for combined heat and power

by

Thomas Schmeister
B.Sc., University of Colorado, 1991
M.Sc., University of Colorado, 1993

Supervisory Committee

Dr. Peter Wild, (Department of Mechanical Engineering)
Co-Supervisor

Dr. Nedjib Djilali, (Department of Mechanical Engineering)
Co-Supervisor

Dr. Andrew Rowe, (Department of Mechanical Engineering)
Departmental Member

Dr. Ashoka Bhat, (Department of Electrical and Computer Engineering)
Outside Member

Abstract

Supervisory Committee
Dr. Peter Wild, (Department of Mechanical Engineering)
Co-Supervisor
Dr. Nedjib Djilali, (Department of Mechanical Engineering)
Co-Supervisor
Dr. Andrew Rowe, (Department of Mechanical Engineering)
Departmental Member
Dr. Ashoka Bhat, (Department of Electrical and Computer Engineering)
Outside Member

This thesis presents experimental and simulated data gathered specifically to assess air-cooled proton exchange membrane (PEM) fuel cells as a heat and electrical power source for residential combined heat and power (CHP). The experiments and simulations focused on the air-cooled Ballard Nexa fuel cell. The experimental characterization provided data to assess the CHP potential of the Nexa and validate the model used for the simulations. The model was designed to be applicable to any air-cooled PEM fuel cell.

Based on hourly load data, four Nexa fuel cells would be required to meet the peak electrical load of a typical coastal British Columbia residence. For a year of operation with the four fuel cells meeting 100% of the electrical load, simultaneous heat generation would meet approximately 96% of the space heating requirements and overall fuel cell efficiency would be 70%. However, the temperature of the coolant expelled from the Nexa varies with load and is typically too low to provide for occupant comfort based on typical ventilation system requirements. For a year of operation, the coolant mean temperature rise is only 8.3 ± 3.4 K above ambient temperature.

To improve performance as a CHP heat engine, the Nexa and other air-cooled PEM fuel cells need to expel coolant at temperatures above 325 K. To determine if PEM fuel cells are capable of achieving this coolant temperature, a model was developed that simulates cooling system heat transfer. The model is specifically designed to determine coolant and stack temperature based on cooling system and stack design (i.e. geometry). Simulations using the model suggest that coolant mass flow through the Nexa can be reduced so that the desired coolant temperatures can be achieved without the Nexa stack exceeding 345 K during normal operation.

Several observations are made from the presented research: 1) PEM fuel cell coolant air can be maintained at 325 K for residential space heating while maintaining the stack at a temperature below the 353 K Nafion design limits chosen for the simulations; 2) The pressure drop through PEM cooling systems needs to be considered for all stack and cooling system design geometries because blower power to overcome the pressure drop can become very large for designs specifically chosen to minimize stack temperature or for stacks with long cooling channels; 3) For the air-cooled Nexa fuel cell stack, heat transfer occurring within the fuel cell cooling channels is better approximated using a constant heat flux mean Nusselt correlation than a constant channel temperature Nusselt correlation. This is particularly true at higher output currents where stack temperature differences can exceed 8 K.

Table of Contents

Tables

Figures

Equations

Nomenclature		**Units**
a, b, c	unknowns in reaction balance	$mole$
A	area	$m^2,\ cm^2$
A_T	Tafel slope	V
B	constant of mass transfer overvoltage equation	V
c_p	specific heat at constant pressure	$J \cdot kg^{-1} \cdot K^{-1}$
$\bar{c}_p$	molar specific heat at constant pressure	$J \cdot mol^{-1} \cdot K^{-1}$
C	empirical constant	-
D_h	hydraulic diameter	m
D_l	laminar equivalent diameter	m
E_{rev}	reversible open circuit voltage	V
f	Fanning friction factor	-
f_{app}	apparent Fanning friction factor	-
F	Faradays constant	$C \cdot mol^{-1}$
g	gravitational acceleration	$m \cdot s^{-2}$
$\Delta\bar{g}_f^o$	molar Gibbs free energy of formation standard conditions	$J \cdot mol^{-1}$
ΔG_f	Gibbs free energy	J
Gr	Grashof number	-
Gz	Graetz number	-
h_f^o	heat of formation at standard conditions	$J \cdot kg^{-1}$
$\overline{h_f^o}$	molar heat of formation at standard conditions	$J \cdot mol^{-1}$

h^o	specific enthalpy at standard conditions	$J \cdot kg^{-1}$
h	specific enthalpy	$J \cdot kg^{-1}$
$\bar{h}$	mean heat transfer coefficient	$W \cdot m^{-2} \cdot K^{-1}$
H	enthalpy	J
H_f^o	enthalpy of formation at standard conditions	J
H_2	hydrogen	-
H^+	hydrogen ion	-
H_2O	water	-
HHV	higher heating value	$J \cdot mol^{-1}$ or $J \cdot kg^{-1}$
i	current density	$mA \cdot cm^{-2}$
i_n	internal and fuel crossover current density	$mA \cdot cm^{-2}$
i_o	exchange current density	$mA \cdot cm^{-2}$
i_l	limiting current density	$mA \cdot cm^{-2}$
I	current	A
k	thermal conductivity	$W \cdot m^{-1} \cdot K^{-1}$
L	characteristic dimension	m
LHV	lower heating value	$J \cdot mol^{-1}$ or $J \cdot kg^{-1}$
$\dot{m}$	mass flow rate	$kg \cdot s^{-1}$
M	molecular mass	$kg \cdot mole^{-1}$

$\dot{N}$	molar flow rate	$mole \cdot s^{-1}$
Nu	Nusselt number	-
O_2	oxygen	-
Δp	channel pressure drop	Pa
P_{da}	absolute pressure of dry air	Pa
$P_{\Delta p}$	power to overcome pressure drop	W
P	channel perimeter	m
Pr	Prandtl number	-
q''	heat flux	$W \cdot m^{-2}$
Q	heat	J
$\dot{Q}$	heat transfer rate	W
r	area specific resistance	$k\Omega \cdot cm^{-2}$
Re	Reynolds number	-
Re_{crit}	critical Reynolds number for laminar to turbulent transition	-
R	gas constant	$J \cdot kg^{-1} \cdot K^{-1}$
Ra	Rayleigh number	-
$\Delta \bar{s}$	molar entropy	$J \cdot mol^{-1} \cdot K$
t	time	s
ΔT	temperature difference	K
ΔT_{LMTD}	log mean temperature difference	K
T	temperature	K
T^o	standard temperature	K

T_b	bulk coolant temperature	K
T_m	average local coolant temperature	K
T_s	local channel temperature	K
u	channel velocity	$m \cdot s^{-1}$
U	overall heat transfer coefficient	$W \cdot m^{-2} \cdot K^{-1}$
V	voltage	V
$\dot{V}$	volumetric flow	$m^3 \cdot s^{-1}$
$\dot{W}$	rate of work performed	W
x_{fd}	thermal entry length	m
x_{hd}	hydrodynamic entry length	m
$x^* = Gz^{-1}$	dimensionless axial channel distance	-
x^+	dimensionless hydrodynamic axial distance	-

Symbols

α	cooling channel aspect ratio	-
μ	dynamic viscosity	$Pa \cdot s$
ϕ	relative humidity	-
λ	oxygen stoichiometry	-
ε	emissivity	-
σ	Stefan-Boltzmann constant	$W \cdot m^{-2} \cdot K^{-4}$
ρ	density	$kg \cdot m^{-3}$
β	volume coefficient of thermal expansion	K^{-1}

Subscripts

air	relating to the properties of air
amb	ambient conditions
app	relating to apparent friction
cool	coolant stream
cell	relating to a single cell of a stack
chan	relating to a single cooling channel
da	dry air
elect	electrical
ex	reaction stream exhaust
f	formation
fc	relating to exposed surface of the fuel cell
fd	relating to thermally fully developed flow
gross	relating to gross power
hd	relating to hydrodynamically fully developed flow
heat	relating to thermal energy
H_2	hydrogen
H_2O	water
i	i^{th} component of a mixture
in	entering fuel cell
lam	relating to fully developed laminar flow
l	liquid state
load	relating to an external load
m	relating to the mean

max	maximum
Nexa	specific to the Nexa fuel cell
nat	natural convection
net	relating to net power
out	exiting fuel cell
O_2	oxygen
para	relating to parasitic load
prod	products of a reaction
rad	radiation
reac	relating to the entire reaction
rev	reversible
stack	relating to stack membrane area
stoich	stoichiometric flow
v	vapour state

Acknowledgements

I would like to thank Rene Proznik for creating the 32 channel temperature, humidity and oxygen sensor data acquisition device. I would also like to thank NSERC, my advisors and my wife for the moral and financial support which made this possible.

Dedication

This thesis is dedicated to my wife and son whom have shown infinite patience while I toiled hours on end over the wording of every paragraph.

Chapter 1

Introduction

1.1 *Background*

Fuel cells have received much attention in the past decade as an environmentally friendly and efficient power source [1]. Although first developed in 1839, the commercial potential of fuel cells only became apparent in the 1960s after NASA successfully used them to provide power during spaceflight [2]. The proton exchange membrane (PEM) fuel cell, used for the Gemini space missions, is receiving much attention today because of its low operating temperature, solid electrolyte, reliability, efficiency, quiet operation and high power density [3]. Considerable advances have been made in PEM fuel cells since the 1960s and they are now considered for transport, portable and stationary power systems.

Combined heat and power (CHP) is one of the proposed stationary applications for PEM fuel cells [4-6]. CHP is the simultaneous generation of useful heat and electrical energy. The heat is recovered and used for applications such as space heating and domestic water heating. Fuel cell CHP systems can potentially achieve lower heating value (LHV) efficiencies as high as 80% [6] compared to efficiencies ranging from 40% to 50% for fuel cell systems which are used to meet only electrical loads.

PEM fuel cells above 10 kW typically use water or another high volumetric heat capacity fluid as the coolant [7]. For CHP integration, the coolant is pumped to a heat recovery system. A water-to-air heat exchange system or water-to-water heat exchange system is

typically used to recover the coolant heat. However, the coolant temperature determines whether or not heat recovery should be considered [4,5]. Table 1.1 lists the desired CHP coolant temperatures that should be maintained to justify heat recovery [4].

Table 1.1 Recommended temperatures to justify CHP heat recovery

Application	**Temperature, K**
Absorption Refrigeration	363 to 393
Space Heating	323 to 393
Domestic Water Heating	323 to 366

If the temperatures can not be maintained for the desired application, heat recovery is typically not justified and a different energy conversion device should be considered (e.g. high temperature fuel cell, microturbine, reciprocating engine, sterling engine, etc). A complete discussion of CHP system components and design criteria are beyond the scope of this thesis; details can be found in the 2008 ASHRAE HVAC Systems and Equipment Handbook, Chapter 7 [4].

The current study focuses on heat recovery from air-cooled PEM fuel cells for residential space heating. Coolant air can be directly used for space heating without the need of a secondary heat exchanger. Air-cooling is utilized for PEM stacks ranging in size from several hundred Watts to 10 kW [7,8]. This power range makes air-cooled PEM fuel cells ideal candidates for residential-scale electrical applications which generally require 1 kW to meet base load and up to 10 kW for peak load [5].

Very little information concerning air-cooled PEM fuel cell heat recovery is available in the literature. No direct application to space heating has been found. The only models

found in the literature use heated coolant air to promote hydrogen desorption from metal hydrides [9,10]; these models do not provide the level of detail required to ensure that PEM fuel cell coolant temperature can maintain comfort conditions within an occupied space.

1.2 *Air-cooled PEM fuel cells for residential space heating*

For an air-cooled PEM fuel cell to be considered for residential space heating, the following operating details must be known:

1. Heat/Electrical power production under all load conditions. This information is necessary to match the electrical and heat generation potential of the fuel cell to the heat and electrical loads of the residence.
2. Where the heat is rejected from the fuel cell (i.e. exhaust gases, coolant, radiation and natural convection from exposed surfaces). This information is necessary to design heat management/recovery systems as well as finding the contribution of the fuel cell to the residential heat load and ventilation requirements because fuel cells can potentially be placed within the occupied space.
3. Temperature and mass flow of the coolant under all load conditions. For PEM fuel cells larger than several hundred Watts, most heat is removed by the cooling system [7]. If the PEM fuel cell coolant temperature is too low to justify recovery or requires additional conditioning before distribution, the overall efficiency may be low and other energy conversion devices will likely be better candidates for CHP integration.

Electrical power and heat production (Detail 1) is widely modelled and experimentally determined in the literature for many different stack designs and cooling systems [1,8-19]. As long as efficiency is provided, the heat generated by the fuel cell can be estimated. For the air-cooled Ballard Nexa fuel cell, which is the focus of the experimental portion of the presented research, heat and power production can be found in the operator's manual [11] with LHV efficiencies as high as 50% at part load and 40% at peak load with the balance rejected as heat.

Because of the low operating temperature of the PEM fuel cell (333 K to 363 K stack temperatures [12]) and the small reactant mass flow (typical air stoichiometry of approximately 2 [8]), the heat dissipated from the fuel cell by natural convection, radiation and sensible heating of the exhaust gases is small relative to the heat dissipated in the cooling system (Detail 2) [7]. The Nexa manual, for example, treats all heat as dissipated in the coolant with natural convection, radiation and sensible heating of the exhaust components disregarded. However, since the physical location of the fuel cell may be in the residence itself, the heat rejected from the stack and possibly the exhaust can be used to calculate the contribution of the fuel cell to the overall residential heat load. In general, knowledge of where the heat is dissipated from the fuel cell allows a heat and ventilation management strategy to be devised.

The discharge temperature of PEM coolant air is not well documented in the literature [Detail 3]. The Nexa manual, for instance, states the temperature rise of the coolant air is approximately 17 K; this temperature rise, however, is only realized near peak operating

current and is not elaborated for the entire range of operation. The coolant temperature over the operating range of the fuel cell is important for CHP system design because heat and electric loads vary over time and the coolant temperature determines whether the coolant can be recovered and utilized without requiring additional conditioning. If sufficient heat is generated to meet the heat load but the temperature is too low, conditioning the coolant before distribution reduces the system efficiency. The discussion thus far leads to the fundamental problem addressed in this thesis: **Detailed coolant temperature data is required to assess air-cooled PEM fuel cells for CHP integration**.

Since PEM cooling system and stack design (i.e. number of cooling channels, stack and cooling channel dimensions) affect heat transfer rates, the coolant temperature rise and mass flow will not be the same for all air-cooled fuel cells and each system ultimately requires individual analysis. For PEM fuel cells under development, a numerical method needs to be employed that allows the coolant temperature rise to be calculated.

1.3 *Considerations for a stack/cooling system model*

The maximum coolant temperature of a PEM fuel cell is bounded by the operating temperature of the stack. However, stack temperature, coolant temperature, coolant mass flow, heat rejection rate, heat transfer coefficients, and cooling system geometry must all be considered simultaneously for heat transfer analysis. A change in any of these variables leads to a change in one or more of the other variables. A natural outcome of PEM fuel cell cooling system modeling is the ability to determine how stack and cooling

channel geometry affects coolant temperature, stack temperature and temperature differences (axial to coolant flow), coolant pressure drop, coolant mass flow, blower power to overcome pressure drop and heat exchange surface area (e.g. material requirements). No model has been found in the literature that considers all these factors.

The cooling system design used for the Nexa fuel cell and considered in this thesis incorporates cooling fins on one side of each bipolar (flow field) plate (Figure 1.1). Rectangular cooling channels are formed when the individual cells are abutted against one another to make a stack. When air is forced through these channels, convective heat transfer takes place. The Nexa uses 47 cells and 48 flow-field plates.

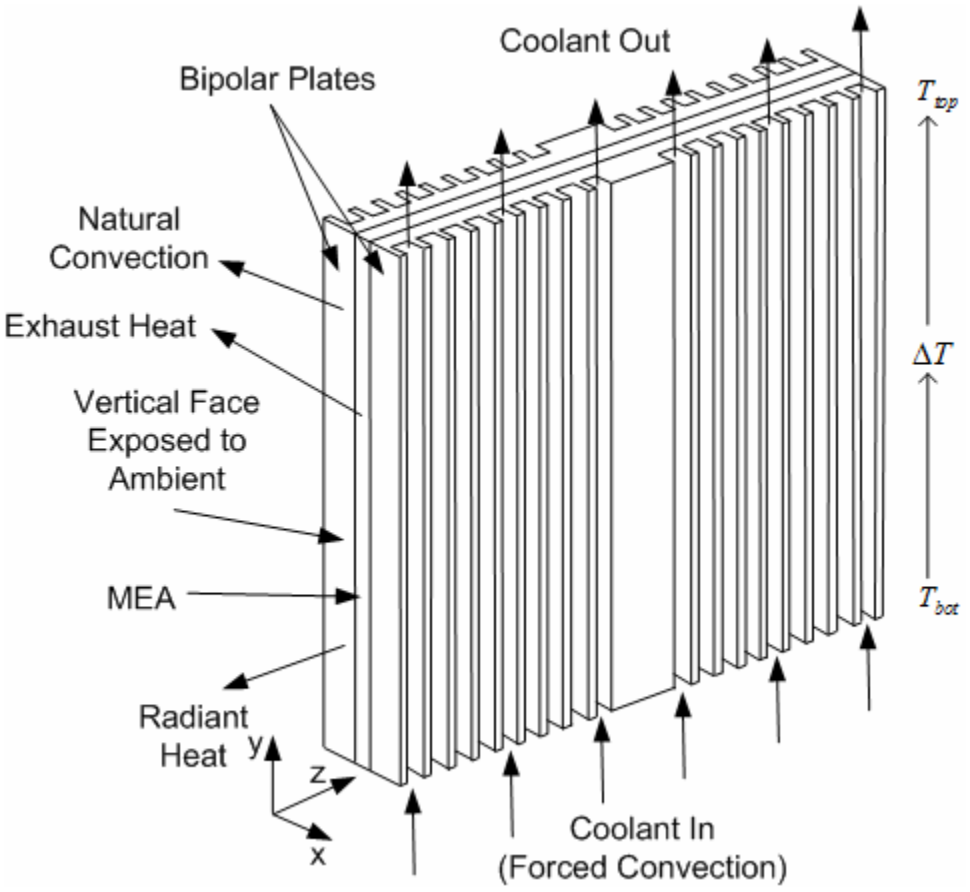

Figure 1.1 Nexa PEM cell design used in the model

1.4 *Limitations of the available PEM fuel cell cooling system models*

The models found in the literature use one or more of the following assumptions in the analysis of cooling system heat transfer:

1) The cooling channels are isothermal – *T* boundary condition
2) The coolant temperature rise is small
3) The heat transfer coefficient is constant
4) Nusselt numbers for rectangular channels can be calculated from circular Nusselt correlations

Since experimentally determined coolant discharge temperatures of PEM fuel cells are typically below the lower limits shown in Table 1.1 [4,11], and may not be acceptable for even space-heating [5,12], accurate predictions of coolant temperature are essential for determining CHP applicability to residential space heating. An erroneous assumption in predicting the coolant temperature can lead an engineer to apply a PEM fuel cell to an application for which it is not suited. The limitations of the models from the literature are discussed below:

1.4.1 *Applying water-cooled heat transfer assumptions to an air-cooled fuel cell*

Many models present in the literature can find the temperature rise of PEM fuel cell coolant [1,9,13-19]. Most of these models have been for water-cooled fuel cells and assume a constant heat transfer coefficient. Assuming a constant heat transfer coefficient greatly simplifies the analysis and is particularly applicable to water-cooled systems because of the low volumetric flow compared to that of air-cooled systems (water has a volumetric heat capacity 4000 times that of air). Conversely, coolant air volumetric flow can have great variability depending on load or stack/cooling system design. The assumption of a constant heat transfer coefficient is only true if the flow will be fully developed laminar under all loads and the entrance effects are negligible.

Zong, et al [13] presents a comprehensive model to simulate the mass and energy transfer process inside a single PEM fuel cell with a non-uniform stack temperature. The energy

balance considers the effects of heat transfer to water and uses a constant overall heat transfer coefficient to find the rate of heat transfer:

$$\dot{Q} = A \cdot U \cdot \Delta T \tag{1.1}$$

where

$\dot{Q}$ = rate of heat transfer to coolant water, W

A = area of heat transfer, m^2

U = overall heat transfer coefficient between stack and coolant, $W \cdot m^{-2} \cdot K^{-1}$

ΔT = temperature difference between stack and coolant, K

Zong, et al, assumes a constant coolant temperature through the length of the cooling passage while the stack temperature is allowed to vary with position. The heat transfer to the coolant allows the simulations to estimate water activity in the membrane and the overall electrical performance of the fuel cell. However, a constant coolant temperature is not a practical assumption for an air-cooled system because the coolant temperature rise can be more than 17 K as seen with the Nexa [11]. An air-cooled fuel cell for CHP should see a temperature rise more on the order of 25 K (for a 298 K ambient and 323 K distributed air temperature) so the assumption of constant coolant temperature is not applicable to the air-cooled model that is required.

Vasu, et al [14], created a model for predicting stack, exiting reactant gases, and exiting coolant temperature for water-cooled PEM fuel cell systems. The power balance used in the model to predict outlet temperatures equates the sensible heat of the water to the convective heat transfer of coolant water:

$$\dot{N} \cdot \bar{c}_p \cdot (T_{out} - T_{in}) = \bar{h} \cdot A \cdot \Delta T_{LMTD} \quad (1.2)$$

where

$\dot{N}$ = molar flow rate of water, $mole \cdot s^{-1}$

$\bar{c}_p$ = molar specific heat of water at constant pressure, $J \cdot mol^{-1} \cdot K^{-1}$

T_{out} = water temperature exiting fuel cell, K

T_{in} = water temperature entering fuel cell, K

$\bar{h}$ = mean heat transfer coefficient, $W \cdot m^{-2} \cdot K^{-1}$

ΔT_{LMTD} = logarithmic mean temperature difference between stack and coolant, K

The model assumes an isothermal stack temperature and a constant heat transfer coefficient obtained from the literature. The ASHRAE Fundamentals Handbook, Chapter 4 [20], discusses calculation of the final coolant temperature for this balance. This is a method commonly used in the literature [1,15-18]. However, for air cooled units, neither the isothermal stack temperature (axial to the coolant flow) nor the constant heat transfer coefficient assumptions are necessarily valid for all the cooling system geometries, coolant temperatures and flows likely to be encountered during operation or considered during the design phase. For example, Adzakpa, et al [19], showed stack temperature differences axial to the coolant flow up to 5 K for the air-cooled Nexa fuel cell. Experimental measurements for this thesis show stack temperature differences greater than 8 K at peak Nexa operation.

1.4.2 *Models that consider air cooling*

The air-cooled models found in the literature use Nusselt numbers to determine heat transfer coefficients.

$$h = \frac{Nu \cdot k}{L} \tag{1.3}$$

where

Nu = Nusselt number

k = coolant thermal conductivity, $W \cdot m^{-1} \cdot K^{-1}$

L = characteristic dimension (diameter for cooling channels), m

Choosing the appropriate Nusselt boundary condition is important for finding the heat transfer coefficient and subsequently the final output temperature and mass flow of the coolant air. The empirical equations and tabular data available to calculate Nusselt numbers are based on two primary assumptions:

1. Constant channel temperature – *T* boundary condition
2. Constant heat flux – *H1* boundary condition with isothermal circumferential channel temperature

The flow regime and channel geometry must also be considered when choosing the Nusselt correlation. The primary flow regimes include:

a. Developing laminar flow

b. Fully developed laminar flow

c. Transitional flow

d. Turbulent flow

Nusselt number correlations for turbulent flow may be applied to both uniform surface temperature and heat flux conditions [21]. Laminar flow and developing laminar flow require individual correlations or tabular data for uniform surface temperature and heat flux conditions. For the air-cooled models found in the literature [9,19], the constant surface temperature Nusselt correlations have been used exclusively.

Using the *T* boundary condition may lead to inaccurate prediction of coolant temperatures. Whether the *T* boundary condition is the best assumption is unknown because no published studies have been found that compare the constant heat flux and constant channel temperature boundary conditions to experimental measurements. A comparison of these assumptions, however, is performed in Chapter 5.

The published models also use circular Nusselt correlations to represent rectangular cooling channels. For rectangular channels, Nusselt numbers are a function of aspect ratio. For laminar flow, using circular correlations can lead to errors in calculating Nusselt numbers and heat transfer coefficients, particularly when sharp corners are encountered [21]. As an example, fully developed laminar flow in a constant temperature channel results in a Nusselt number of 3.66 for a circular channel and 5.6 for a rectangular channel with a 1:8 aspect ratio. The use of rectangular correlations eliminates erroneous Nusselt calculations introduced by using circular correlations.

The air-cooled models found in the literature use a one Newton's Law of cooling as shown in Equation 1.4 to calculate heat flux.

$$q'' = h \cdot \Delta T \tag{1.4}$$

where

q'' = channel heat flux, $W \cdot m^{-2}$

Adzakpa [19], et al, uses experimentally measured axial coolant temperatures and mass flows to compute the average cooling channel heat transfer coefficient for the Nexa fuel cell. The model relies upon experimental measurements to supply temperature and mass flow variables that would be unknown during the design phase of a cooling system. Turbulent and transitional flows are not considered in their model. The air-cooled PEM fuel cell model by Graf, et al [9], is similar but includes turbulent and transitional flows.

Choosing the Nusselt correlation and boundary condition that provides the most accurate coolant air temperature and mass flow predictions is desirable for determining CHP applicability. However, without a comparison of the *T* and *H1* boundary conditions, the correlation that provides the most realistic prediction of coolant temperature and stack temperature remains unknown. To be useful from a design perspective, the model must be capable of determining variables independent of observations made for a specific PEM fuel cell.

1.5 *Objectives*

Two primary objectives are achieved in this thesis:

1. **Determine the operating parameters of the Nexa fuel cell necessary to evaluate it for residential space heating CHP application.** The measurements include:
    a) Coolant temperature and mass flow.
    b) System power balance.
    c) Stack surface temperature differences.

    Power balance curves are developed to evaluate the Nexa for CHP application.
2. **Develop a model for characterizing a PEM fuel cell cooling system with rectangular cooling channels.** The following list of goals are achieved with the model:
    a. Allow the effects of channel geometry on the heat transfer rates to be investigated. Only rectangular channels are considered, with aspect ratio and channel length user defined variables.
    b. Predict the mass balance, energy balance, stack and coolant temperatures of PEM fuel cells using empirical equations and general variables valid for any Nafion membrane PEM stack. The ability to simulate these parameters is essential for assessing the CHP potential of air-cooled PEM fuel cells.
    c. Consider both the *T* and *H1* boundary conditions for the cooling system mass and energy balance. Determine which boundary condition best fits the experimental Nexa data.

d. Allow different flow regimes to be considered for the cooling system, including developing laminar flow, fully developed laminar flow, transitional flow and turbulent flow for Reynolds numbers up to 10^6.
e. Include coolant mass flow and pressure drop calculations to assess power requirements to overcome pressure drop.

The research presented in this thesis contributes to the literature by providing:

1. Experimental data necessary to evaluate the Nexa PEM fuel cell for CHP application. The current literature lacks substantive coolant temperature data.
2. A PEM cooling system model that considers both the constant heat flux and constant temperature Nusselt correlations for air-cooled PEM fuel cell heat exchanger design. The model uses rectangular Nusselt correlations instead of the circular correlations previously used in the literature.
3. Simulations showing that the Nexa coolant output temperatures can be increased to improve CHP applicability.

1.6 *Thesis layout*

Chapter 2: Experiment Methodology

Chapter 2 describes the design of the experiments used for finding the power balance, temperatures and mass flows of the Nexa fuel cell. The experiments provide baseline operating parameters for validating the model developed in Chapter 4 and evaluating the Nexa fuel cell for CHP applications. Details include:

1. Nexa data acquisition from the Integrated Renewable Energy Experiment (IRENE).
2. Location of additional sensors necessary for finding a Nexa power/mass balance.
3. Equations for calculating the power balance and temperatures.

Chapter 3: Experiment Results

The inputs and outputs observed during operation of the Nexa fuel cell are presented in Chapter 3. The chapter includes:

1. Stack power balance for the operating range of the Nexa.
2. Coolant temperatures.
3. Average stack surface temperatures
4. Heat balance diagram
5. Simplified analysis of the Nexa for CHP application to coastal British Columbia residences.

Chapter 4: Model Development

Chapter 4 describes the fundamental equations necessary for developing a model for analyzing coolant heat exchange in PEM fuel cell stacks and includes:

1. Stack electrical production.
2. Stack heat production.
3. Reactant/coolant mass and power balances.
4. Exhaust, radiation, natural convection and forced convection heat transfer.

Chapter 5: Model Results

Chapter 5 presents validation of the model by comparing simulated operation of the Nexa fuel cell with the experimental operation shown in Chapter 3. Simulations are performed to determine changes that can be made to the Nexa fuel cell to improve performance as a heat and power supply for CHP applications.

Chapter 6: Conclusions and Discussion

Chapter 6 discusses suitability of the Nexa for CHP applications based on experiments and simulated operation. Recommendations for future study are proposed.

Appendix

The appendix contains additional experimental measurements, simulations and equations not presented in the main text.

Chapter 2

Nexa Experiment Methodology

2.1 *Introduction*

This chapter presents the experiment procedures used to find the mass and power balance of the Ballard Nexa PEM fuel cell. The Integrated Renewable Energy Experiment (IRENE) at the University of Victoria acted as the test bed and provided Nexa control, subsystem control (e.g. load banks, inverters, power supplies, etc.), sensors for electrical characterization and data acquisition [22]. Additional sensors necessary to characterize the heat output of the Nexa were integrated into IRENE's data acquisition systems and are discussed in this chapter. The experimental procedures and characterization are specifically designed to allow the Nexa to be evaluated for integration into a CHP system and to validate the cooling system model developed in Chapter 4.

2.2 *Basic Nexa power balance*

For steady operation at a constant stack temperature, the Nexa requires the rate of energy input to balance with the rate that energy is output from the system. The thermodynamic power balance of the Nexa is expressed as:

$$\dot{Q}_{\Delta H} = \dot{Q}_{heat} + \dot{W}_{elect} \tag{2.1}$$

where

$\dot{Q}_{\Delta H}$ = rate at which energy enters the fuel cell, W

$\dot{Q}_{heat}$ = rate at which heat is rejected from the fuel cell, W

$\dot{W}_{elect}$ = rate at which electrical energy is generated by the fuel cell, W

The temperature, voltage, current and mass flow measurements performed in the experiments allow all three variables of Equation 2.1 to be evaluated independently. Figure 2.1 provides a visual representation of the energy and mass flows of the Nexa.

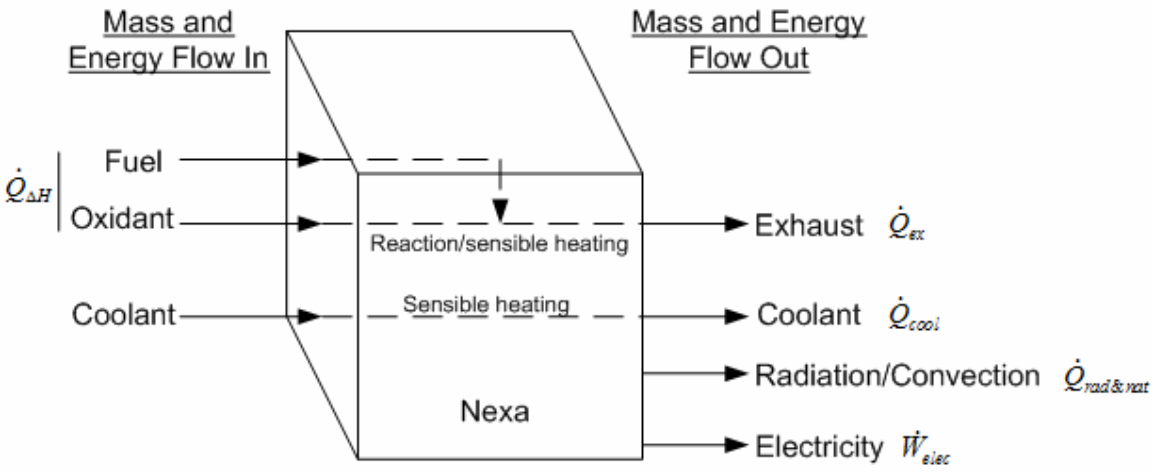

Figure 2.1 Mass and energy flow of the Nexa fuel cell

where

$$\dot{Q}_{heat} = \dot{Q}_{cool} + \dot{Q}_{rad\&nat} + \dot{Q}_{ex}$$

$\dot{Q}_{cool}$ = rate heat is carried from the fuel cell in the coolant, W

$\dot{Q}_{rad\&nat}$ = rate heat is dissipated by the exposed stack surface, W

$\dot{Q}_{ex}$ = rate heat is carried from the fuel cell in the exhaust, W

The energy input and heat rejected from the fuel cell are calculated with respect to ambient temperature. Heat and electrical generation are all determined during steady state operation. Since coolant and exhaust temperature rise for PEM fuel cells are small (e.g. $\approx$ 17 K for the Nexa [11]) and the coolant air specific heat varies little over the

temperature range encountered, the analysis of sensible heating assumes ideal gases and constant specific heats.

2.2.1 *Rate energy enters the Nexa,* $\dot{Q}_{\Delta H}$

The rate that energy enters the fuel cell depends upon the mass flow rate of the reactants, the ambient temperature, and the final state of the by-product water [23]. Assuming a constant pressure reaction, the change in enthalpy is equal to the heat evolved in the reaction. The enthalpy change for the reaction is shown in Figure 2.2 relative to ambient. The enthalpy diagram is a representation of Hess's Law which states that the enthalpy of a reaction is equivalent to the enthalpy sum of the individual steps in the reaction.

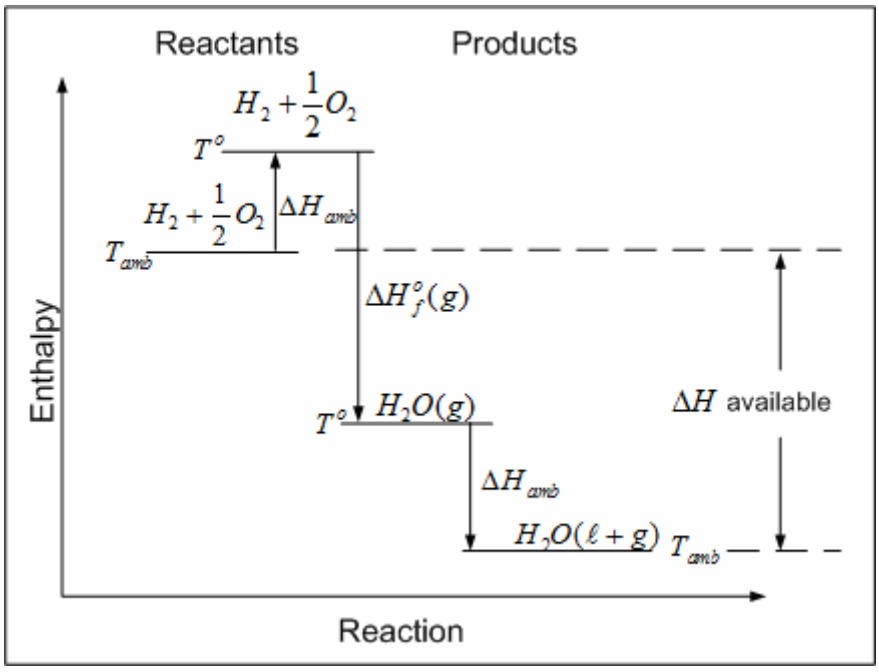

Figure 2.2 Enthalpy diagram for a redox reaction of hydrogen and oxygen

where

T_{amb} = ambient temperature, K

T^o = standard temperature, 298 K

ΔH_{amb} = change in enthalpy to bring products or reactants to standard temperature, J

$\Delta H_f^o(g)$ = enthalpy of combustion at standard temperature, J

ΔH available = total enthalpy evolved in the reaction, J

Equation 2.2 gives the rate at which energy is liberated due to the electrochemical reaction within the fuel cell. The energy entering the cell is treated as a positive value.

$$\dot{Q}_{\Delta H} = -\left[\sum_{prod}[\dot{m}(\Delta h_f^o + h_{amb} - h^o)]_i - \sum_{react}[\dot{m}(\Delta h_f^o + h_{amb} - h^o)]_i\right] \quad (2.2)$$

where

$\dot{m}$ = mass flow rate of the individual product or reactant species, $kg \cdot s^{-1}$

Δh_f^o = heat of formation for products or reactants, $J \cdot kg^{-1}$

h_{amb} = specific enthalpy of the products or reactants at ambient, $J \cdot kg^{-1}$

h^o = standard specific enthalpy of products or reactants at 298 K, $J \cdot kg^{-1}$

The latent heat of condensation is accounted for in Equation 2.2 if the mass flow rate of both the liquid product and the vapour product are known. This is because the heat of formation at standard conditions is defined for both a liquid or vapour product. When the fraction of vapour and liquid product are unknown, the entire product is treated as a vapour because liquid water is seldom formed during fuel cell reactions [8]. This equation is simplified in the analysis because the heat of formation of the reactants is zero,

ambient temperature for the experiments was approximately standard temperature (i.e. $h_{amb} \approx h^o$), and the total enthalpy is determined with respect to ambient temperature. The simplified equation is shown below:

$$\dot{Q}_{\Delta H} = -\sum_{prod} [\dot{m} \cdot \Delta h_f^o]_i \tag{2.3}$$

Equation 2.3 is equal to the heating value of the fuel consumed.

2.2.2 *Rate of heat rejection,* $\dot{Q}_{heat}$

The rate heat is rejected from the Nexa equals the sum of the coolant, natural convection and radiation, and exhaust heat rejection rates (Figure 2.1). The rate of coolant heat rejection from the Nexa can be calculated from the sensible heat change of the coolant air mass flow. For the experiments, relative humidity was measured and the heat rejected in the coolant air includes sensible heating of dry air and sensible heating of water vapour.

$$\dot{Q}_{cool} = \sum_{cool} (\dot{m} \cdot c_p \cdot (T_{cool} - T_{amb}))_i \tag{2.4}$$

where

c_p = specific heat of dry air or water vapour at constant pressure, $J \cdot kg^{-1} \cdot K^{-1}$

T_{cool} = temperature of coolant air rejected from fuel cell, K

Appendix A1 discusses computation of the mass of water vapour and dry air based on relative humidity.

The temperature difference between the stack surface and ambient drives radiation and natural convection heat rejection. For the calculation of Nexa surface heat loss, a combined heat transfer coefficient was used [20]:

$$h_{rad\&nat} = h_{rad} + h_{nat} \tag{2.5}$$

where

h_{rad} = radiation heat transfer coefficient, $W \cdot m^{-2} \cdot K^{-1}$

h_{nat} = natural convection heat transfer coefficient, $W \cdot m^{-2} \cdot K^{-1}$

Using the combined heat transfer coefficient, the rate heat is rejected from the Nexa stack surface can be found with Equation 2.6 [20]:

$$\dot{Q}_{rad\&nat} = h_{rad\&nat} \cdot A \cdot (T_{fc} - T_{amb}) \tag{2.6}$$

where

A = stack surface area exposed to ambient environment, m^2

T_{fc} = average stack temperature, K

As the surface area of the Nexa is small compared to the room in which it is housed, the radiation heat transfer coefficient can be estimated using Equation 2.7 [20].

$$h_{rad} = \sigma \cdot \varepsilon_{fc} \cdot ({T_{amb}}^2 + {T_{fc}}^2) \cdot (T_{amb} + T_{fc}) \tag{2.7}$$

where

σ = Stefan-Boltzmann constant, 5.67 x 10^{-8} $W \cdot m^{-2} \cdot K^{-4}$

ε_{fc} = emissivity of stack surface

Emissivity of the surface is approximated as impervious graphite ($\varepsilon_{fc} = 0.75$ [20]).

The natural convection heat transfer coefficient is not as easy to determine. The natural convection heat transfer coefficient requires several dimensionless numbers to be

calculated including the Grashof number (Gr), the Prandtl number (Pr), and the Rayleigh number (Ra). Solving for the Rayleigh number allows the proper Nusselt correlation (Nu) to be determined. Appendix A2 shows the solution of the dimensionless correlations and the resulting Nusselt correlation. Once the Nusselt number has been determined, the natural convection heat transfer coefficient can be found from equation 2.8 (same as equation 1.3 except vertical height is now the characteristic dimension):

$$h_{nat} = \frac{Nu \cdot k}{L} \tag{2.8}$$

where

k = thermal conductivity of coolant, $W \cdot m^{-1} \cdot K^{-1}$

L = characteristic dimension = height of the Nexa, m

The exhaust consists of vapour water, liquid water and un-reacted air. The sensible heat rejected in the exhaust is the sum of the heat transfer rates for each individual exhaust component as shown in Equation 2.9.

$$\dot{Q}_{ex} = \sum_{ex} (\dot{m} \cdot c_p \cdot (T_{ex} - T_{amb}))_i \tag{2.9}$$

where

T_{ex} = exhaust temperature, K

For the analysis of the Nexa, air is considered to consist of nitrogen, oxygen and water vapour due to relative humidity. Since liquid water production was measured but could not be consistently reproduced, all water formed in the reaction is treated as a vapour as

suggested by Larminie and Dicks. Appendix A3 discusses the rate at which liquid water was produced at different Nexa currents.

2.2.3 *Rate at which electrical energy is produced,* $\dot{W}_{elect}$

The electrical power production is the sum of the parasitic load (i.e. the Nexa blower, compressor, and control system load) and the primary load (e.g. residential load).

$$\dot{W}_{elect} = \dot{W}_{para} + \dot{W}_{load} \tag{2.10}$$

where

$\dot{W}_{para}$ = Nexa parasitic power consumption, W

$\dot{W}_{load}$ = power consumed by an external load, W

The external load is calculated directly from the voltage and current measured at the load.

$$\dot{W}_{load} = I_{load} \cdot V_{load} \tag{2.11}$$

where

I_{load} = current measured at the external load, A

V_{load} = voltage measured at the external load, V

Assuming all hydrogen is reacted, for every mole of hydrogen consumed, two moles of electrons become available. Using Faraday's constant, the molar flow rate of hydrogen and the number of cells in the stack, a theoretical current for the Nexa can be found using Equation 2.12:

$$I_{Nexa} = \frac{2 \cdot F \cdot \dot{N}_{H2}}{47} \tag{2.12}$$

where

F = Faraday's constant, 96,485 $C \cdot mo1^{-1}$

$\dot{N}_{H_2}$ = molar flow rate of hydrogen, $mole \cdot s^{-1}$

2 = moles of electrons per mole of hydrogen

47 = number of cells in the Nexa stack

The total theoretical electrical power output of the Nexa can be computed using the voltage of the stack.

$$\dot{W}_{elect} = I_{Nexa} \cdot V_{Nexa} \tag{2.13}$$

where

V_{Nexa} = voltage of the Nexa stack, V

Parasitic loads are estimated as the difference between the primary load and the theoretical electrical power calculated from fuel consumption because power consumption by the individual Nexa subsystems was not measured.

$$\dot{W}_{para} = \dot{W}_{elect} - \dot{W}_{load} \tag{2.14}$$

2.3 *Experiment setup*

To assess the power balance described in Section 2.2 and to allow the Nexa to be used for model validation, many different voltages, mass flows, currents and temperatures need to be measured. The current, voltage and hydrogen mass flow datum are collected by

sensors essential for control of IRENE operation. Details of IRENE can be found in Bergen, et al [22]. Temperatures, coolant mass flow and reactant air mass flow are measured by secondary sensors not required for operation of IRENE and are detailed below.

To fully characterize Nexa operation, temperature and mass flow measurements need to be obtained. The placement of the temperature and mass flow sensors to make these measurements is shown in Figure 2.3.

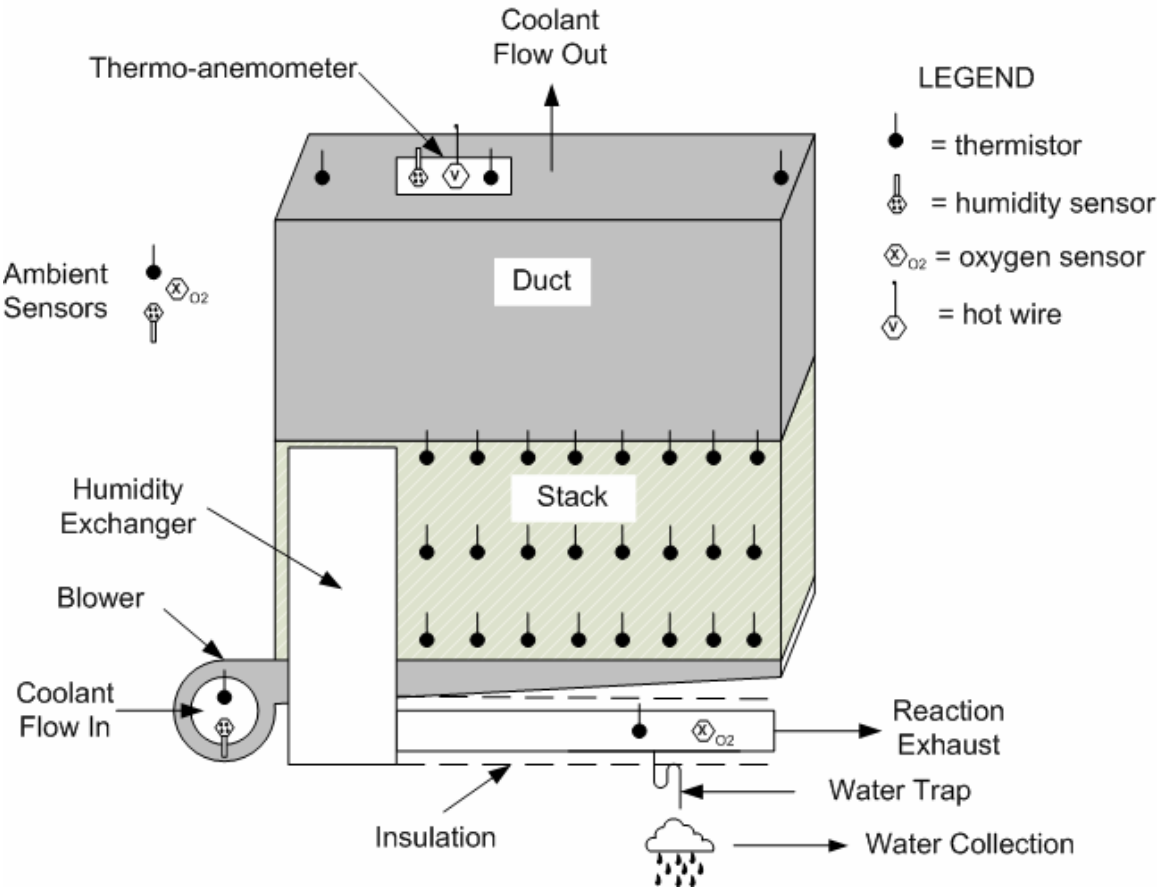

Figure 2.3 Placement of sensors on the Nexa

Note that a duct has been fitted to the top of the Nexa to confine the coolant flow so that a single anemometer and a log-Tchebycheff duct traverse can be used to find the average overall coolant mass flow. Appendix A4 discusses the measurement of duct velocity with the log-Tchebycheff traverse. The sensor specifications are presented in Appendix A5 and their placement is summarized as follows:

1. **Temperature:** Linear response thermistors were placed on the exterior surface of the stack, in the coolant output flow, in the coolant input flow, in the exhaust flow and in the ambient environment to measure temperature.

   Stack temperature

   The stack temperature was measured with 24 thermistors placed in 3 rows along the length of the stack, with 8 thermistors in each row (as shown in Figure 2.3). The thermistor package is approximately 5 mm x 5 mm. The midpoint of each thermistor in the top and bottom rows was approximately 1.5 cm from the edge of the stack. The thermistors were evenly spaced along the length of the stack up to the Nexa humidification system. Only one side of the Nexa stack had temperatures measured as access to the opposite side was limited due to control wiring. The temperature sensors allowed the stack temperature differences parallel and perpendicular to coolant flow to be found.

   Coolant temperature

   Coolant temperature was measured with two thermistors placed in the duct on opposite sides of the stack and a third temperature sensor integrated into the hot wire anemometer placed at a position of average coolant velocity as shown in Figure 2.3.

Ambient, coolant intake and exhaust temperature

Ambient, coolant intake and exhaust temperatures were each measured by a thermistor placed as shown in the figure.

2. **Humidity:** Relative humidity was measured in the coolant blower intake, at a support bracket in the ambient environment, and with the thermo-anemometer placed in the coolant duct. The relative humidity allowed water vapour in the air to be considered for the calculation of heat rejected in the coolant.
3. **Anemometer:** A hot wire anemometer (TSI Velocicalc model 8386) was used to measure coolant velocity in the duct placed atop the Nexa stack. A log-Tchebycheff rule duct traverse was used to find the average velocity of the coolant air for the range of currents at which the Nexa operates. The average coolant velocities determined from the traverses allowed the mass and volume flows of coolant air to be determined. The overall duct velocity also allowed the average velocity of air travelling through each cooling channel to be found for Reynolds number calculations.
4. **Oxygen Sensors:** Oxygen sensors were placed in the exhaust and ambient air to determine the molar fraction of oxygen present in the reactant air and the exhaust by-products. The measurements of oxygen were taken during steady-state operation. The oxygen measurements allowed the mass flow of exhaust gases to be computed as well as the oxygen stoichiometry by solving the following molar balance on a dry basis [20,23]:

$$aH_2 + b(O_2 + 3.76N_2) \rightarrow cO_2 + (1-c)N_2 + aH_2O \qquad (2.15)$$

where

a = moles of hydrogen and water involved in the reaction

b = moles of dry air in the reaction

c = measured molar oxygen percent in the exhaust

3.76 = nitrogen to oxygen molar ratio in air

The solution to this molar balance, considering the measured flow of hydrogen, is elaborated in Appendix A6. The stoichiometry of the oxygen can be calculated once the mass balance of Equation 2.15 is solved.

$$\lambda = \frac{\dot{m}_{O2}(in)}{\dot{m}_{O2}(stoich)} \tag{2.16}$$

where

$\dot{m}_{O2}$ = mass flow rate of reactant oxygen, $kg \cdot s^{-1}$

Oxygen stoichiometry for the Nexa is shown graphically in Appendix A6.

5. **Un-reacted hydrogen in the exhaust**: Measurement of the hydrogen content of the exhaust and coolant was also periodically measured with a portable leak detector. If hydrogen was present in these streams, it was at levels too low to be detected by the leak detector. In the analysis of the mass and power balance, all hydrogen is assumed to react and form water.

2.4 *Summary*

This chapter presented the equations and sensor measurements necessary to characterize the Nexa fuel cell. The measurements taken include stack temperature and temperature difference, coolant velocity, hydrogen consumption, load current and voltage, relative humidity and exhaust gas oxygen concentration. These variables allow the Nexa fuel cell to be characterized with a power balance so the electrical and heat production rates can be determined for the operating range of the Nexa. The temperature measurements, particularly for the coolant, allow the quality of the heat rejected by the fuel cell to be assessed for heat recovery. Chapter 3 presents the characterization of the Nexa resulting from the measurements.

Chapter 3

Nexa Characterization and CHP analysis

3.1 *Introduction*

This chapter presents heat and electrical power production, polarization and coolant dry bulb temperature data for a Nexa PEM fuel cell. The data is presented in a heat balance graph which provides a visual representation of the thermal output characteristics of the Nexa based on the fractional load encountered. This graph can be used to estimate CHP potential. The heat balance graph is subsequently used to determine how much heat can be recovered from the Nexa for space heating a typical coastal British Columbia household.

This chapter is broken down into several sections: First, Section 3.2 lists the ambient conditions and sample collection time for the Nexa data presented in this chapter. Next, Section 3.3 presents the Nexa polarization, heat and electrical power, coolant temperature, and heat balance graphs for the conditions described in section 3.2. Once the baseline operation of the Nexa is known, Section 3.4 analyzes the Nexa as a heat and power source for a typical coastal British Columbia residence using hourly BC Hydro load data and the heat balance graph. Finally, Section 3.5 summarizes the Nexa CHP viability based on desired residential heating and ventilating design conditions.

3.2 *Operating conditions during data acquisition*

The Nexa uses ambient air for cooling and as the source of oxygen for the reduction/oxidation reaction occurring in the stack. During the Nexa characterization,

ambient dry bulb temperature and humidity were controlled by the laboratory ventilation system. The data presented in this chapter is valid for the following ambient temperature and relative humidity ranges:

1. Relative humidity: $37.0 \leq \phi \leq 39.0$ %
2. Dry Bulb Temperature: $296.55 \leq T_{amb} \leq 298.85\,\mathrm{K}$

The Nexa also undergoes purge cycles to remove liquid water and nitrogen that collects in the anode and cathode. The purge cycles occur periodically and result in hydrogen being flushed through the system and released into the coolant stream. Ballard notes that less than 1% of the fuel consumed by the Nexa is purged from the fuel cell [11]. Purge cycles increase in frequency as the load increases. Appendix A7 presents hydrogen mass flow data for steady state operation at several different loads and includes purge cycles. To simplify the analysis, the mean hydrogen consumption rate, which is used to calculate input power, comes from contiguous data and includes purge cycles. The mean values are calculated from a minimum of 2 minutes of un-interrupted data collection during steady state operation. Determination of steady state is discussed in Appendix A8.

3.3 *Results*

The performance of the Nexa PEM fuel cell is presented in this section and is limited to polarization, power, and temperature graphs; these variables are of primary importance to CHP analysis of the Nexa fuel cell. Additional Nexa performance data such as air stoichiometry, hydrogen consumption, and coolant mass flow rates are presented in Appendices A6, A7, and A9, respectively.

3.3.1 *Nexa Polarization Curves*

Polarization and electrical power curves for the Nexa are shown in Figure 3.1.

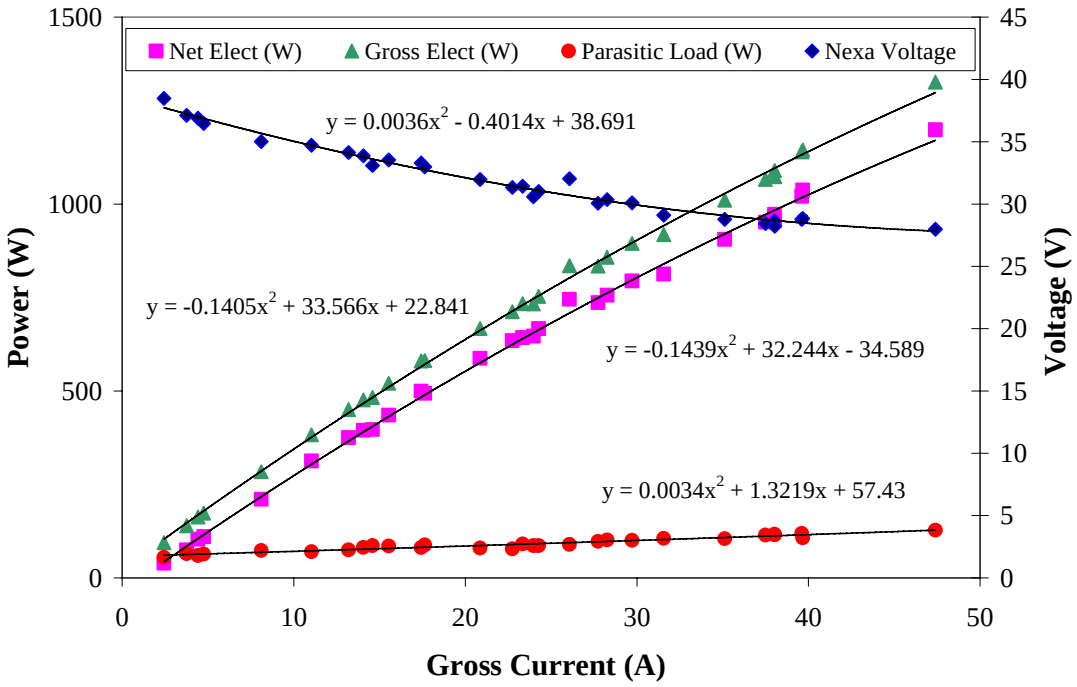

Figure 3.1 Nexa Polarization and Power curves

The Nexa fuel cell is rated for operation up to 1.2 kW net power output. For the experiments, the net load power ranged from 39 Watts to 1199 Watts. This load range translates to a gross electrical output power of approximately 94 Watts to 1326 Watts. The corresponding stack voltage ranged from 38.5 volts to 28.0 volts. The parasitic load, which is the difference between the net load and gross load, never exceeded 128 Watts. Parasitic loads include the Nexa blower, compressor, and electronic control subsystems. The voltage and net power curves come from direct system measurements while the gross

power curve is calculated from hydrogen flow assuming all fuel participates in the oxidation/reduction reaction.

3.3.2 *Total heat rejected*

The heat generated by the Nexa is the difference between the heating value of the fuel consumed and the gross electrical power as depicted in the polarization curves. Stack temperature, coolant temperature, exhaust mass flow and coolant mass flow are measured so sensible and radiant heat transfer can be computed independently for each of the different areas from which heat is rejected. Figure 3.2 shows the rate heat is rejected from the Nexa. The figure includes the lower heating value of the fuel and the gross electrical power generated.

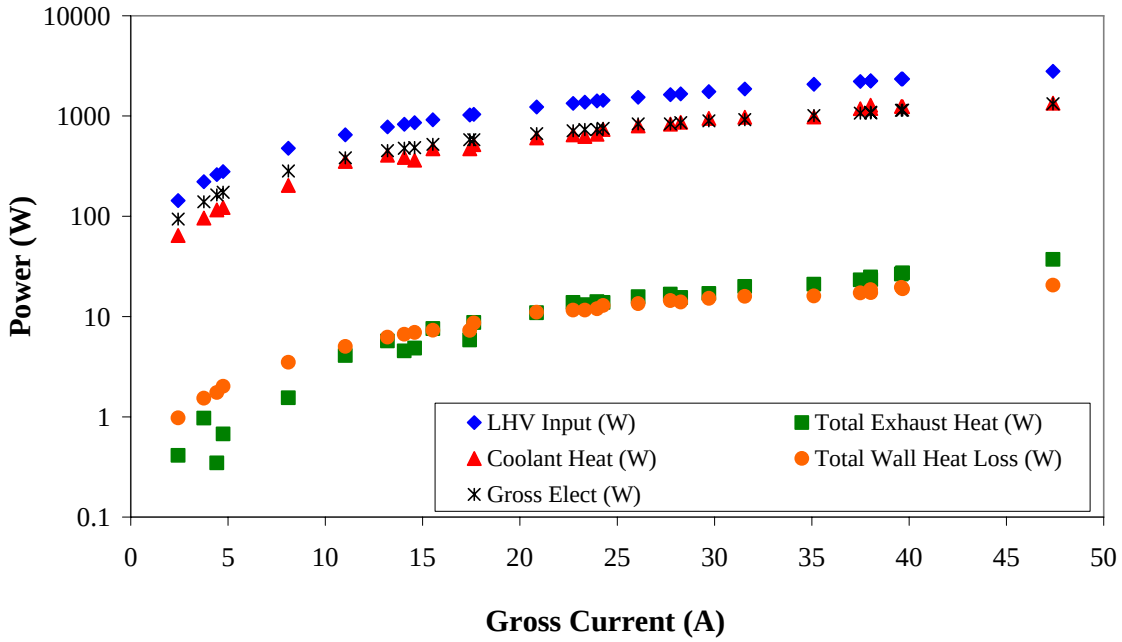

Figure 3.2 Nexa heat dissipated from the exhaust, coolant and exposed surfaces

The sum of heat dissipated through radiation, natural convection and the exhaust is more than an order of magnitude smaller than the heat dissipated through the coolant air. At peak power, the exhaust gases, natural convection and radiation transfer a combined 57 Watts of heat to the ambient environment. This compares to 1345 Watts of heat dissipated by the coolant; hence, as anticipated from the literature [1,4,8,11], the coolant is the only thermal energy carrier considered for heat recovery. The rate of coolant heat rejection is of similar magnitude to the gross electrical power at all load conditions.

3.3.3 *Temperature measurements*

The data presented in Figures 3.1 and 3.2 are similar to Nexa fuel cell characterizations previously published previously in the literature [11,24]. However, for the Nexa to be considered for CHP, the temperature of the coolant needs to be known. The coolant temperatures for the load range and ambient temperatures discussed previously are shown in Figure 3.3.

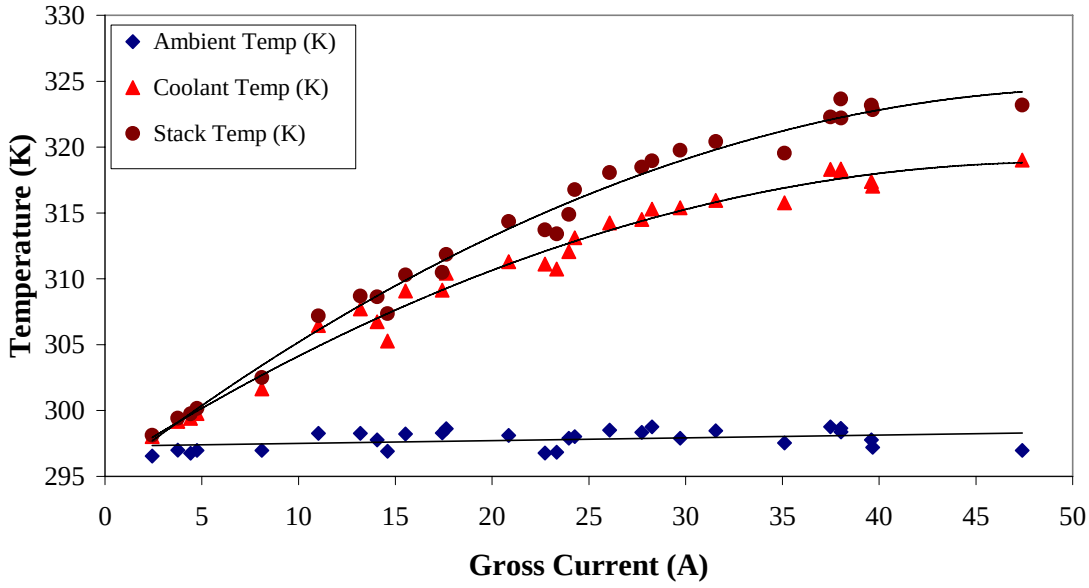

Figure 3.3 Stack, ambient, and coolant temperatures of a Nexa fuel cell

Figure 3.3 also includes the ambient temperature for finding the temperature rise at any given load current, and the average stack surface temperature used for model validation in Chapter 5. The stack and coolant temperatures rise as the Nexa current increases.

The Nexa User's Manual [11] states that the temperature rise of the coolant is approximately 17 K. As can be seen from Figure 3.3, this temperature rise only occurs at gross currents greater than 30 Amps (894 Watts gross power). The maximum observed temperature rise was 22.1 K, resulting in a coolant temperature of approximately 319 K.

3.3.4 *Overall Nexa power balance*

Figures 3.1 to 3.3 can be combined into a single heat balance graph. Figure 3.4 shows the heat balance graph for the Nexa using the rated net power of 1.2 kW as 100% full load. The sum of the four "% Fuel Energy" curves at any fractional load equals 100 % of the fuel energy input to the fuel cell. For any given load, the heat and electrical production of the Nexa can be found from the figure.

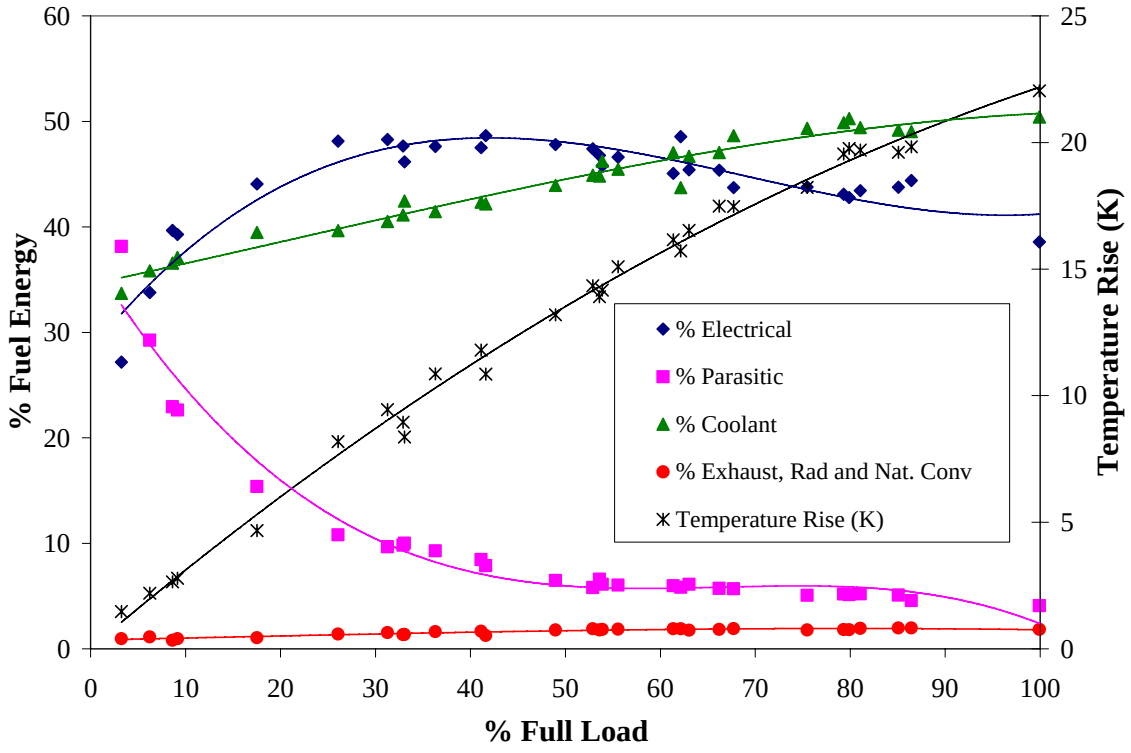

Figure 3.4 Heat balance for a Nexa fuel cell at $\overline{T}_{amb} = 298.0 \pm 0.7$ K

The parasitic load reduces the net electrical power available for external loads. Although the parasitic load increases as the power output of the Nexa increases (Figure 3.1), the overall fraction of fuel energy consumed by the parasitic load decreases (% Parasitic curve in Figure 3.4). During operation at loads below 30% full load, the parasitic load of the Nexa consumes between 10% and 30% of the fuel energy entering the system compared to less than 5% at peak load. For maximum electrical efficiency of approximately 48%, the Nexa should be operated at about 42% full load. However, for maximum coolant temperature rise which is desirable for CHP, the Nexa should be operated at 100% full load. At this peak load, the electrical efficiency falls to

approximately 41%. Operation below 20% full load is undesirable for all applications because both the electrical efficiency and coolant temperature are at a minimum.

Figure 3.4 allows the power balance of multiple Nexa units to be considered simultaneously as long each unit shares the same proportion of the load. For instance, to meet a peak load of 3.8 kW, four Nexa stacks would be required. If all 4 units share the load equally, Figure 3.4 can be used to determine the amount of heat and electrical power that will be produced at any given load.

3.4 *Nexa for CHP integration in a typical coastal British Columbia residence*

This section uses Figure 3.4 to assess the Nexa fuel cell as a heat and power source for residential applications. The Nexa is evaluated as a total energy system and hence must provide all heat and electricity. For space heating, the minimum recommended temperature of the coolant carrying the heat is 323 K (Table 1.1). This minimum temperature is typical for water-cooled PEM fuel cells which must use a heat exchanger to transfer the heat to the ambient air for space heating. Unlike water-cooled PEM fuel cells, the cooling air of the Nexa can be used directly in a ventilation system without the need of a heat exchanger. This is possible because the cooling air is not part of the reactant stream and can be re-circulated through the house like air in a typical forced convection furnace. However, since the goal of a residential heating and ventilation system is to maintain thermal comfort, the temperature at which air is supplied to the living space must still be maintained at certain minimum levels. Typically, the

ventilation system must be able to maintain a room at temperatures near 295 to 298 K with air velocities less than 0.25 m/s in the occupied space [25].

Forced convection heating systems ideally discharge air from the diffusers into the occupied space at a temperature near 325 K [26]; the Nexa is incapable of producing coolant at this temperature. However, heating systems with a temperature rise of approximately 13 K can be implemented as long as the ventilation system is designed to minimize the perception of “cool” drafts [4]; this temperature rise is used in this section to evaluate the Nexa as a residential CHP heat source.

The following assumptions are made for residential application of the Nexa:

- The residence is independent of the grid and all electricity must be provided by the four Nexa stacks.
- If the temperature rise of the coolant is below the desired temperature rise, the coolant is not recovered.
- Heat energy is not stored but must be used when generated.
- Supplementary heat to bring either the Nexa coolant up to an acceptable temperature or to meet heating demand is not considered.
- Indoor temperature is maintained at 298 K.

A real system will undoubtedly have a supplementary furnace that can condition the discharge coolant of the fuel cell before distribution throughout the residence or to provide heat when the fuel cell discharge coolant heat is insufficient to meet the load.

However, the highest CHP system efficiency will be obtained when the coolant discharged from the fuel cell can be used without expending energy to raise the temperature. The analysis presented hence does not consider supplementary heating.

Table 3.1 lists the average yearly heat and electrical energy consumption of a typical coastal British Columbia residence. Appendix A10 contains a heat and electrical load graph for a single January day.

Table 3.1 Coastal British Columbia average residential energy use for 1 year

Electrical Consumption kWh	Heat Consumption kWh	Peak Electric Load kW	Peak Heat kW
12971	6635	3.82	3.70

Four Nexa fuel cells would be required to meet the peak residential power demand shown in Table 3.1 because a single Nexa is rated for 1.2 kW. Using Figure 3.4 and the hourly electrical load data, the heat generated by the Nexa can be found. Appendix A10 shows an example of finding the heat generated by the Nexa based on the electric load. Figure 3.4 can also be used to find the temperature of the coolant based on the load.

Table 3.2 provides a summary of Nexa heat recovery for space heating using a 0 K, 13 K, and 20 K minimum coolant temperature rise; any coolant that does not exceed the desired temperature rise would not be recovered for this study: Appendix A10 discusses how this table is developed.

Table 3.2 Heat recovery from 4 Nexa fuel cells for 1 year of operation

Minimum Coolant Temperature Rise	0 K	13 K	20 K	No heat recovery
Heat Generated (kWh)	11568	11568	11568	11568
Heat Recovered (kWh)	6395	2075	3	0
Heat Dumped (kWh)	5173	9493	11565	11568
Supplementary Heat (kWh)	240	4560	6632	6635
LHV efficiency (%)	70.0	54.4	46.9	46.9
Heat Demand Met (%)	96.4	31.3	0.0	0.0
Average % full load	30.8	30.8	30.8	30.8

Column 2 requires the coolant rejected from the Nexa to undergo an increase in temperature of 0 K above ambient temperature for recovery to occur (i.e. distribution throughout the occupied space of the residence); hence all heat generated by the Nexa could be recovered for this scenario if the residence required heating. Based on operation over a year, the by-product heat generated by the Nexa would meet 96.4% of the residential heat load (no thermal energy storage is considered). That is, if the four Nexa stacks were to meet 100% of the yearly residential electrical load, the by-product heat generated would meet 96.4% of the heat load. Since the residence does not require continuous heating, 5173 kWh of by-product heat would not be recovered.

In contrast, if heat recovery only occurs for a coolant temperature rise above 20 K (coolant temperature of approximately 318 K), only 3 kWh of heat would be recovered for the year. The four Nexa stacks would have to operate above 79% full load to generate coolant at 318 K. During the course of the year, 79% full load only happens a few times. Under these conditions, the Nexa would not be used for CHP.

The four Nexas operate at approximately 31% full load based on the average hourly electrical requirement; this indicates the Nexa stacks would be typically operating below peak electrical and thermal efficiency. Ideally, the stacks should operate near 42% full load for maximum electrical efficiency or near 100% full load for maximum thermal efficiency and coolant temperature.

If a single Nexa can be operated for short durations at 1.27 kW, three Nexa stacks can potentially meet the electrical demands of the residence and also increase the coolant temperature and electrical efficiency. Table 3.3 summarizes the residential heat recovery options if three fuel cells are used to meet the electrical demand:

Table 3.3 Nexa heat recovered for 3 fuel cell stacks for a year of operation

Nexa Coolant Temperature Rise	0 K	13 K	20 K	No heat recovery
Heat Generated (kWh)	12247	12247	12247	12247
Heat Recovered (kWh)	6421	3874	494	0
Heat Dumped (kWh)	5826	8373	11753	12247
Supplementary Heat (kWh)	214	2761	6141	6635
LHV efficiency (%)	69.8	60.6	48.5	46.7
Heat Demand Met (%)	96.8	58.4	7.4	0.0
Average % full load	41.1	41.1	41.1	41.1

With three Nexa stacks, even though the electrical output is the same as with four stacks, almost 700 kWh more heat is produced for the year. This is because the three fuel cells will each have to operate at higher loads when compared to the four fuel cell scenario. During operation, a larger fraction of the fuel energy input to the system is being converted to heat and electricity and not used for parasitic loads when compared to the four stack scenario. The three Nexa stacks operate, on average, at 41% full load which is almost the peak electrical efficiency. If heat is recovered for a minimum 13 K coolant

temperature rise, 58.4% of the residential heat load can be met strictly from the heat generated by the 3 Nexa stacks; this compares to 4 stacks meeting only 31.3% of the yearly heat load.

3.5 *Summary*

A heat balance diagram was developed in this chapter for the Nexa fuel cell. The heat balance diagram shows the relationship between fuel consumption, thermal efficiency and electrical efficiency based on fractional loads. The heat balance diagram simplifies analysis of the Nexa for CHP integration. The diagram shows that maximum electrical efficiency of the Nexa occurs when the fuel cell operates at 42% full load; the diagram also shows that maximum coolant temperature and thermal efficiency occur at 100% full load.

This chapter also presented an analysis of the Nexa fuel cell for residential heat and power applications. Based on hourly residential power consumption, 4 Nexa fuel cells would be required to meet the electrical demands of a typical British Columbia residence. Using the heat balance diagram, the analysis presented in this chapter shows the Nexa CHP system can potentially meet the electrical load and 96% of the heating load of a typical residence if heat recovery occurred irrespective of the coolant temperature. However, if an ambient of 298 K is desired for the occupied space and a 13 K or 20 K temperature rise is required for the coolant, only 31.3% or 0.0% of the heat load would be met, respectively. Ideally, the Nexa coolant temperature rise should be approximately 25 K for all loads. Chapter 4 presents a model to determine whether the Nexa can achieve

this coolant temperature rise without exceeding the suggested operating temperatures for Nafion membranes.

Chapter 4

PEM fuel cell cooling system analysis

4.1 *Introduction*

This chapter presents equations and a model to simulate and analyze the cooling system of air-cooled PEM fuel cells. The PEM fuel cell is treated as a heat exchanger with internal heat generation. Heat generated during normal operation of the fuel cell is eliminated from the fuel cell through radiation, natural convection and forced convection. The choice of equations and modular design of the model allows cooling system geometry and heat exchange surface area (i.e. number of cooling channels, cooling channel dimensions, stack dimensions, number of cells in stack) to be modified. Simulations can be run to determine the effects of cooling system and stack design on coolant temperature rise, coolant mass flow, stack temperature, or stack temperature difference axial to flow and pressure drops through the cooling system. The model is limited to cooling systems with straight rectangular cooling channels, stacks with a rectangular geometry (i.e. the cooling channel length is the same for all channels), and air as the cooling fluid.

The following assumptions are made for the model:

1. Radiation and natural convection heat transfer occur at the mean stack temperature.
2. Exhaust gases exit the fuel cell at the mean stack temperature.
3. Water vapour is formed during the reaction.

This chapter is comprised of 3 subsections as follows:

1. Section 4.2 describes the equations for determining heat and electrical power generation of a PEM fuel cell.
2. Section 4.3 presents the empirical equations and tabular data used to simulate heat transfer.
3. Section 4.4 discusses the range and limitations for the model.

4.2 *PEM fuel cell heat and electrical power generations*

Proton exchange membrane fuel cells can be viewed as both an electrical power generating device and a heat engine. The general reaction of the PEM fuel cell is shown in Figure 4.1.

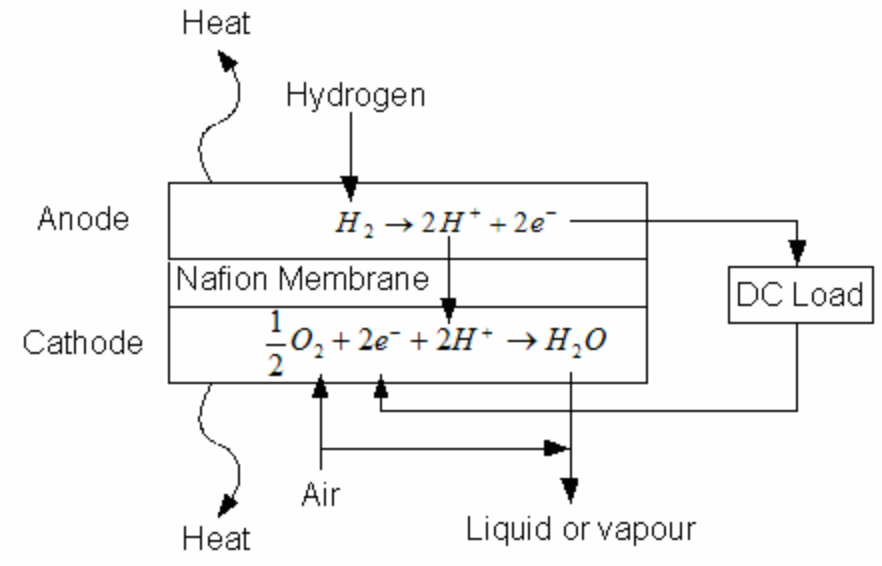

Figure 4.1 PEM fuel cell chemical reactions

The overall reaction occurring in the fuel cell is shown in Equation 4.1 and is a combination of the half-cell reactions shown in Figure 4.1.

$$H_2 + \frac{1}{2}O_2 \xrightarrow{\dot{Q}_{\Delta H}} H_2O \tag{4.1}$$

where

$\dot{Q}_{\Delta H}$ = the rate at which energy enters the fuel cell, W

For the reaction to progress to completion, the electrons liberated by hydrogen oxidation must pass through an external circuit, driven by a potential difference between the anode and cathode. For every mole of hydrogen reacted, 2 moles of electrons pass through the external circuit. For a continuous current, the molar flow rate of hydrogen necessary to maintain the reaction can be calculated from:

$$I = A_{stack} \cdot \frac{i}{1000} = 2 \cdot F \cdot \dot{N}_{H_2} \tag{4.2}$$

where

I = circuit current, A

i = current density, $mA \cdot cm^{-2}$

A_{stack} = stack cross sectional area involved in the reaction, cm^2

F = Faradays constant, $C \cdot mol^{-1}$

$\dot{N}_{H_2}$ = molar flow rate of hydrogen, $mole \cdot s^{-1}$

For simulating the operation of a PEM stack, the current density, i, is the independent variable.

4.2.1 *Total heat energy generated by the PEM fuel cell*

The total energy (enthalpy) liberated by the electrochemical reaction in Figure 4.1 equals the molar enthalpy of reaction. The molar enthalpy of reaction can be calculated from the difference between the molar enthalpy of formation for the products and the reactants as shown in Equation 4.3, and is an application of Hess's Law of heat summation:

$$(\Delta\bar{h}_f)_{reac} = (\Delta\bar{h}_f)_{H_2O} - \left[(\Delta\bar{h}_f)_{H_2} + \frac{1}{2}(\Delta\bar{h}_f)_{O_2}\right] \tag{4.3}$$

where

$\Delta\bar{h}_f$ = molar enthalpy of reaction or formation, $J \cdot mol^{-1}$

The molar enthalpy of formation for the reactants and products varies with temperature and can be calculated with equation 4.4 [8]:

$$\Delta\bar{h}_T = \Delta\bar{h}_f^o + \int_{298.15K}^{T} \bar{c}_p dT \tag{4.4}$$

where

$\Delta\bar{h}_T$ = molar enthalpy of formation at temperature T, $J \cdot mol^{-1}$

$\Delta\bar{h}_f^o$ = molar enthalpy of formation at standard conditions, $J \cdot mol^{-1}$ (Table 4.1)

$\bar{c}_p$ = molar specific heat capacity, $J \cdot mol^{-1} \cdot K^{-1}$

Table 4.1 Heat of formation and entropy at standard conditions (298 K, 1 atm)

	$\Delta\bar{h}_f^o \quad J \cdot mol^{-1}$	$\Delta\bar{s}^o \quad J \cdot mol^{-1} \cdot K^{-1}$
$H_2O(l)$ liquid water	-285,830	70.05
$H_2O(v)$ vapour water	-241,820	188.83
H_2	0	130.59
O_2	0	205.14

The molar specific heat capacity can be determined from Equations 4.5 to 4.8 [8,20,23].

$$(\bar{c}_p)_{H_2O(v)} = 143.05 - 58.040 \cdot T^{0.25} + 8.2751 \cdot T^{0.5} - 0.036989 \cdot T \quad (4.5)$$

$$(\bar{c}_p)_{H_2(v)} = 56.505 - 22222.6 \cdot T^{-0.75} + 116500 \cdot T^{-1} - 560700 \cdot T^{-1.5} \quad (4.6)$$

$$(\bar{c}_p)_{O_2(v)} = 37.432 + 2.0102 \cdot 10^{-5} \cdot T^{1.5} - 178570 \cdot T^{-1.5} + 2368800 \cdot T^{-2} \quad (4.7)$$

$$(\bar{c}_p)_{H_2O(l)} = 741.03 - 7.9178 \cdot T + 0.0353 \cdot T^2 - 7 \cdot 10^{-5} \cdot T^3 + 5 \cdot 10^{-8} \cdot T^4 \quad (4.8)$$

where T is in Kelvin and Equation 4.8 a polynomial fit of tabular data

Solving equation 4.3 for ambient temperature gives the reaction enthalpy per mole of hydrogen consumed. At an ambient of 298 K, the molar enthalpy is simply the lower or higher heating value of the fuel (LHV = -241.82 $kJ \cdot mol^{-1}$ and HHV = -285.83 $kJ \cdot mol^{-1}$). The difference between the LHV and HHV of the fuel is the latent heat of condensation at standard conditions. Multiplying the ambient temperature solution of equation 4.3 by the molar flow rate of hydrogen gives the total power generated by the fuel cell (Equation 4.9):

$$\dot{Q}_{\Delta H} = -\Delta\bar{h}_{f_{amb}} \cdot \dot{N}_{H_2} \quad (4.9)$$

The value calculated in 4.9 is the rate heat energy would be liberated for a combustion reaction. However, the reaction is an electrochemical reaction so a portion of the power produced is available to perform electrical work as described in section 4.2.2.

4.2.2 *Electrical energy generated by the fuel cell*

The theoretical maximum electrical work that can be performed equals the Gibbs free energy (Equation 4.10) [27].

$$W_{\max} = -\Delta G_f \tag{4.10}$$

where

$W_{\max}$ = maximum work performed by the fuel cell, *J*

ΔG_f = Gibbs free energy, *J*

Since the model is concerned with reactant and product flow rates, the molar Gibbs free energy is more useful to complete a fuel cell power balance. The molar Gibbs free energy of formation is equal to the difference between the molar enthalpy of formation and the product of the absolute temperature and change in entropy for the reaction (Equation 4.11).

$$\Delta \bar{g}_f = \Delta \bar{h}_f - T\Delta \bar{s} \tag{4.11}$$

where

$\Delta \bar{g}_f$ = molar Gibbs free energy, $J \cdot mol^{-1}$

$\Delta \bar{s}$ = molar entropy, $J \cdot mol^{-1} \cdot K$

However, the molar entropy changes with temperature. Equation 4.12 and 4.13 along with the entropy values given in Table 4.1 and molar specific heat equations 4.5 to 4.8 can be used to find the change in molar entropy for the reaction at any temperature and thus solve equation 4.11 for the molar Gibbs free energy.

$$\Delta\bar{s} = (\Delta\bar{s})_{H_2O} - \left[(\Delta\bar{s})_{H_2} + \frac{1}{2}(\Delta\bar{s})_{O_2} \right] \tag{4.12}$$

$$\Delta\bar{s}_T = \bar{s}_{298.15K} + \int_{298.15K}^{T} \frac{1}{T}\bar{c}_p dT \tag{4.13}$$

For a reversible system, the molar Gibbs free energy can be equated to the maximum theoretical electrical work of a hydrogen/oxygen fuel cell:

$$\Delta\bar{g}_f = -2 \cdot E_{rev} \cdot F \tag{4.14}$$

where

E_{rev} = the reversible cell voltage, V

Thus,

$$E_{rev} = -\frac{\Delta\bar{g}_f}{2 \cdot F} \tag{4.15}$$

The fuel cell does not operate at the reversible cell voltage. Activation losses, fuel crossover, ohmic losses and mass transport losses all result in a lower cell voltage. Equation 4.16, described by Larminie and Dicks [8], provides an empirical relation to account for these losses:

$$V_{cell} = E_{rev} - (i + i_n) \cdot r - A \cdot \ln(\frac{i + i_n}{i_o}) + B \cdot \ln(1 - \frac{i + i_n}{i_l}) \tag{4.16}$$

where

V_{cell} = voltage of the fuel cell found, V

The other variable descriptions, units and PEM fuel cell values used in the model to simulate cell voltage are shown in Table 4.2. These variables are presented by Larminie and Dicks and were found to give an excellent fit to real fuel cells [8].

Table 4.2 Variables used to calculate PEM fuel cell voltage

Variable	Value	Units	Description
E_{rev}	Eqn. 4.15	volts	Reversible open circuit voltage
i	Model looping variable	$mA \cdot cm^{-2}$	Cell current density
i_n	2	$mA \cdot cm^{-2}$	Internal and fuel crossover current density
i_o	0.067	$mA \cdot cm^{-2}$	Exchange current density
i_l	900	$mA \cdot cm^{-2}$	Limiting current density
A_T	0.06	volts	Tafel slope
B	0.05	volts	Constant of mass transfer overvoltage equation
r	30 x 10^{-6}	$k\Omega \cdot cm^{-2}$	Area specific resistance

Figure 4.2 shows the voltage calculated from the model subroutine implementing equations 4.3 through 4.16 for both a vapour and liquid product using the mean Nexa stack temperatures shown in Chapter 3 taking a 94 cm^2 active surface area per cell and 47 cells per stack. The 94 cm^2 per cell is estimated from the exterior dimensions of 11.7 x 11.7 cm assuming a 1 cm boundary around the outer edge of the MEA is not active (no flow fields). Other estimates of Nexa active area found in the literature include: 100 cm^2 [28], 115.8 cm^2 [29] and 122 cm^2 [30].

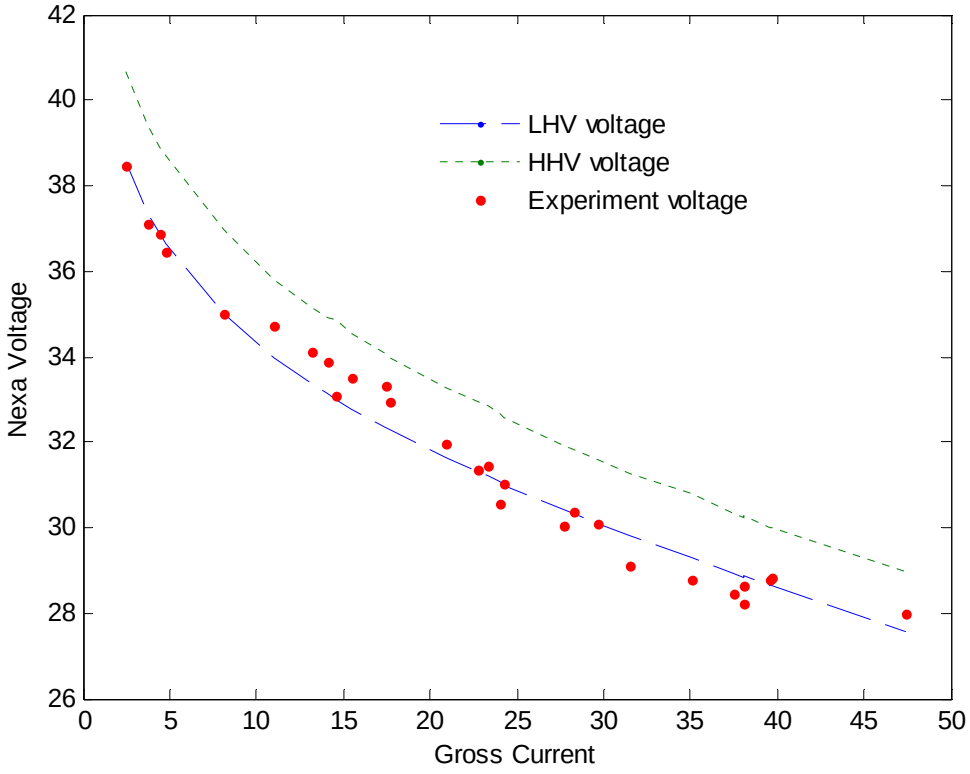

Figure 4.2 Experimental and predicted Nexa polarization values

Figure 4.2 shows that the voltage calculated from empirical Equation 4.16 with the parameters given in Table 4.2 provides a good approximation of the actual experimental voltage for the Nexa.

4.2.3 *Heat generated by PEM fuel cells*

The electrical power generation of the fuel cell is the product of the cell voltage and current as shown in Equation 4.17.

$$\dot{W}_{elect} = I_{cell} \cdot V_{cell} \tag{4.17}$$

The rate of heat generation by the fuel cell is the difference between the electric power generated and the total power generated by the reaction:

$$\dot{Q}_{heat} = \dot{Q}_{\Delta H} - \dot{W}_{elect} \tag{4.18}$$

At 298 K using the lower heating value of the fuel, Equation 4.18 is equivalent to the heat generation equation given by Larminie and Dicks ($I_{cell} \cdot (1.25 - V_{cell})$) where 1.25 is the cell voltage if all the enthalpy of reaction (LHV) were converted into electrical energy [8].

4.2.4 *Reactant and by-product mass flow rates*

For any given current, the stoichiometric mass flow rate of the products and reactants can readily be determined (Appendix A6). These flow rates are required to calculate heat rejected due to forced convection in the exhaust as well as the total enthalpy of the reaction. In the model, the actual flow of the reactant air is chosen by the fuel cell designer; for the simulations, the stoichiometry is chosen at twice the required flow [8].

4.2.5 *Heat rejection from a PEM fuel cell*

As discussed in Chapter 2, forced convection, natural convection and radiation heat transfer carry energy from the fuel cell to the environment. Equations 2.4 through 2.9 are used in the model to simulate heat transfer rates due to natural convection, radiation and sensible heating of exhaust gases while Equation 4.18 gives the total heat generated. Once the stack temperature, ambient temperature and reactant air stoichiometry are known, the rate at which heat must be removed from the fuel cell by sensible heating of the coolant air can be found from Equation 4.19 (Refer to Figure 2.1):

$$\dot{Q}_{cool} = \dot{Q}_{heat} - (\dot{Q}_{rad\&nat} + \dot{Q}_{ex}) \tag{4.19}$$

4.3 *Cooling system model*

The cooling system must remove heat at the rate determined from Equation 4.19. The cooling system model presented in this section uses empirical correlations found in Incropera, et al [21], Kakac, et al [31], and Rohsenow, et al [32] to find the coolant air mass flow rate and temperature rise with respect to the stack temperature and rate heat is dissipated. The correlations presented are for rectangular channel geometries. These Nusselt number correlations (i.e. heat transfer coefficients) are used in a power balance to equate heat power generated with heat power dissipated by forced convection. The correlations presented correspond to the isothermal channel temperature (T boundary condition) and constant heat flux with uniform circumferential temperature cases ($H1$ boundary condition). The model developed to simulate the heat transfer of the cooling system analyzes the heat transfer of one cooling channel (Figure 4.3).

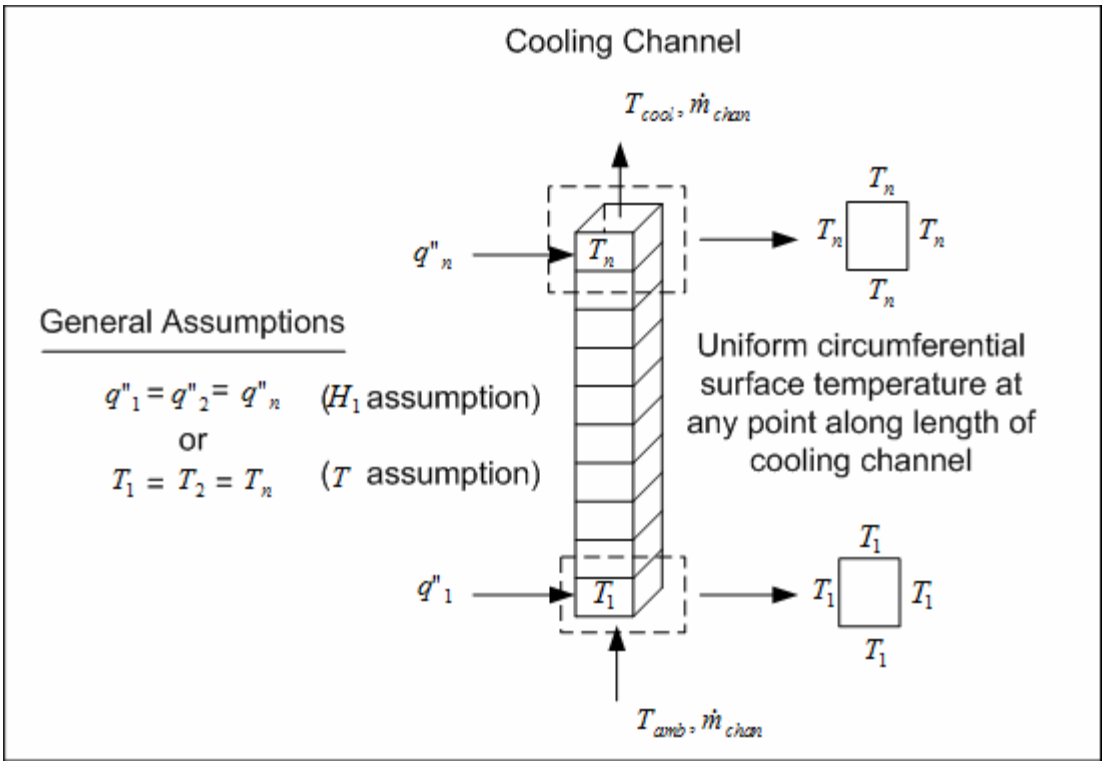

Figure 4.3 Single channel used in the model with the 2 boundary conditions considered

where

q''_n = heat flux at any position in the channel, $W \cdot m^{-2}$

T_n = channel surface temperature at any position in the channel, K

T_{amb} = ambient temperature, K

T_{cool} = final coolant temperature, K

$\dot{m}_{chan}$ = coolant mass flow through a single channel, $kg \cdot s^{-1}$

The model assumes:

1. Air is the coolant.
2. The entrance region for laminar flow is characterized by simultaneously developing flow (a valid assumption for air as the coolant [21]).

3. When Reynolds numbers are greater than the critical Reynolds number (i.e. the flow is turbulent), fully developed flow exists through the entire channel. This assumption is valid for turbulent flow of air when the length to diameter ratio is greater than 10 ($L/D_H \geq 10$) [32].
4. Operating conditions are identical for every channel.

4.3.1 *Nusselt correlations*

Correlations, typically obtained from experimental data, are usually given in terms of the non-dimensional heat transfer coefficient, i.e. the Nusselt number defined as:

$$Nu = \frac{h \cdot D_h}{k} \tag{4.20}$$

where

Nu = Nusselt number determined from appropriate correlation

h = mean or local heat transfer coefficient, $W \cdot m^{-2} \cdot K^{-1}$

D_h = characteristic dimension (hydraulic diameter) = $4 \cdot \frac{A_c}{P}$, m

A_c = channel cross sectional area for flow, m^2

P = channel perimeter, m

k = fluid thermal conductivity, $W \cdot m^{-1} \cdot K^{-1}$

Developing laminar flow

Nusselt numbers in the developing laminar flow region of the channel for either the *H1* or T boundary conditions are determined from tabular data. The tabular data is dependent

upon channel aspect ratio, α^*, and the Graetz number, Gz, defined in equations 4.21 and 4.22, respectively.

$$\alpha^* = \frac{a}{b} = \text{cooling channel aspect ratio as shown in Figure 4.4} \qquad (4.21)$$

where

a = short perimeter wall, m

b = long perimeter wall, m

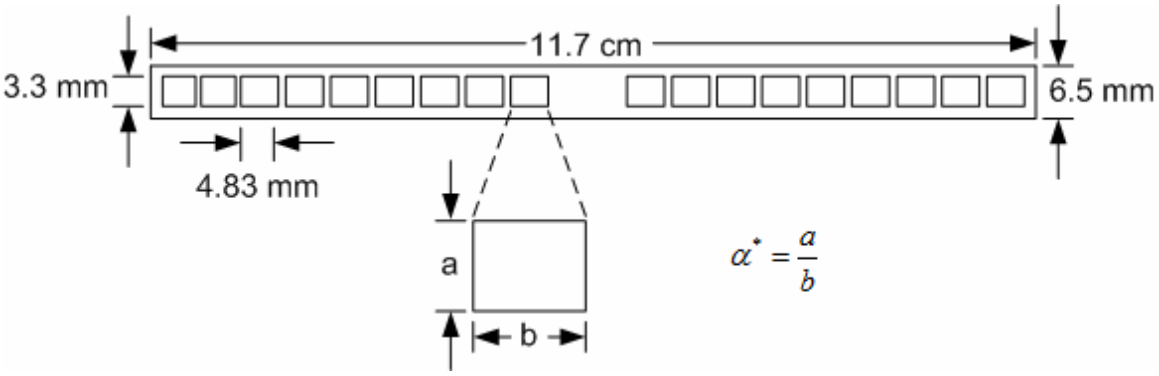

Figure 4.4 Aspect ratio of Nexa fuel cell

$$Gz = \frac{\mathrm{Re} \cdot \mathrm{Pr} \cdot D_h}{x} \qquad (4.22)$$

The Graetz number characterized the extent of the entrance region, with the other parameters defined as follows:

$\mathrm{Re} = \frac{\dot{m}_{chan} \cdot D_h}{A_c \cdot \mu}$ = Reynolds number

Pr = Prandtl number

μ = dynamic viscosity of air, $kg \cdot m^{-1} \cdot s^{-1}$

Appendix A12 presents the tabular developing laminar flow Nusselt data for both the $H1$ and T boundary conditions. Based on plots of the rectangular Nusselt data versus inverse Graetz data and recommendations by Incropera, et al [21], fully developed laminar flow occurs at an inverse Graetz of approximately of 0.05. The physical distance into the channel at which developing flow becomes fully developed flow can then be estimated with Equation 4.23:

$$x_{fd} = 0.05 \cdot \mathrm{Re} \cdot \mathrm{Pr} \cdot D_h \tag{4.23}$$

where

x_{fd} = distance in channel to thermally fully developed flow, m

Equation 4.23 is for simultaneously developing flow and is used to estimate the point where fully developed thermal flow is achieved. To estimate fully developed hydrodynamic flow, Equation 4.24 is used:

$$x_{hd} = \frac{x_{fd}}{\mathrm{Pr}} \tag{4.24}$$

where

x_{hd} = distance in channel to hydrodynamically fully developed flow, m

The pressure drop in the hydrodynamically developing laminar flow region to some position, *x*, is estimated using tabular data for the apparent Fanning friction factor shown in Figure 4.5 and Equation 4.25 [33].

$$\Delta p = \frac{2 \cdot (f_{app} \cdot \mathrm{Re}) \cdot \mu_{air} \cdot u_m \cdot x}{D_h^2} \tag{4.25}$$

where

Δp = channel pressure drop, Pa

f_{app} = apparent Fanning friction factor

ρ_{air} = air density, $kg \cdot m^{-3}$

u_m = mean channel velocity, $m \cdot s^{-1}$

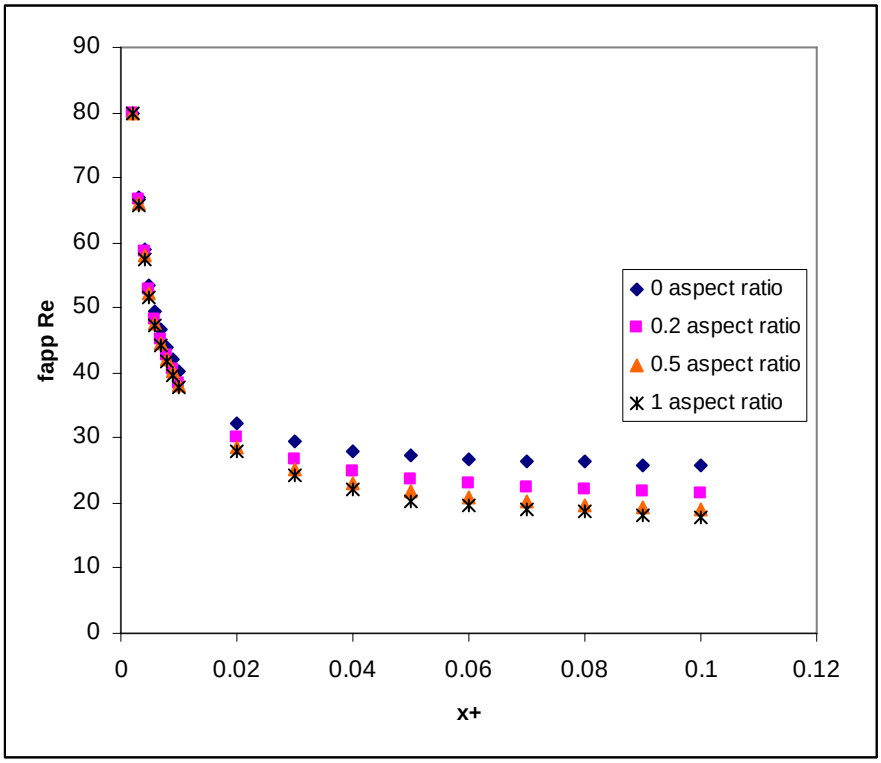

Figure 4.5 Apparent Fanning friction factor for hydrodynamically developing flow in rectangular channels adapted from [32].

where

$x^+ = \dfrac{x}{D_h \cdot \mathrm{Re}}$ = dimensionless hydrodynamic axial distance

Using the overall channel length in Equation 4.25 gives the total pressure drop. Equation 4.25 is also valid for the fully developed laminar flow regime and is used in the model to

find total pressure drop through the channel as long as the Reynolds number remains below the critical Reynolds number (i.e. the flow is in the laminar regime).

Fully developed laminar flow

For the $H1$ and T boundary conditions and fully developed laminar flow, Equations 4.26 and 4.27, respectively, are used in the model to predict the Nusselt number for different channel aspect ratios [31,32].

$$Nu_{H1} = 8.235 \cdot (1 - 2.0421 \cdot \alpha^{*} + 3.0853 \cdot \alpha^{*2} - 2.4765 \cdot \alpha^{*3} + 1.0578 \cdot \alpha^{*4} - 0.1861 \cdot \alpha^{*5}) \tag{4.26}$$

$$Nu_{T} = 7.541 \cdot (1 - 2.610 \cdot \alpha^{*} + 4.970 \cdot \alpha^{*2} - 5.119 \cdot \alpha^{*3} + 2.702 \cdot \alpha^{*4} - 0.548 \cdot \alpha^{*5}) \tag{4.27}$$

The Fanning friction factor in the fully developed laminar flow region is given by Equation 4.28:

$$f_{lam} = \frac{24 \cdot (1 - 1.3553 \cdot \alpha^{*} \cdot 1.9467 \cdot \alpha^{*2} - 1.7012 \cdot \alpha^{*3} + 0.9564 \cdot \alpha^{*4} - 0.2537 \cdot \alpha^{*5})}{\mathrm{Re}} \tag{4.28}$$

The Fanning friction factor for fully developed laminar flow, transitional flow and turbulent flow can be used in Equation 4.29 to estimate pressure drops:

$$\Delta p = \frac{f \cdot 2 \cdot \rho_{air} \cdot u_m^2 \cdot L}{D_h} \tag{4.29}$$

where

L = channel length, m

However, since developing laminar flow can occur through much of the channel length and entrance effects can be substantial, equation 4.25 and the apparent Fanning friction factor is used for Reynolds numbers below the critical Reynolds number. Equation 4.29 and the Fanning friction factor are used for Reynolds numbers above the critical Reynolds number (turbulent flow).

Determining laminar or transitional flow

For Reynolds numbers above the critical Reynolds number, the flow is turbulent. Equation 4.30 is used to find the critical Reynolds number for rectangular channels with an abrupt entrance (i.e. not bevelled).

$$\mathrm{Re}_{crit} = \frac{4650}{(u_{\max}/u_m)} \tag{4.30}$$

where

$u_{\max}$ = maximum channel velocity, $m \cdot s^{-1}$

The ratio of maximum channel velocity to mean channel velocity for rectangular ducts can be approximated with equation 4.31 [31]:

$$\frac{u_{\max}}{u_m} = \left(\frac{m+1}{m}\right) \cdot \left(\frac{n+1}{n}\right) \tag{4.31}$$

where

$$m = 1.7 + 0.5 \cdot (\alpha^*)^{-1.4}$$

$$n = 2 \qquad \text{for } \alpha^* \leq \frac{1}{3}$$

$$n = 2 + 0.3 \cdot \left(\alpha^* - \frac{1}{3} \right) \qquad \text{for } \alpha^* \geq \frac{1}{3}$$

For the Nexa fuel cell channel dimensions (Figure 4.4), the critical Reynolds number is 2265 as calculated from Equation 4.31.

Transitional and turbulent flow

For the turbulent flow regime, as suggested by Kakac, et al [31], the circular Nusselt correlations provide sufficiently accurate predictions when the laminar equivalent diameter is used (Equation 4.32).

$$D_l = \frac{2}{3} \cdot D_h + \frac{11}{24} \cdot \alpha^* \cdot \left(2 - \alpha^* \right) \tag{4.32}$$

Transitional flow and turbulent flow can be modelled with a Nusselt correlation that spans both flow regimes. The circular Nusselt correlations for turbulent flow apply to both the constant heat flux and constant channel temperature assumptions provided the correct variables are used as presented in Equation 4.33:

$$Nu^{10} = Nu_l^{10} + \left[\frac{\exp\left[\frac{2200 - \mathrm{Re}}{365} \right]}{Nu_l^2} + \frac{1}{Nu_t^2} \right]^{-5} \tag{4.33}$$

where

$Nu_l = 3.657$ *T* boundary condition

$Nu_l = 4.364$ *H1* boundary condition

$$Nu_t = Nu_0 + \frac{0.079 \cdot \left[\frac{f}{2}\right]^{\frac{1}{2}} \cdot \mathrm{Re} \cdot \mathrm{Pr}}{(1 + \mathrm{Pr}^{\frac{4}{5}})^{\frac{5}{6}}}$$

$Nu_0 = 4.8$ *T* boundary condition

$Nu_0 = 6.3$ *H1* boundary condition

To solve Equation 4.33, the developing or turbulent Fanning friction factor needs to be found (Equation 4.34)

$$f = A + \frac{B}{\mathrm{Re}^{\frac{1}{m}}} \tag{4.34}$$

where

$A = 0.0054,\ B = 2.3 \cdot 10^{-8},\ m = -\frac{2}{3}$ for $2100 < \mathrm{Re} \leq 4000$

$A = 1.28 \cdot 10^{-3},\ B = 0.1143,\ m = 3.2154$ for $\mathrm{Re} > 4000$

The Fanning friction factor can also be used in Equation 4.29 to estimate the pressure drop through the channel. The correlation for transitional and turbulent flow is valid up to a Reynolds number of 10^6, but it should be noted that equation 4.34 assumes a smooth duct surface.

4.3.2 *Power balance equations*

For the channel shown in Figure 4.3, the rate of heat transfer due to sensible heating of the coolant air is given by Equation 4.35:

$$\dot{Q}_{chan} = \dot{m}_{chan} \cdot c_p \cdot (T_{cool} - T_{amb}) \quad (4.35)$$

where

$\dot{Q}_{chan}$ = rate of heat transfer for a single cooling channel, W

Constant heat flux assumption

For the constant heat flux assumption, the mean temperature of the coolant at any position within the channel can be found by applying the first law of thermodynamics (Equation 4.36) [20,21]:

$$\dot{m}_{chan} \cdot c_p \cdot (T_m(x) - T_{amb}) = q'' \cdot P \cdot x \qquad q'' = \text{heat flux for 1 channel = constant} \quad (4.36)$$

where

$T_m(x)$ = coolant temperature at any position within the cooling channel, K

Setting $x = L$ in Equation 4.36 gives the output temperature of the coolant. The coolant temperature can also be used to find the stack temperature at any channel position using Newton's law of cooling (equation 4.37).

$$q'' = h_c \cdot (T_s(x) - T_m(x)) \quad (4.37)$$

where

T_s = channel surface temperature, K

Isothermal channel temperature assumption

For an isothermal channel temperature, the coolant temperature at any position within the channel can be found with equation 4.38 [20,21]:

$$\ln\left(\frac{T_s - T_m(x)}{T_s - T_{amb}}\right) = -\frac{P \cdot x \cdot \bar{h}}{\dot{m}_{chan} \cdot c_p} \qquad T_s = \text{constant} \tag{4.38}$$

where

$\bar{h}$ = mean channel heat transfer coefficient, $W \cdot m^{-2} \cdot K^{-1}$

4.4. *Summary*

The cooling system model presented in this chapter equates power output with power input (generated) for a PEM fuel cell. The power balance allows the relationship between stack temperature, coolant temperature, coolant mass flow, reactant mass flow, cooling system channel geometry, and cell voltage to be investigated. Due to the interdependence of these variables, most solutions need to be iterated based on initial guesses. As an example, Appendix A13 gives a flow chart showing the iterative process by which the MATLAB code solves for the stack temperature when the user defines the coolant temperature rise and ambient temperature.

The constant wall temperature or constant heat flux assumptions used for the model represent the two limit conditions at which heat transfer can occur. For most real systems, actual heat transfer occurs somewhere between these two limits (conjugate problem) due to heat conduction in the channel walls. The conjugate problem is not addressed in this thesis; however, usually either the constant wall temperature or constant heat flux approximation provide sufficiently accurate approximations of the heat transfer coefficients [21]. Chapter 5 compares the models with experimental data for these two boundary conditions.

Chapter 5

PEM fuel cell cooling system simulations

5.1 *Introduction*

Prior to building an air-cooled PEM fuel cell, the stack designer must determine if the prospective cooling system design will maintain a stack temperature that does not promote drying or flooding of the membrane electrode assembly. In addition, if the stack is to be used for combined heat and power, the designer must ensure the coolant rejected from the fuel cell can be maintained at a temperature sufficient to justify heat recovery. Pressure drops and mass flow must also be considered for any stack or cooling system design because cooling system power consumption directly impacts the efficiency of the fuel cell. Simulations are necessary to determine these factors prior to manufacture. Simulations can also be used with existing fuel cells to predict how changes to one parameter, such as coolant mass flow, will affect temperature and other variables of interest.

The equations presented in Chapter 4 are used to predict PEM fuel cell coolant and stack temperatures (also mass flow, pressure drop, heat production, natural convection heat loss, radiation heat loss, and polarization curves). The goal of this chapter is to determine the accuracy and limitations of the forced convection heat transfer simulations compared to the experimental measurements obtained for the air-cooled Nexa proton exchange membrane fuel cell. Once the limitations are known, simulations are conducted to determine if the coolant temperature of the Nexa can be increased so that CHP heat recovery can be justified for all operating currents and to minimize the need for

supplementary residential heating to compensate for low discharge temperatures. The chapter addresses these issues as follows:

5.2: Validate the cooling model and determine which empirical heat transfer correlation (constant heat flux or constant temperature) best predicts the stack temperature of the Nexa PEM fuel cell over the entire power output range.

5.3: Perform simulations to determine if the Nexa PEM fuel cell coolant air can be maintained at a minimum temperature of 325 K for residential combined heat and power application while ensuring the stack temperature does not exceed the threshold operating temperature of 353 K at which cell electrical efficiency drops (Song, et al [34]).

5.4: Perform simulations to estimate the stack temperature and pressure drop through the Nexa if the number of cooling channels and heat exchange area were increased.

5.5: Estimate the Reynolds number and pressure drop through the Nexa if the stack height were doubled while maintaining the same overall membrane area and number of cells in the stack.

5.2 *Cooling system model validation*

The stack polarization curves and heat transfer rates are temperature dependent. As shown previously in Figure 4.2, the equations and variables presented by Larminie and Dicks provide an approximation of the Nexa polarization curves based on the average Nexa stack temperature and hence will not be discussed further. Alternate variables and

polarization equations with various degrees of complexity and accuracy are available in the literature [1,19,34] but are not tested in this thesis. The heat transfer characteristics of forced convection air-cooled PEM fuel cells are the focus of this chapter.

5.2.1 *Determining the Nexa flow regime*

Before the Nusselt correlations can be applied and simulations performed, the flow regime occurring in the cooling channels must be determined. From the experimental data obtained for the Nexa, flow velocity leads to Reynolds numbers that never exceed the critical Reynolds number at which transition to turbulence occurs. The Reynolds numbers computed by the simulations for the flows observed in the experimental data are shown in Figure 5.1. The Reynolds numbers shown are for coolant air flow in a single cooling channel, previously depicted in Figure 4.4.

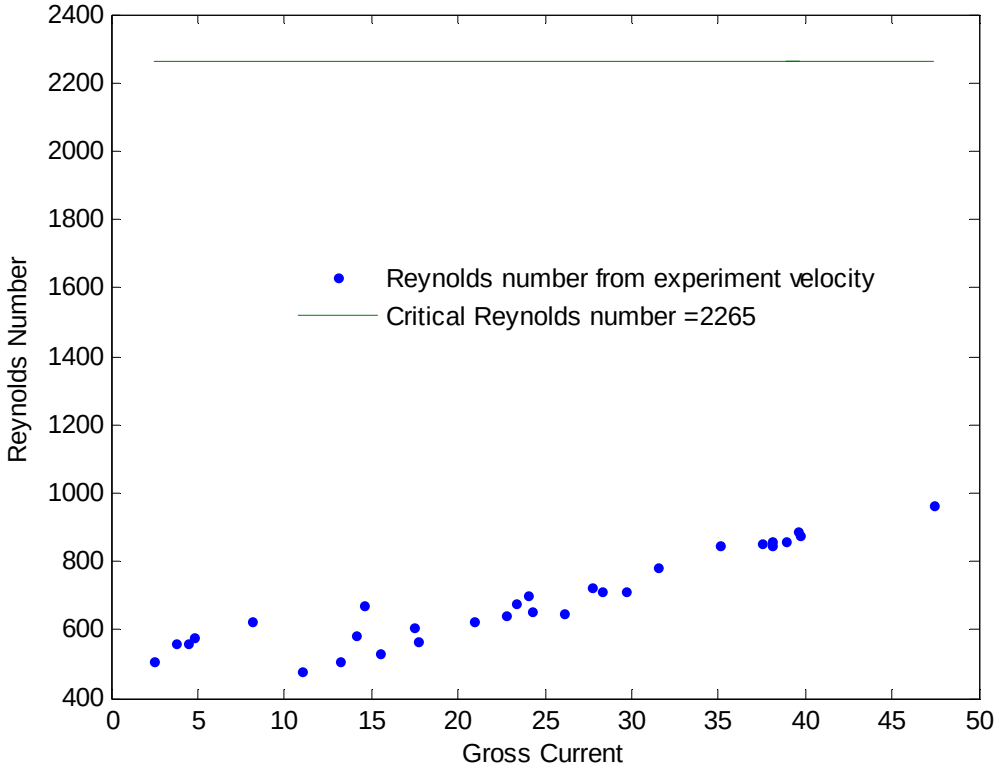

Figure 5.1 Nexa cooling channel Reynolds number

The Reynolds number can be used to determine the flow regime encountered throughout the length of the cooling channel. For the entire operating range of the Nexa, the flow must be either developing laminar flow or a combination of developing laminar flow and fully developed laminar flow. The approximate transition from simultaneously developing flow to fully developed flow occurs at a Gz^{-1} greater than 0.05 [21] (refer to equation 4.22). Figure 5.2 shows the approximate location of this transition point at 3 different operating currents representing the range of Nexa operation:

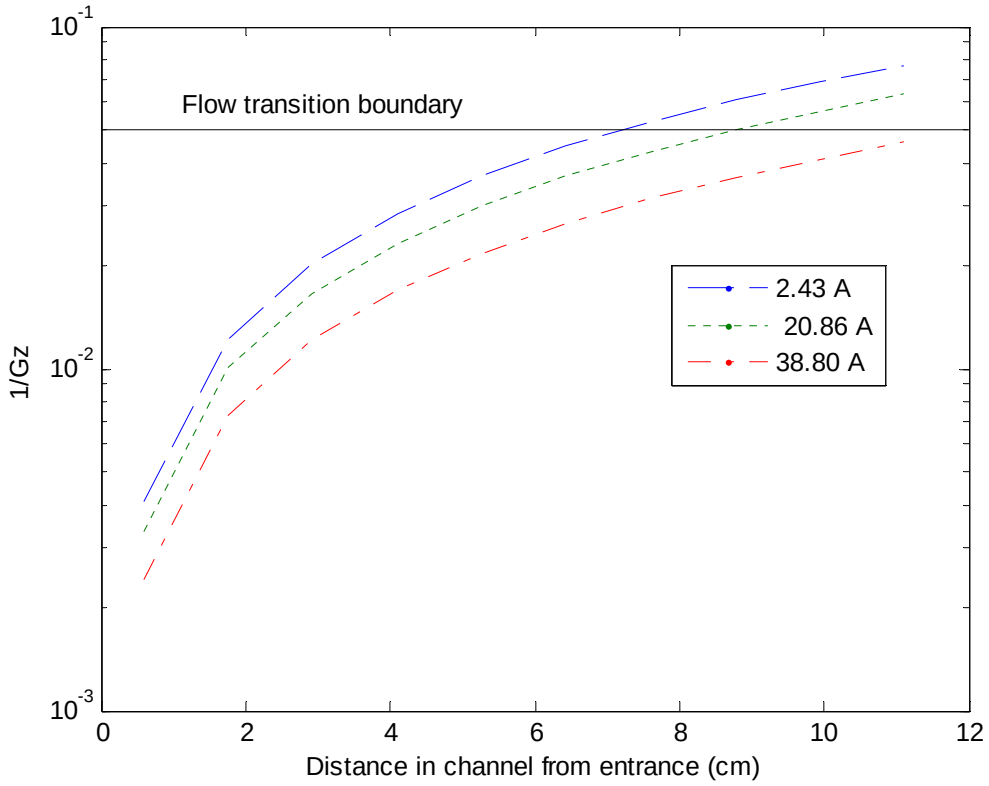

Figure 5.2 Nexa cooling channel approximate transition point from developing to fully developed laminar flow

As can be seen in Figure 5.2, the flow is developing laminar flow for the entire Nexa cooling channel at a 38.80 amp current. At the lowest Nexa current (when the fuel cell is idling and providing for only parasitic loads), the flow is developing laminar for more than 60% of the channel length. For all measured Nexa coolant velocities, developing laminar flow is the primary flow regime as determined from the Graetz number. Since the Nusselt numbers for developing laminar flow in rectangular channels can not be represented with a single equation, tabular data must be used to estimate the heat transfer occurring in the cooling channels. Figures 5.1 and 5.2 also indicate that as Reynolds numbers increase (i.e. flow velocity increases) the extent of the developing laminar flow

region also increases. For the Nexa, only small Reynolds numbers (<400) would result in more than 50% of the cooling channel experiencing fully developed laminar flow.

5.2.2 *Application of the Nusselt correlations to the Nexa cooling channels*

The Nusselt correlations for fully developed laminar, transitional and turbulent flow for both the *H1* and *T* boundary conditions are available as equations that are dependent upon channel aspect ratio. The developing laminar flow correlations are available as tabular data dependent upon channel aspect ratio and Graetz number. For air as the coolant (Pr $\approx$ 0.72), the model assumes simultaneously developing flow (i.e. both hydrodynamically and thermally developing flow) and the correlation data is chosen accordingly. Data for strictly hydrodynamically developing flow or thermally developing flow are not applied to the model except for computing pressure drops which depend upon hydrodynamic conditions. The model and simulations are only applicable to cooling fluids with Prandtl numbers that approximate those of air ($\mathrm{Pr} \approx 0.72$)

Tabular Nusselt data for three simultaneously developing flow regimes are available in the literature and applied during the simulations and include: 1) *T* boundary condition *mean* Nusselt number, 2) *H1* boundary condition *mean* Nusselt number, and 3) *H1* boundary condition *local* Nusselt number. Figure 5.3 shows the *H1 local* Nusselt numbers from Kakac, et al [31] for 4 aspect ratios and the developing flow Nusselt curve predicted by the model for the Nexa cooling channels; the figure also shows the fully developed laminar flow Nusselt number computed from equation 4.26.

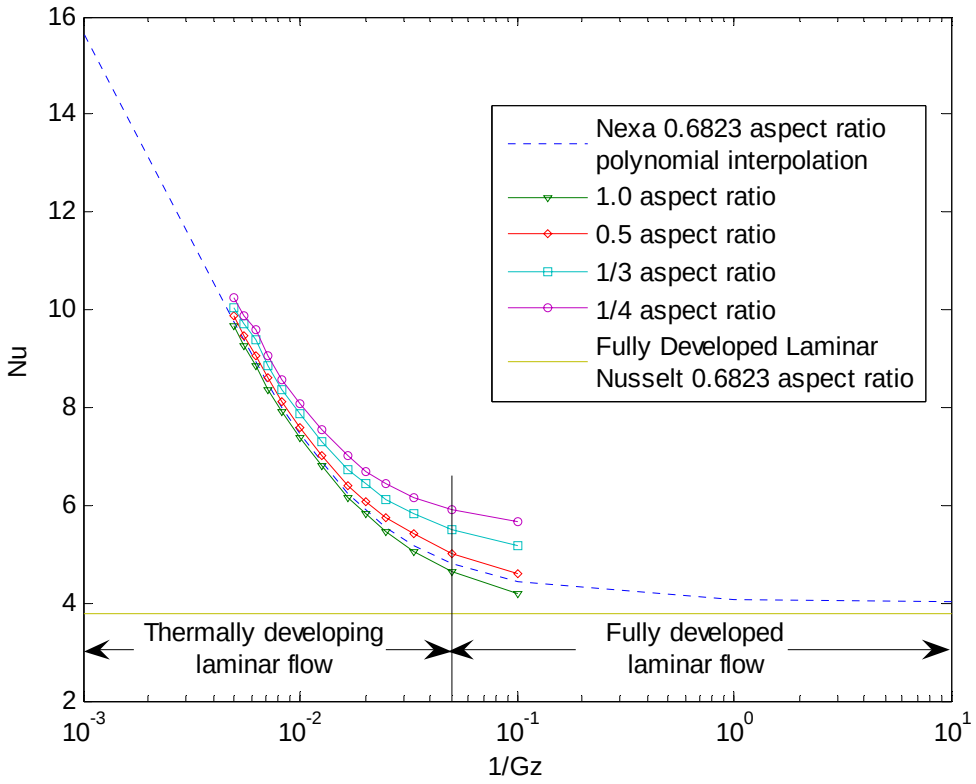

Figure 5.3 Simultaneously developing flow Nusselt numbers for the *H1 local* boundary condition

The Nusselt vs. Gz^{-1} graphs for the *T* and *H1 mean* Nusselt data are not shown but are quite satisfactorily similar to Figure 5.3. As can be seen in Figure 5.3, the model predicts the Nusselt numbers for the Nexa with the developing laminar flow *H1* Nexa Nusselt numbers falling between the 1.0 and 0.5 aspect ratio curves. This figure also shows that the Nusselt number predicted by the code for the developing flow region approaches the fully developed Nusselt number predicted by equation 4.26 as Gz^{-1} increases. For the simulations, since the developing laminar flow polynomial curve fit of Nusselt data also predict the fully developed laminar flow Nusselt numbers, the developing laminar flow fits are used to estimate Nusselt numbers for all Reynolds numbers below the critical Reynolds number.

5.2.3 *Stack temperature predictions using the Nusselt correlation data*

This section simulates operation of the Nexa fuel cell cooling system with emphasis on predicting stack temperatures. Table 5.1 contains the experimental values used as the boundary conditions for the simulations; these values represent the operating range of the Nexa.

Table 5.1 Nexa simulation boundary conditions

Gross Current (A)	Voltage (V)	Coolant Temp (K)	Ambient Temp (K)
2.4	38.5	298.1	296.6
20.9	32.0	311.4	298.2
38.8	28.7	317.1	298.0

For the simulations, the channels are broken into 10 equal area segments as previously shown in Figure 4.3. The local stack temperatures are determined for the midpoint of each channel segment. The stack temperatures predicted using the Nusselt correlations and the above boundary conditions are shown in Figures 5.4 through 5.6. The figures also include the boundary condition temperatures for reference.

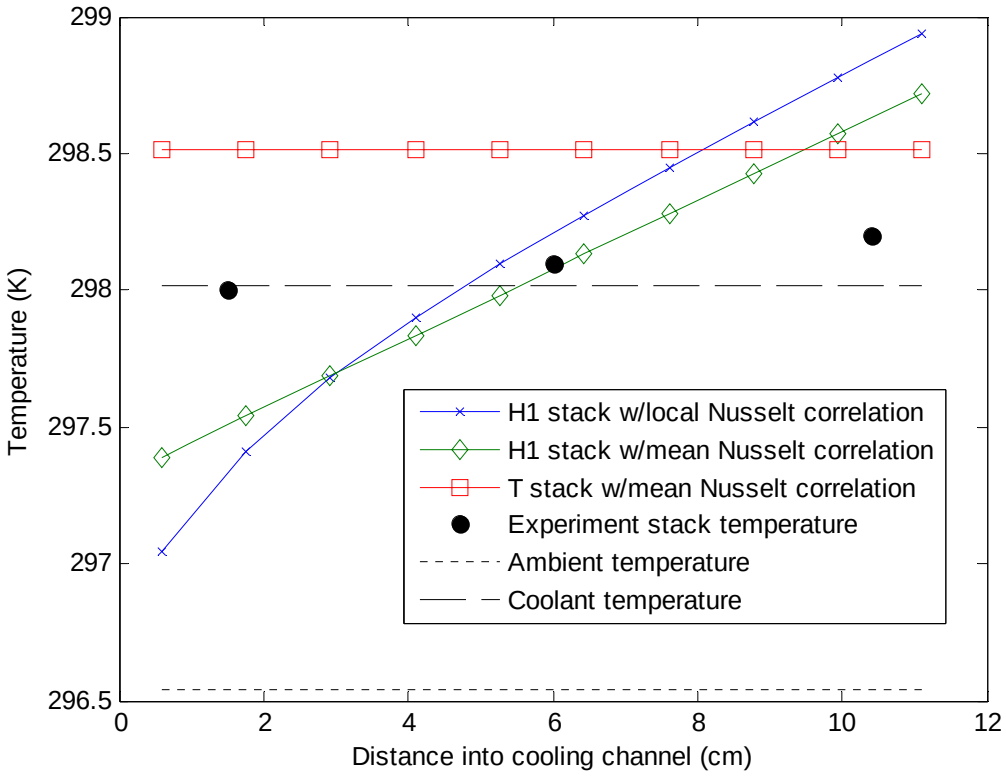

Figure 5.4 Local stack temperature at 2.4 amp gross current for *H1* and *T* boundary conditions

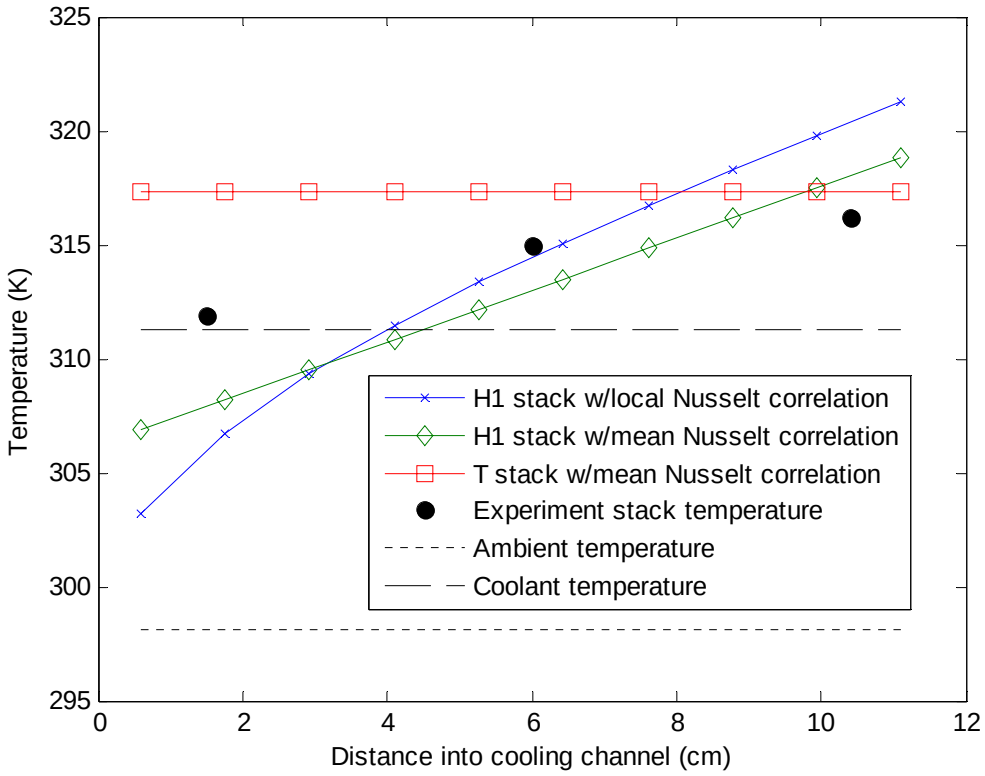

Figure 5.5 Local stack temperature at 20.9 amp gross current for *H1* and *T* boundary conditions

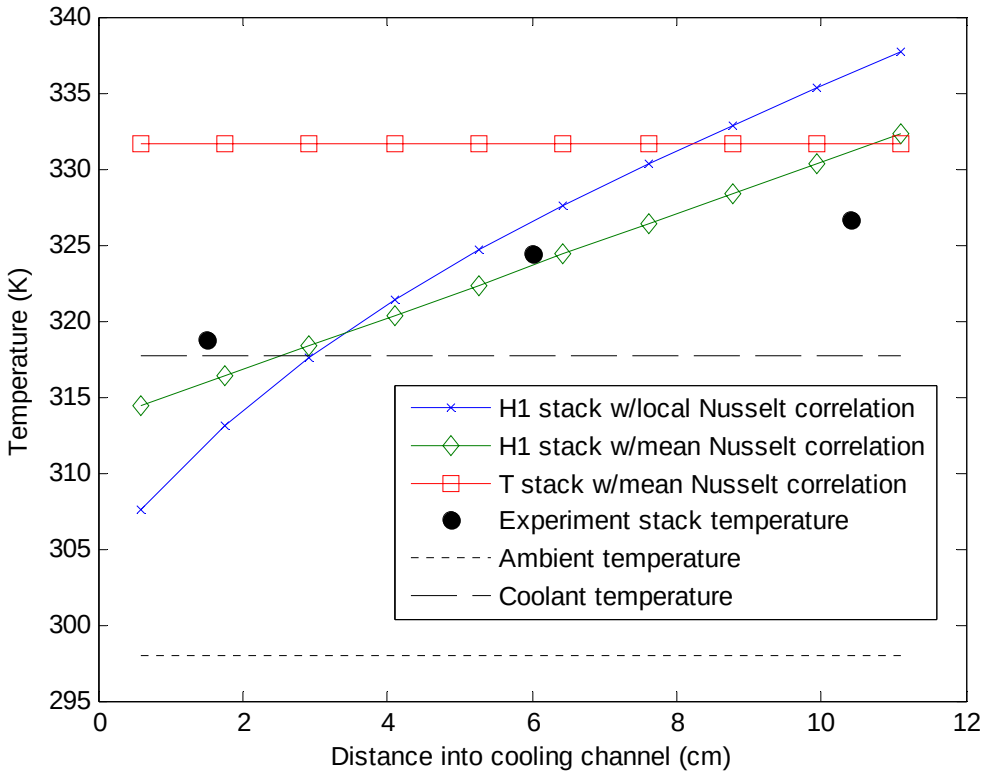

Figure 5.6 Local stack temperature at 38.8 amp gross current for *H1* and *T* boundary conditions

5.2.4 *T boundary condition*

As can be seen from Figures 5.4 to 5.6, the stack temperature predicted using the *T* boundary condition correlation is always higher than the experimentally measured stack temperature. This indicates that the heat transfer coefficients (Nusselt numbers) predicted by the constant stack temperature correlation are smaller than heat transfer coefficients seen in practice. Since previously published Nexa models uses the constant stack temperature assumption and set the stack temperature as a boundary condition, they will likely overestimate the mass of coolant required to cool the stack and underestimate the final coolant temperature.

Table 5.2 shows the mean Nusselt numbers predicted by the *T* boundary condition correlation as well as the Nusselt numbers necessary for the model to predict the experimentally measured axial mid-point stack temperature (mid-point temperature taken at approximately 6 cm from cooling channel entrance) and the maximum experimentally measured stack temperature (temperature measured approximately 10.2 cm from cooling channel entrance). The table also contains the Nusselt number and heat transfer coefficient used by Adzakpa, et al [19], for comparison.

Table 5.2 Nusselt numbers for the *T* boundary condition correlation

Nexa Gross Current (A)	Nu from correlation	Nu for mid-point stack temperature	Nu for maximum stack temperature	Nu used by Adzakpa
2.4	4.2	8.5	6.8	5.1
20.9	4.3	5.7	4.9	5.1
38.8	4.6	7.0	6.0	5.1

As can be seen in Table 5.2, the *T* boundary condition correlation predicts Nusselt numbers (column 2) below the value necessary for the entire stack to be at the experimentally measured mid-point temperature (column 3) or the 10.2 cm temperature (column 4). For the Nexa operating at 38.8 Amps, using the constant stack temperature Nusselt correlations can lead to stack temperature predictions more than 13 K greater than the experimentally measured temperature approximately 1.5 cm from the cooling channel entrance.

The Nexa channel dimensions and cooling air velocity used by Adzakpa (3.66 × 5.23 mm and 3 $m \cdot s^{-1}$) differ from those measured for this thesis (3.30 × 4.83 mm and 2.97 to 4.74 $m \cdot s^{-1}$) and hence are only presented for comparison. The ambient temperature is also not presented by Adzakpa; since the coolant mass flow requirements (channel velocity) to

maintain stack temperature decreases as the ambient temperature is lowered, more information about the operating conditions of the Adzakpa experiments is required to use their data for additional comparison to the model and experimental results presented in this thesis.

5.2.5 *H1 local boundary condition*

The *H1 local* correlation predicts a stack temperature difference much larger than observed in practice. At the 38.8 amp Nexa operating current, the *H1 local* correlation predicts a stack temperature difference greater than 25 K (based on temperature at the same channel axial position as in the experiments) compared to the experiment value of 8 K. However, the mid-point temperature of the stack predicted by the *H1 local* correlation is within 2 K from the experimentally measured mid-point temperature at the 38.8 amp operating current. For all operating currents, the mid-point stack temperatures predicted by the *H1 local* simulations are similar to the experimental mid-point temperatures. However, the stack temperature predictions near the cooling channel entrance and exit can be more than 10 K from the experimental temperatures at peak power.

5.2.6 *H1 mean boundary condition*

The *H1 mean* Nusselt data provides the most realistic prediction of the experimentally determined Nexa stack temperatures. The *H1 mean* Nusselt correlations eliminate the extreme Nusselt numbers predicted for the entry region of the channel with the *H1 local* correlations. Instead, the *H1 mean* data assumes a constant Nusselt number throughout the channel length. Although the temperature difference predicted by the *H1 mean*

Nusselt data is larger than the experimentally observed value (14 K vs. 8 K at 38.8 amp current), the discrepancy decreases with increasing stack current and is smaller than the *H1 local* boundary condition predictions. Furthermore, the stack temperature predictions at all operating currents and axial positions up to a distance of 10 cm (more than 80% of the channel length) are closer to the measured temperatures compared to the temperatures predicted by the *T mean* boundary condition data. Based on the 3 locations where stack temperatures were tested, the stack temperature predicted by the *H1 mean* Nusselt data differs on average by less than 2.55 K from the experiment data. Like the *H1 local* correlation, the *H1 mean* correlation predicts a temperature rise that intersects the experimentally measured stack temperature rise near the cooling channel axial mid-point. The Nusselt numbers predicted for the 2.4 amp, 20.9 amp and 38.8 amp boundary conditions are respectively 5.8, 6.1 and 6.6.

5.2.7 *Choosing the most applicable Nusselt correlations*

Whenever the heat transfer correlations are applied to predicting coolant temperature rise or stack temperature, the user must realize that the correlations are developed for situations where heat conduction in the walls is not considered, such as heat generation occurring at the channel surface. For the Nexa, the heat is not generated at the surface and must conduct through a thickness of material before being transferred to the coolant. Ideally, the thermal conductivity of the material must be considered in the stack temperature predictions as per the *conjugate problem*. Solving the *conjugate problem* was not performed in this thesis as the goal was to use empirical correlations available in the literature. With this limitation, the *H1 mean* correlation is the best predictor of the

temperatures observed in the experiments. However, the best correlation for different stack component thicknesses and materials has not been determined experimentally. The *H1 mean* assumption will likely be valid for many different stack materials, physical dimensions and heat generation rates. However, since this cannot be proven without additional experiments, the model compensates by using both the *T mean* and *H1 mean* boundary conditions to provide an estimate of the temperatures that may be encountered. For most real systems, actual temperatures should fall somewhere between the temperatures predicted by these two boundary conditions.

5.3 *Optimizing Nexa output temperature for combined heat and power*

One of the objectives of the simulations is to determine if the coolant output temperature of the Nexa can be increased so that CHP heat recovery is justified over the operating range of the fuel cell and to also minimize the need for auxiliary heating. The simulations must simultaneously ensure that the stack temperature of the Nexa does not exceed the temperature allowed for the Nafion membrane (353 K for the simulations). The analyses of the Nexa utilize the channel geometry as shown in Figure 4.4 and iterate the stack temperature until the coolant output temperature is 325 K, which is an adequate air temperature for residential heating [25] if the air is used directly for space heating. The boundary conditions used in the simulations are shown in Table 5.3.

Table 5.3 Boundary conditions for Nexa CHP application

Boundary Condition	**Value**
Ambient Temperature (K)	298
Min/Max Allowed Stack Temperature (K)	298/353
Coolant Output Temperature (K)	325
Stack Current (A)	1-48
Polarization Variables	See Table 4.2
Cooling Channel Dimensions (cm)	11.7 x 0.483 x 0.33
Cell Dimensions (cm)	11.7 x 11.7 x 0.65
Cooling Channels per Cell	18
Cells per Stack	47

Figure 5.7 shows the predicted *H1 mean* temperature difference and *T mean* stack temperature to achieve the desired Nexa coolant output temperature with the variables shown in Table 5.3. Again, for these simulations, the stack is broken into 10 equal area segments with the *H1 mean* entrance and exit temperatures predicted at the midpoint of the first and last segment respectively:

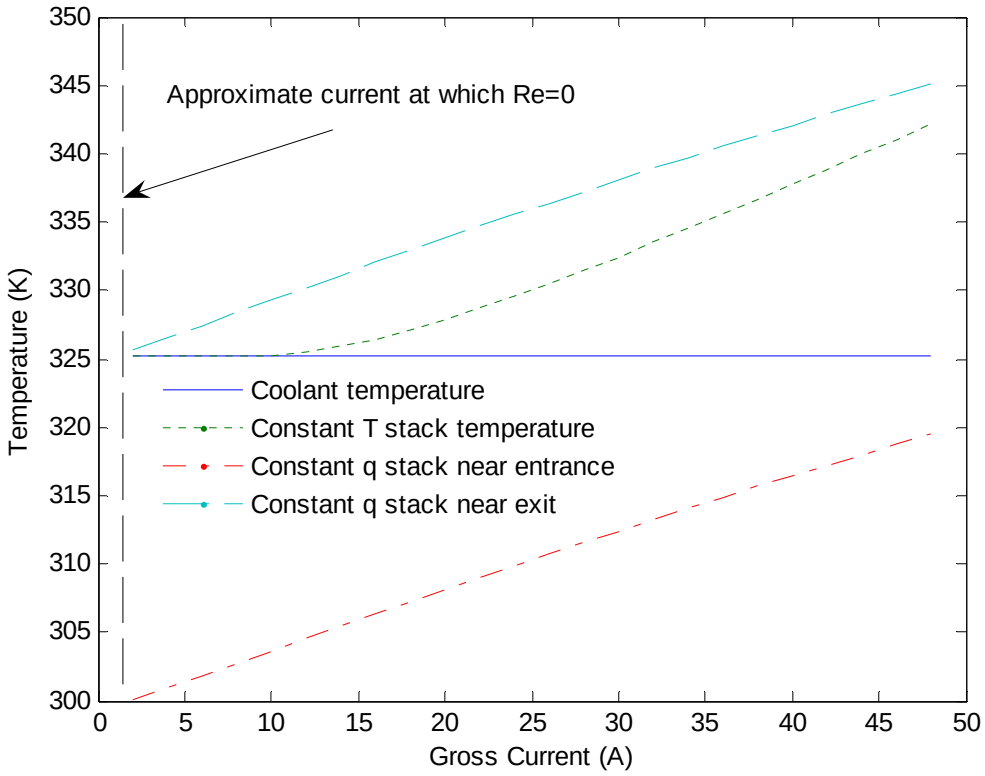

Figure 5.7 Predicted Nexa stack temperature to maintain a coolant temperature of 325 K in a 298 K ambient environment

Both the *H1 mean* boundary condition correlation and *T* boundary condition correlation predict that the Nexa can maintain the 325 K coolant air temperature while operating in ambient conditions of 298 K. The stack temperature never exceeds 346 K (*H1 mean* prediction at 48 amp gross current, the approximate maximum current at which the Nexa operates), which is below the 353 K boundary condition. However, at currents below 1.5 Amps, the simulations predict coolant flow velocities that result in Reynolds numbers approaching 0 (i.e. no coolant flow). Below this current, heat dissipated by natural convection, radiation and heating of the exhaust by-products passively cools the stack without the need for forced convection cooling.

As shown previously in Tables 3.2 and 3.3, by increasing the output coolant air temperature of the Nexa, over 96% of the hourly heat demand for a typical coastal British Columbia residence could be met with Nexa coolant heat without needing to raise the discharge air temperature before distributing it throughout the residence. That is, during normal operation of the Nexa, the *quantity* and *quality* of the heat generated could meet most residential heat and comfort demand. Auxiliary heating will still be required, particularly during high heat load winter conditions; however, when the Nexa produces sufficient heat and auxiliary heating is not required, coolant air distributed throughout the residence will feel comfortable to most occupants.

This simulation suggests that the coolant mass flow rates of the Nexa can be reduced to increase stack and coolant temperature. A reduction in the mass flow rates through the cooling channels also results in a smaller pressure drop which can reduce the cooling system power requirements. Figure 5.8 shows the estimated pressure drops for both the experiment and simulations.

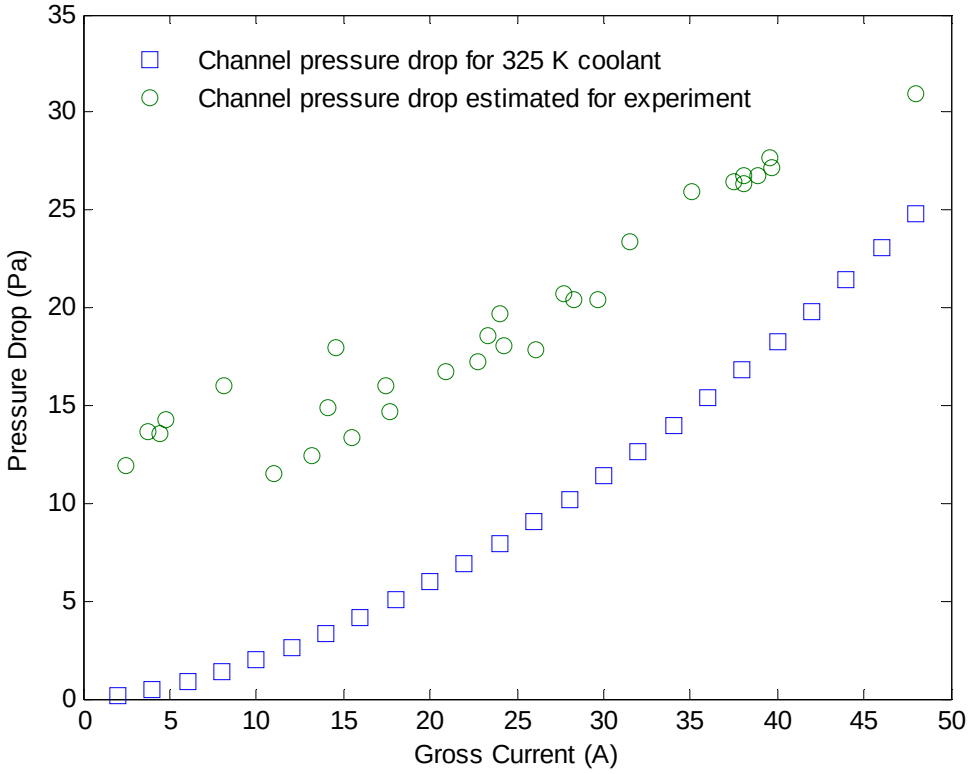

Figure 5.8 Estimated pressure drops through a single Nexa cooling channel

Since the pressure drop is proportional to the Reynolds number (Equation 4.25), decreasing the flow velocity through each channel to increase stack and coolant temperature results in a simulation pressure drop that is lower than the experimentally determined pressure drop.

The power to overcome the pressure drop can be estimated with equation 5.1 and depends upon the efficiency of the Nexa fan and motor.

$$P_{\Delta p} = \frac{\Delta p \cdot \dot{V}_{cool} \cdot N_{chan}}{\eta_{fan} \cdot \eta_{motor}} \tag{5.1}$$

where

$P_{\Delta p}$ = power to overcome pressure drop, W

Δp = pressure drop through a single channel, Pa

$\dot{V}$ = coolant volumetric flow rate through a single channel, $m^3 \cdot s^{-1}$

N_{chan} = number of cooling channels

η = efficiency

Assuming a 100% efficient blower assembly, the power to overcome the pressure drop through the stack is 1.3 Watts for the 38.8 amp experiment Nexa current; for the reduced flow simulations, the power to overcome the pressure drop is approximately 0.65 Watts at a 38.8 amp current.

5.4 *Decreasing the aspect ratio of the Nexa cooling channels*

Reducing the cooling channel dimensions and increasing cooling system heat transfer surface area can increase heat transfer rate and decrease the temperature of the stack. For example, if an additional fin were placed in the middle of each of the Nexa cooling channels, thereby doubling the number of channels, and 325 K were still the desired coolant temperature, the overall temperature of the stack will be lower than shown previously in section 5.3. Figure 5.9 shows the modified configuration of the Nexa channels for cooling the stack:

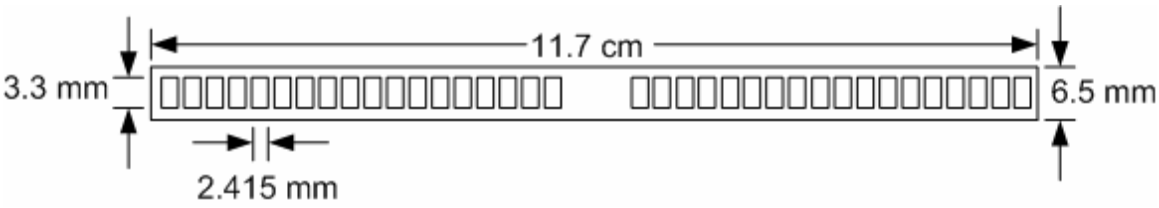

Figure 5.9 Doubling the number of Nexa channels

However, decreasing the channel dimensions also increases the pressure drop that will be seen across each channel. Figure 5.10 shows the effect of reducing the dimensions of the Nexa cooling channels on the predicted stack temperature and individual channel pressure drop:

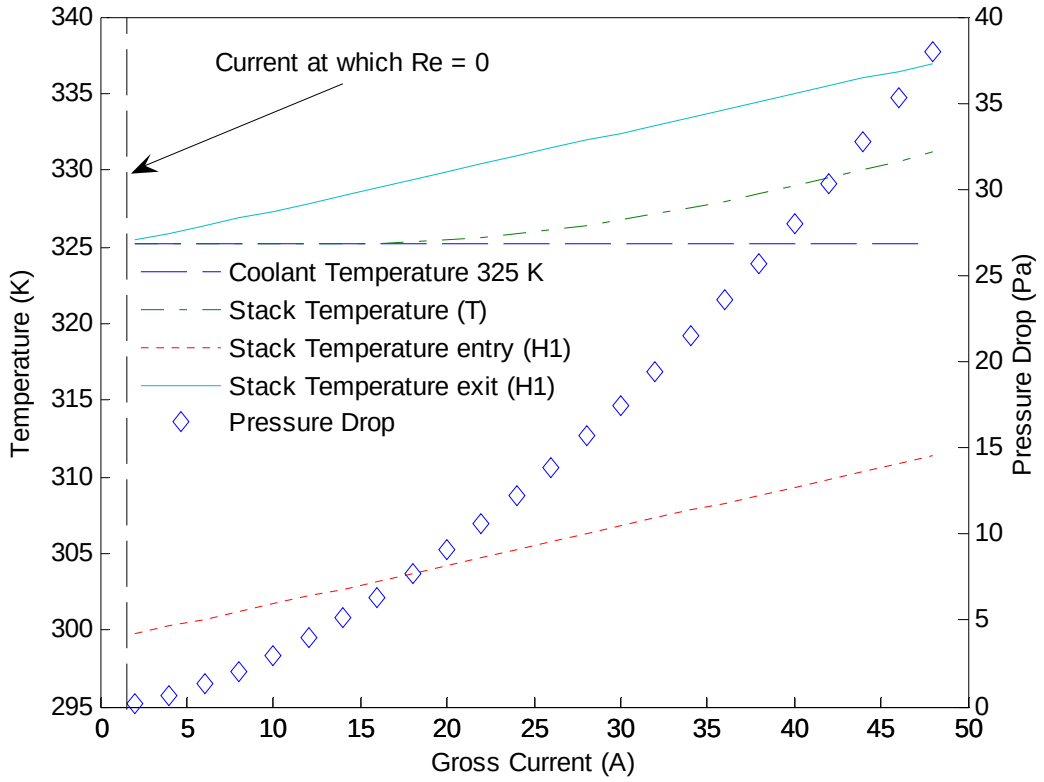

Figure 5.10 Stack temperature and pressure drop for smaller Nexa channels

With these modifications to the Nexa cooling channels, the maximum stack temperature predicted by both the *T* and *H1 mean* boundary conditions are lower than those seen in Figure 5.7 for the un-modified Nexa, particularly at the higher output currents. Decreasing the channel dimensions essentially reduces the slope of the stack temperature

vs. gross current graph. However, even though the stack temperature is reduced, the pressure drop increases for each channel and the number of channels doubles. Any design of the stack cooling system must consider the pressure drop because as the cooling system power consumption increases, the overall efficiency of the fuel cell will decrease. For this modified cooling system, at 38.8 Amps, the power to overcome the stack pressure drop is now approximately 1.02 Watts.

5.5 *Cooling system evaluation doubling the height of the Nexa stack*

The model also allows the stack dimensions to be modified. The simulation shown in this section uses the boundary conditions set in Table 5.3 except the Nexa stack height is doubled and the stack width and number of cooling channels is cut in half. Essentially, the simulations performed in this section are for a Nexa fuel cell cut in half perpendicular to the membrane with one half placed atop the other (i.e. individual cell dimensions changed from 11.7 x 11.7 cm to 23.4 x 5.85 cm). Table 5.4 shows the boundary conditions used for the simulations performed in this section:

Table 5.4 Boundary conditions for section 5.5 simulations

Boundary Condition	**Value**
Ambient Temperature (K)	298
Min/Max Allowed Stack Temperature (K)	298/353
Coolant Output Temperature (K)	325
Stack Current (A)	1-48
Polarization Variables	See Table 4.2
Cooling Channel Dimensions (cm)	23.4 x 0.483 x 0.33
Cell Dimensions (cm)	23.4 x 5.85 x 0.65
Cooling Channels per Cell	9
Cells per Stack	47

The resulting stack temperature vs. gross current graph is the same as Figure 5.7. However, the temperature rise of the stack now occurs over a height of 23.4 cm instead of 11.7 cm. The stack still meets the criterion of providing heated air at a temperature of 325 K without exceeding a stack temperature of 353 K.

Figure 5.11 compares the Reynolds numbers and pressure drop through each channel with those predicted with the boundary conditions of Table 5.3:

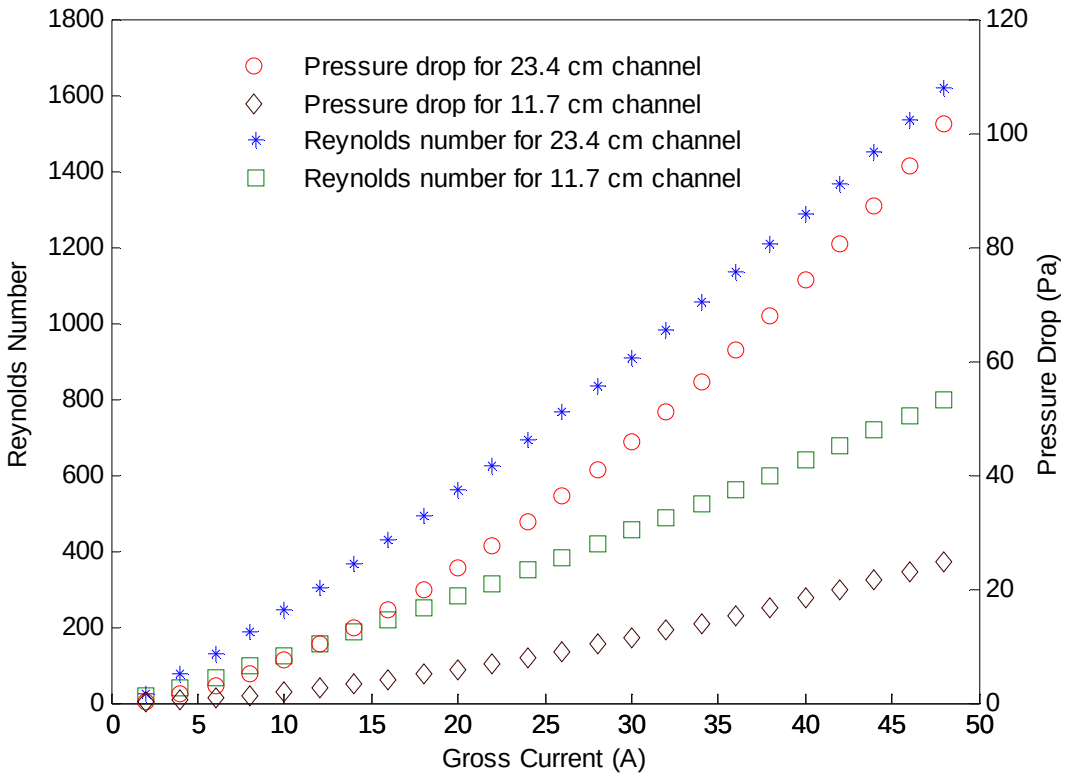

Figure 5.11 Reynolds Number and pressure drop for a Nexa stack with 11.7 cm and 23.4 cm stack height

With half as many cooling channels and the same heat production as the previous simulations, the mass of coolant air passing through each channel must double. Doubling the mass flow through each channel also doubles the Reynolds number as shown in

Figure 5.11. However, since the cooling channel length has also been doubled, the pressure drop through each channel has quadrupled (as per Equation 4.25). According to Equation 5.1, the power required to overcome the pressure drop across the stack will also be quadrupled when compared to the stack modelled in section 5.3. At 38.8 Amps, power to overcome this pressure drop for the stack is approximately 2.6 Watts compared to 0.65 Watts for the shorter channel lengths (assuming a 100% efficient blower).

5.6 *Conclusions*

This chapter showed that the *H1 mean* Nusselt correlations are the best equations for predicting the stack temperature of a Nexa PEM fuel cell. The *T* boundary condition Nusselt correlations predict stack temperatures that are larger than seen experimentally while the *H1 local* boundary condition correlations predict stack temperature differences that are much larger than seen in the experiments. The model used correlations for Prandtl numbers of air; the model is applicable to other Prandtl numbers if the appropriate correlations are used.

Simulations using both the *H1 mean* and *T* boundary conditions show that the output temperature of the Nexa fuel cell can be increased to a temperature of 325 K without the stack exceeding 353 K. With the coolant temperature increased to 325 K, the Nexa can be used for CHP applications without having to heat the coolant air before distributing it throughout the residence.

Finally, this chapter showed that different stack or cooling channel configurations can be used to successfully cool the Nexa PEM fuel cell. However, pressure drops increase as cooling channel aspect ratios are decreased or channel lengths are increased. The cooling system must provide power to overcome the pressure drops and the overall efficiency of the fuel cell will decrease as pressure drops increase.

Chapter 6

Summary, Recommendations and Conclusions

6.1 *Summary*

This thesis has presented an analysis of the Nexa PEM fuel cell as a heat/power source for residential CHP. As a power source, the maximum electrical efficiency of the Nexa occurs when it operates at 42% full load (approximately 500 Watts net power). However, maximum thermal efficiency and coolant temperature occur when the Nexa operates at 100% full load. At full load, the temperature rise of the coolant is 22 K. For residential space heating, this temperature rise would likely be acceptable for air that is distributed throughout the occupied space as long as ventilation system design ensures occupants do not feel "cool" drafts and living spaces are maintained at the desired temperature (295 K to 298 K are typical design temperatures).

However, residential electrical loads are not constant; at the average hourly load for a typical British Columbia residence, a four Nexa system would output coolant air at a temperature rise of approximately 8 K; this temperature rise is too low for most residential space heating ventilation systems. However, space heating guidelines are subject to the preference of the design engineer and the design of the heating and ventilation system. Higher temperatures, in general, are preferred; however, physical layout of the residence, minimum/maximum allowed ventilation system mass flow, control of heat distribution, system efficiency, complexity of ventilation system design, control system design, expected lifetime, initial costs, maintenance costs, net metering and supplementary heating all need to be considered during design of a CHP system. The

heat balance graph presented in Chapter 3 permits the Nexa coolant temperature, heat and electrical output to be included in this type of full system analysis.

This thesis has also presented a model that can be used to analyze the coolant air that is rejected from an air-cooled PEM fuel cell. The model allows prediction of stack temperature, coolant mass flow, coolant temperature and pressure drop based on cooling system and stack design geometry. The model can be used to design air-cooled PEM cooling systems and assess coolant output temperatures and mass flow for CHP consideration.

Based on simulations using the model and Nexa stack and cooling system geometry, the air flow through the Nexa can be reduced so that the coolant exits the fuel cell 27 K above ambient which is near the desired output temperature of diffusion grilles on a residential ventilation system. As long as the Nexa operates above a minimum gross current of approximately 1.5 Amps, the 27 K temperature rise can be maintained.

Simulations also show that the channel geometry can be modified to reduce the maximum observed stack temperature or magnitude of the temperature rise per unit channel length. In general, the simulations show the Nexa can be designed to operate with stack temperatures maintained below 353 K and a coolant temperature rise above 27 K. However, for any cooling system design, the power to overcome pressure drops must be considered because pressure drops can become very large for small channel aspect ratios or for long channels. The cooling system designer must judiciously choose when air-

cooling is no longer efficient and different coolants need to be considered. The model allows this type of cooling system design analysis to be conducted.

6.2 *Recommendations*

The data collected for the Nexa fuel cell is applicable to an ambient temperature of approximately 298 K. However, data presented in the literature show that ambient temperature has a significant effect on the electrical efficiency of the Nexa. Data collected for this thesis also shows that ambient temperature affects the final discharge temperature of the coolant, where a decrease in ambient results in a proportional decrease in the coolant temperature rejected from the fuel cell. Ideally, the same type of analysis as presented in Chapter 3 needs to be performed with control of ambient temperatures. From analyses at other ambient temperatures, a transfer function could be devised so that the heat balance diagram can be translated for any ambient temperature.

The humidification system should be characterized and modelled. Heat transfer occurring in the humidification system may be responsible for condensed water observed in the exhaust stream. More information concerning heat transfer in the humidification system would allow the model to incorporate latent heat into the energy balance. However, the most important aspect of including a humidification system in the model is the ability to determine whether or not the membrane can be kept hydrated for the stack temperatures predicted by the model. Even though the simulations show that the Nexa stack temperature and coolant output temperatures can be increased, the ability of the humidification system to maintain membrane hydration has not been determined.

6.3 *Conclusions*

Two primary conclusions are noted from this thesis that may aid other engineers interested in air-cooled fuel cells for CHP applications or fuel cell thermal modelling: First, the Nexa fuel cell is not an ideal candidate for residential CHP applications because the coolant temperature is too low during normal operation. However, this conclusion is only valid for the Nexa "out of the box" because modelling evidence suggests coolant temperature can be increased without the stack exceeding the maximum allowable design temperatures; Secondly, the mean *H1* Nusselt correlation data provides the best approximation of stack temperatures that a fuel cell will encounter during normal operation. When comparing the modelled results to the experimental results for the Nexa fuel cell, the mean *T* Nusselt correlation data over-estimates stack temperature while the local *H1* Nusselt correlation data over-estimates the temperature difference. Future thermal models of the Nexa and other air-cooled PEM fuel cells should consider using the *H1 mean* correlation data because a real system will have temperature differences axial to the coolant flow in addition to temperature differences through the thickness of stack materials.

References

[1] C. Spiegel, “Designing and building fuel cells”, The McGraw Hill Company 2007

[2] S. Thomas and M. Zalbowitz, Fuel Cells – Green power, Los Alamos National Laboratory, LA-UR-99-3231

[3] C. Rayment and S. Sherwin, “Introduction to fuel cell technology”, Department of Aerospace and Mechanical Engineering, University of Notre Dame, 2003, http://www.nd.edu/~msen/Teaching/DirStudies/FuelCells.pdf, last accessed 12 July 2010

[4] 2008 ASHRAE Handbook, “HVAC Systems and Equipment”, Chapter 7 *Combined Heat and Power Systems*, American Society of Heating, Refrigerating and Air-Conditioning Engineers, 2008

[5] R. Zogg, K. Roth and J. Brodrick, Combined heat and power for residences, ASHRAE Journal Vol. 47 (7), July 2005, 142-143

[6] H. I. Onovwiona and V. I. Ugursal, Residential cogeneration systems: review of the current technology, Renewable and Sustainable Energy Reviews, 10 (2006) 389-431

[7] A. Faghri and Z. Guo, Challenges and opportunities of thermal management issues related to fuel cell technology and modeling, Int. J. Heat and Mass Transfer 48 (2005) 3891-3920

[8] J. Larminie and A. Dicks, “Fuel Cell Systems Explained”, John Wiley and Sons Ltd., 2003

[9] C. Graf, A. Vath, and N. Nicoloso, Modeling of the heat transfer in a portable PEFC system within MATLAB-Simulink, J. Power Sources 155 (2006) 52-59

[10] B. D. MacDonald and A. M. Rowe, A thermally coupled metal hydride hydrogen storage and fuel cell system, J. Power Sources, 161 (2006) 346-355

[11] Nexa Power Module Users Manual, MAN5100078, June 16, 2003

[12] S. Lasher, R. Zogg, E. Carlson, P. Couch, M. Hooks, K. Roth, and J. Brodrick, PEM Fuel Cells for Distributed Generation, ASHRAE Journal Vol. 48, Nov 2006

[13] Y. Zong, B. Zhou and A. Sobiesiak, Water and thermal management in a single PEM fuel cell with non-uniform stack temperature, J. Power Sources 161 (2006) 143-159

[14] G. Vasu and A. K. Tangirala, Control-oriented thermal model for proton-exchange membrane fuel cell systems, J. Power Sources, 183 (2008) 98-108

[15] Y. Zhang, M. Ouyang, Q. Lu, J. Luo and X. Li, A model predicting performance of proton exchange membrane fuel cell stack thermal systems, Applied Thermal Engineering, 24 (2004) 501-513

[16] X. Yu, B. Zhou and A. Sobiesiak, Water and thermal management for Ballard PEM fuel cell stack, J. Power Sources 147 (2005) 184-195

[17] A. J. Real, A. Arce and C. Bordons, Development and experimental validation of a PEM fuel cell dynamic model, J. Power Sources, 173 (2007) 310-324

[18] S. Yu and D. Jung, Thermal management strategy for a proton exchange membrane fuel cell system with a large active cell area, Renewable Energy 33 (2008) 2540-2548

[19] K. P. Adzakpa, J. Ramousse, Y. Dube, H. Akremi, K. Agbossou, M. Dostie, A. Poulin, M. Fournier, Transient air cooling thermal modeling of a PEM fuel cell, Journal of Power Sources 179 (2008) 164-176

[20] 2009 ASHRAE Handbook, “Fundamentals”, American Society of Heating, Refrigerating, and Air Conditioning Engineers Inc., 2009

[21] F.P Incropera, D.P. DeWitt, T.L. Bergman and A.S. Lavine, “Introduction to Heat Transfer”, John Wiley and Sons, Inc., 2007

[22] A. Bergen, T. Schmeister, L. Pitt, A. Rowe, N. Djilali, P. Wild, Development of a dynamic regenerative fuel cell system, Journal of Power Sources, 164 (2007) 624-630

[23] M.C. Potter and C.W. Somerton, “Thermodynamics for Engineers”, Schaum’s Outline Series, McGraw-Hill, 1995

[24] K. Choi, H. Kim, H. Yoon, M. Forrest and P. Erickson, Effects of ambient temperature and relative humidity on the performance of Nexa fuel cell, J. Energy Conversion and Management, 49 (2008) 3505-3511

[25] 2007 ASHRAE Handbook, “HVAC Applications”, American Society of Heating, Refrigerating, and Air Conditioning Engineers Inc., 2007

[26] A.D. Althouse, C.H. Turnquist, and A.F. Bracciano, “Modern Refrigeration and Air Conditioning”, The Goodheart-Willcox Co, Inc., 1982

[27] J.E. Brady and G.E. Humiston, “General Chemistry Principles and Structure”, John Wiley and Sons Inc., 1982

[28] H. Kim, C. Y. Cho, J. H. Nam, D. Shin and T. Y. Chung, A simple dynamic model for polymer electrolyte membrane fuel cell (PEMFC) power modules: Parameter estimation and model prediction, Int. J. Hydrogen Energy, Vol. 35, Issue 8, (2010) 3656-3663

[29] A. Sripakagorn and N. Limwuthigraijirat, Experimental assessment of fuel cell/supercapacitor hybrid system for scooters, Int. J. Hydrogen Energy, Vol. 34, Issue 15, (2009) 6036-6044

[30] W. H. Zhu, R. U. Payne, R. M. Nelms and B. J. Tatarchuk, Equivalent circuit elements for PSpice simulation of PEM stacks at pulse load, J. Power Sources, Vol. 178, Issue 1, (2008) Pages 197-206

[31] S. Kakac, R. K. Shah, and W. Aung, “Handbook, of Single-Phase Convective Heat Transfer”, John Wiley and Sons Ltd, 1987

[32] W.M. Rohsenow, J.P. Hartnett, and Y.I. Cho, “Handbook of Heat Transfer”, McGraw-Hill, 1998

[33] M.E. Steinke and S.G. Kandlikar, Single-phase liquid friction factors in microchannels, Int. J. Thermal Sciences, 45 (2006) 1073-1083

[34] C. Song, Y. Tang, J.L. Zhang, J. Zhang, H. Wang, J. Shen, S. McDermid, J. Li, and P. Kozak, PEM fuel cell reaction kinetics in the temperature range of 23-120 ^{o}C, Electrochimica Acta 52(2007) 2552-2561

[35] W. H. Zhu, R. U. Payne, D. R. Cahela and B. J. Tatarchuk, Uniformity analysis at MEA and stack levels for a Nexa PEM fuel cell system, J. Power Sources, 128 (2004) 231-238

Appendix

A1 - Water vapour in air from relative humidity

The components of cooling air for the calculation of heat flow are dry air and water vapour. Since relative humidity is found during the experiment, the partial pressure of the components of air can be found by using an empirical relation for water saturation pressure where temperature is in absolute temperature [20].

$$\ln(P_{H_2O}(s)) = \frac{C1}{T_{cool}} + C2 + (C3 \cdot T_{cool}) + (C4 \cdot T_{cool}^2) + (C5 \cdot T_{cool}^3) + C6 \cdot \ln(T_{cool}) \qquad \text{(A1.1)}$$

where

$P_{H_2O}(s)$ = saturation pressure, Pa

T_{cool} = absolute temperature coolant discharge, K

$C1 = -5.8002206 \cdot 10^3$

$C2 = 1.3914993 \cdot 10^0$

$C3 = -4.8640239 \cdot 10^{-2}$

$C4 = 4.1764768 \cdot 10^{-5}$

$C5 = -1.4452093 \cdot 10^{-8}$

$C6 = 6.5459673 \cdot 10^0$

The relative humidity can then be used to find the real water vapour pressure in the air and subsequently the dry air pressure (standard sea level operation).

$$P_{H_2O}(v) = \phi \cdot P_{H_2O}(s) \qquad \text{(A1.2)}$$

$$P_{da} = 101325 - P_{H_2O}(v) \qquad \text{(A1.3)}$$

where

$P_{H_2O}(v)$ = water vapour pressure in the air, Pa

ϕ = relative humidity in coolant discharge

P_{da} = dry air pressure, Pa

Since the bulk velocity of the airflow through the fuel cell is measured and the duct discharge dimensions known, the volumetric flow is known. From this, the mass flow can be found based on the partial pressure of the air constituents. Using ideal gas relations:

$$\dot{m}_{da} = \frac{P_{da} \cdot \dot{V}_{cool}}{R_{da} \cdot T_{cool}} \tag{A1.4}$$

$$\dot{m}_{H_2O} = \frac{P_{H_2O} \cdot \dot{V}_{cool}}{R_{H_2O} \cdot T_{cool}} \tag{A1.5}$$

where

$\dot{m}_{da}$ = mass flow rate of dry air, $kg \cdot s^{-1}$

$\dot{m}_{H_2O}$ = mass flow rate of water vapour, $kg \cdot s^{-1}$

$\dot{V}_{cool}$ = volumetric flow rate of air, $m^3 \cdot s^{-1}$

R = specific gas constant for water or dry air, $J \cdot kg^{-1} \cdot K^{-1}$

A2 - Nusselt numbers for natural convection

To determine heat transfer coefficients for natural convection, the proper Nusselt correlation must first be determined. The walls of the Nexa are treated as vertical plates

and the correlations are chosen for this orientation. The process for finding the proper Nusselt correlation is as follows:

Find the Grashof, Prandtl and Rayleigh numbers with properties evaluated at $\frac{(T_{fc} + T_{amb})}{2}$ except β evaluated at T_{amb}.

$$Gr = \frac{g \cdot \beta \cdot \rho_{air}^2 \cdot (T_{fc} - T_{amb}) \cdot L^3}{\mu^2} \tag{A2.1}$$

where

g = gravitational acceleration, $m \cdot s^{-2}$

β = volume coefficient of thermal expansion, K^{-1}

ρ_{air} = density of air, $kg \cdot m^{-3}$

T_{fc} = mean fuel cell temperature, K

T_{amb} = ambient temperature, K

L = height of fuel cell, m

μ = dynamic viscosity, $Pa \cdot s$

$$\mathrm{Pr} = \frac{c_p \cdot \mu}{k} \tag{A2.2}$$

where

c_p = specific heat at constant pressure, $J \cdot kg^{-1} \cdot K^{-1}$

k = air thermal conductivity, $W \cdot m^{-1} \cdot K^{-1}$

$$Ra = Gr \cdot \Pr \tag{A2.3}$$

The Rayleigh number computed from these equations and the experimental measurements falls in the range $10^{-1} < Ra < 10^{9}$, leading to the following Nusselt number correlation; the Nusselt correlation is then used to find the natural convection heat transfer coefficient [20]:

$$Nu = 0.68 + \frac{0.67 \cdot Ra^{1/4}}{[1 + (0.492/\Pr)^{9/16}]^{4/9}} \tag{A2.4}$$

Other possible Nusselt correlations are as follows:

$$Nu = \left\{ 0.825 + \frac{0.387 \cdot Ra^{1/6}}{[1 + (0.492/\Pr)^{9/16}]^{8/27}} \right\}^2 \qquad 10^{9} < Ra < 10^{12} \tag{A2.5}$$

$$Nu = \left\{ 0.825 + \frac{0.387 \cdot Ra^{1/6}}{[1 + (0.437/\Pr)^{9/16}]^{8/27}} \right\}^2 \qquad 10^{-1} < Ra < 10^{12} \tag{A2.6}$$

A3 – Fraction of by-product water condensed

Liquid water produced by the Nexa fuel cell was measured for many different currents. The exhaust hose was flexible and had a U-bend placed in it. At the bottom of the U-bend, a trap was installed allowing water to drain into a graduated cylinder and the exhaust gas could continue through the hose. However, this data could not be reproduced and seems to be very dependent upon ambient temperature, which was beyond experiment control. Evaporation from the graduated cylinder was also possible because at low currents (< 10 Amps) water collection took up to 30 minutes for the meniscus to be near a gradation. The measurement was visual, so that is also a source of error. The

data is presented only for curiosity sake and is not used directly for any of the calculations presented in the thesis.

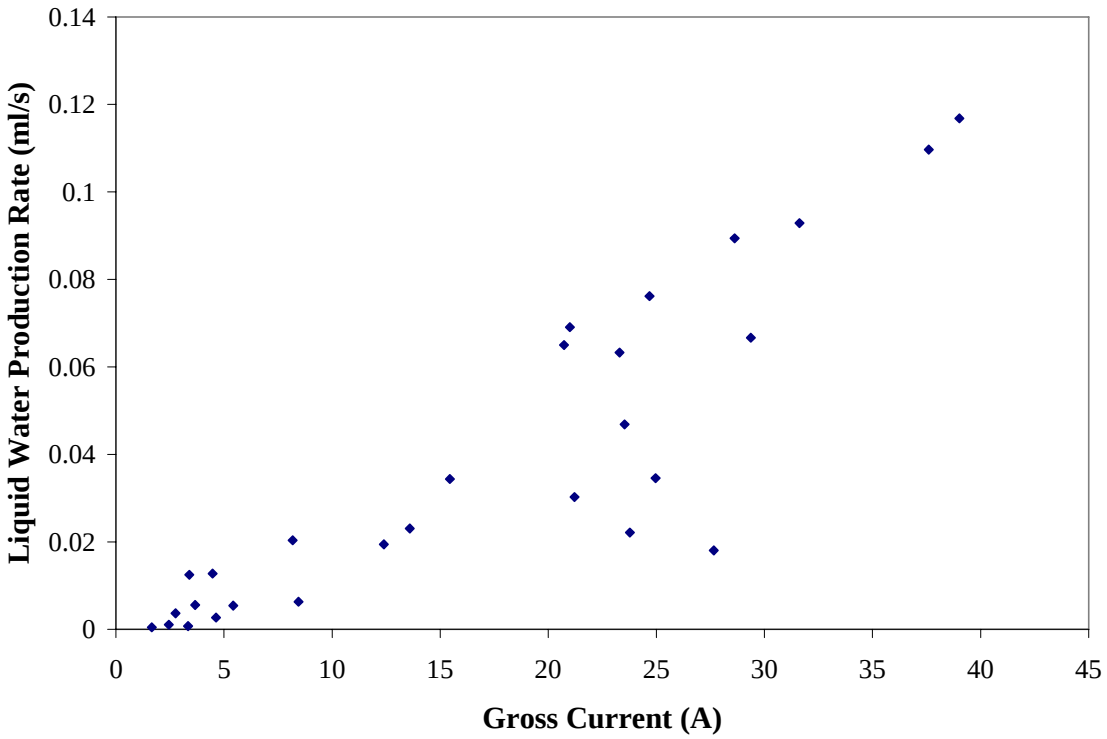

Figure A3.1 Time average rate of liquid water production for the Nexa

Dividing the values in Figure A3.1 by the rate that water was produced yields the fraction of water that was condensed.

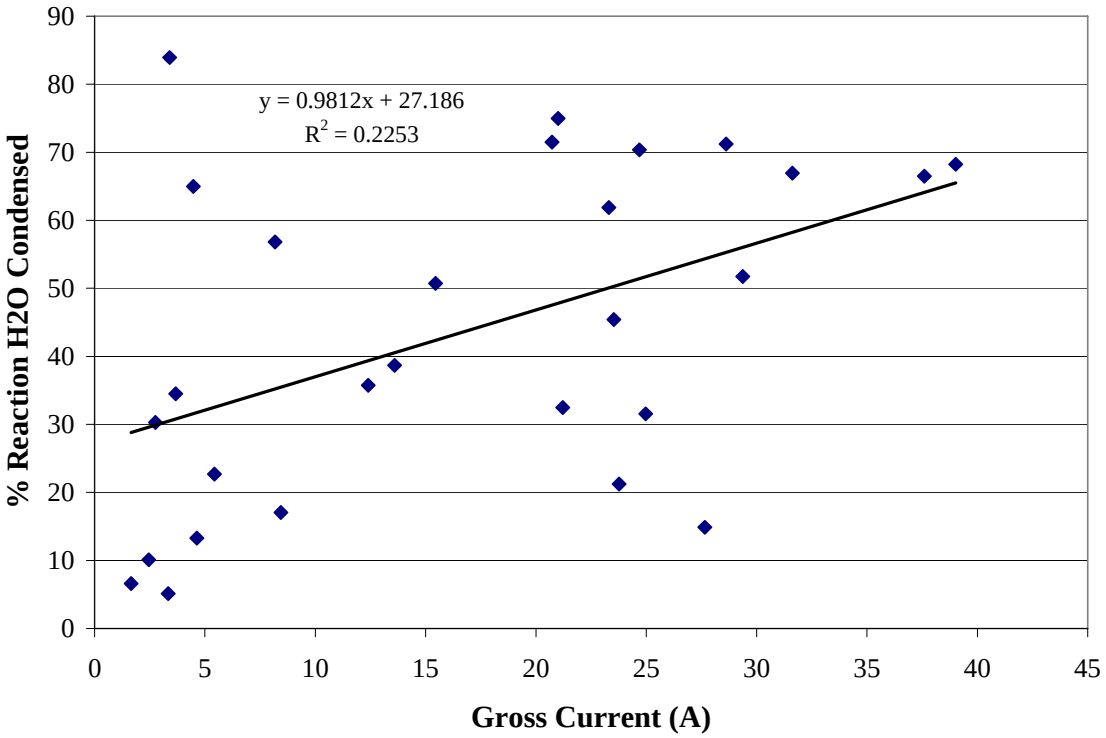

Figure A3.2 Fraction of water condensed based on liquid measurements and hydrogen flow rate

As can be seen in Figure A3.2, the fraction of water condensed is scattered and the curve fit yields very large errors.

A4 – Duct traverse for finding average coolant velocity

The average coolant air velocity through the Nexa fuel cell is determined by using a log-Tchebycheff rule duct traverse for the laminate duct placed at the coolant discharge opening [20]. Figure A4.1 gives the position at which the hot-wire anemometer velocity measurements were taken for the duct traverse, where the perspective is looking into the duct with W and H the duct dimensions.

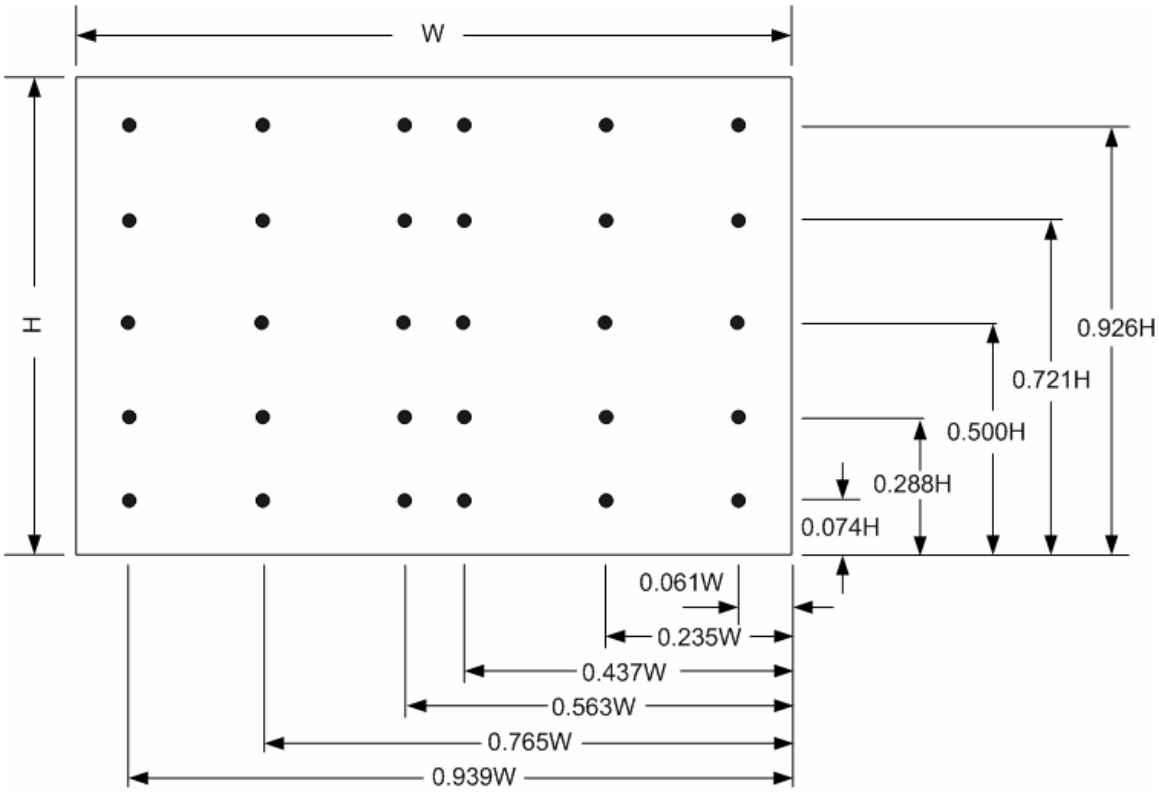

Figure A4.1 Log Tchebycheff rule duct traverse points

The straight average of the 30 points gives the mean air velocity in the duct. The average velocity was determined for a range of Nexa operating currents (from approximately 2 Amps to 38 Amps in increments of 6 Amps). A position along the 0.500H centerline at which anemometer velocity measurements were equal to the duct traverse velocity for that current was found by trial and error. For the experiment data presented, the anemometer was placed midway between the 2 amp and 38 amp mean velocity locations on the centerline.

A5 – Temperature, oxygen and humidity sensors

The sensors, multiplexer and microcontroller used for data acquisition of molar oxygen content, temperature, and relative humidity are presented in Table A5.1.

Table A5.1 Data acquisition components for Nexa characterization

Device	**Sensing Resolution**	**Operating Range**
Analog Devices AD22100 Temperature Sensor	< 1 K	273 to 373 K Calibrated range
Honeywell HIH-4000 Relative Humidity Sensor	3% Relative Humidity	0 to 100% Relative Humidity
CiTicel A02 oxygen sensor	< 1% O_2	0 to 25% O_2
Microchip PIC16F874/20 microcontroller		
Microchip MCP6S28 multiplexer		

The 32 channel data acquisition system comprised of the above components contained 29 channels of temperature sensors, 2 channels of relative humidity sensors and one channel of oxygen sensing. The data collected by this system was transmitted via an RS232 port to the LabVIEW data acquisition system that controlled IRENE operation.

A6 – Finding exhaust mass flow

The general reaction occurring within a hydrogen fuel cell is shown in Equation A6.1:

$$aH_2 + b(O_2 + 3.76N_2) \rightarrow cO_2 + (1-c)N_2 + aH_2O \qquad \text{(A6.1)}$$

where

a = moles of hydrogen and water involved in the reaction

b = moles of dry air in the reaction

c = measured molar oxygen percent in the exhaust

Since c is measured in the experiments, the molar balance of b and a can be solved as follows assuming a dry product:

$$b = \frac{(1-c)}{3.76} \tag{A6.2}$$

$$a = (b-c)\cdot 2 \tag{A6.3}$$

With the chemical reaction balanced, the molar fraction of nitrogen to hydrogen entering the fuel cell can be found:

$$f_{N_2} = \frac{b}{a}\cdot 3.76 \tag{A6.4}$$

The mass flow of hydrogen and the ratio of nitrogen to hydrogen molecular mass can be used to estimate the mass flow of nitrogen:

$$\dot{m}_{N_2} = \frac{M_{N_2}}{M_{H_2}}\cdot f_{N_2}\cdot \dot{m}_{H_2} \tag{A6.5}$$

where

M = molecular mass, $kg\cdot mole^{-1}$

$\dot{m}$ = mass flow, $kg\cdot s^{-1}$

The molar fraction of oxygen to hydrogen entering the fuel cell can be similarly found:

$$f_{O_2}(in) = \frac{b}{a} \tag{A6.6}$$

The mass flow of oxygen entering the fuel cell is then:

$$\dot{m}_{O_2}(in) = \frac{M_{O_2}}{M_{H_2}}\cdot f_{O_2}(in)\cdot \dot{m}_{H_2} \tag{A6.7}$$

And the fraction and mass of un-reacted oxygen:

$$f_{O_2}(out) = \frac{c}{a} \tag{A6.8}$$

$$\dot{m}_{O_2}(out) = \frac{M_{O_2}}{M_{H_2}} \cdot f_{O_2}(out) \cdot \dot{m}_{H_2} \tag{A6.9}$$

With the mass flow rates of nitrogen and oxygen known, the actual stoichiometry of the air flow can be found. This is the ratio of the actual oxygen mass flow to the stoichiometric oxygen mass flow. Assuming all hydrogen is reacted, stoichiometric flow is found from the chemical balance of 1 mol H_2 reacting with ½ mol O_2. Then, since we know the hydrogen flow rate, the stoichiometric mass flow rate of oxygen and actual stoichiometry can be found:

$$\dot{m}_{O2}(stoich) = \frac{M_{O2}}{M_{H2}} \cdot \frac{\frac{1}{2} mol_{O2}}{1 mol_{H2}} \cdot \dot{m}_{H2} \tag{A6.10}$$

$$\lambda = \frac{\dot{m}_{O2}(in)}{\dot{m}_{O2}(stoich)} \tag{A6.11}$$

For the Nexa fuel cell experiments, the stoichiometry determined from equations A6.1 to A6.11 is shown in Figure A6.1. The figure shows that at low currents (< 2A), the stoichiometry is approximately 11; as the current increases, the stoichiometry approaches the value of 2, which is the expected value as presented by Larminie and Dicks [8].

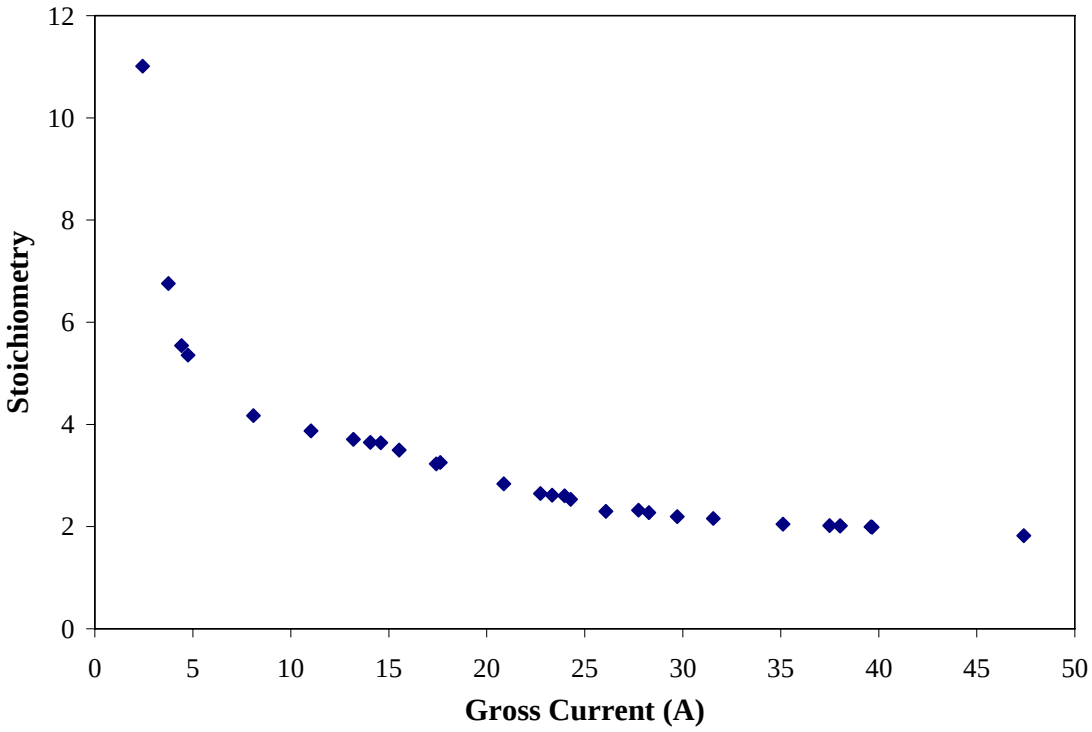

Figure A6.1 Stoichiometry of oxygen (air) flow in the Nexa fuel cell

A7 – Nexa purge cycles and hydrogen flow rates

The purge cycles are difficult to isolate from the experiment measurements and are hence included in the data. This means that all hydrogen flowing into the fuel cell is assumed to react even though some of it passes through the system solely to purge liquid water from the cell. The mass of un-reacted hydrogen passing through the system is small because at no time did the hydrogen leak detector that was periodically used to test coolant and exhaust gas show any hydrogen readings. Figure A7.1 shows hydrogen flow for 3 different average gross currents over 11 minutes of operation. As can be seen in the

figure, hydrogen spikes become more prevalent at high current operation, but the quantity of hydrogen used in the purges can not be determined from this data.

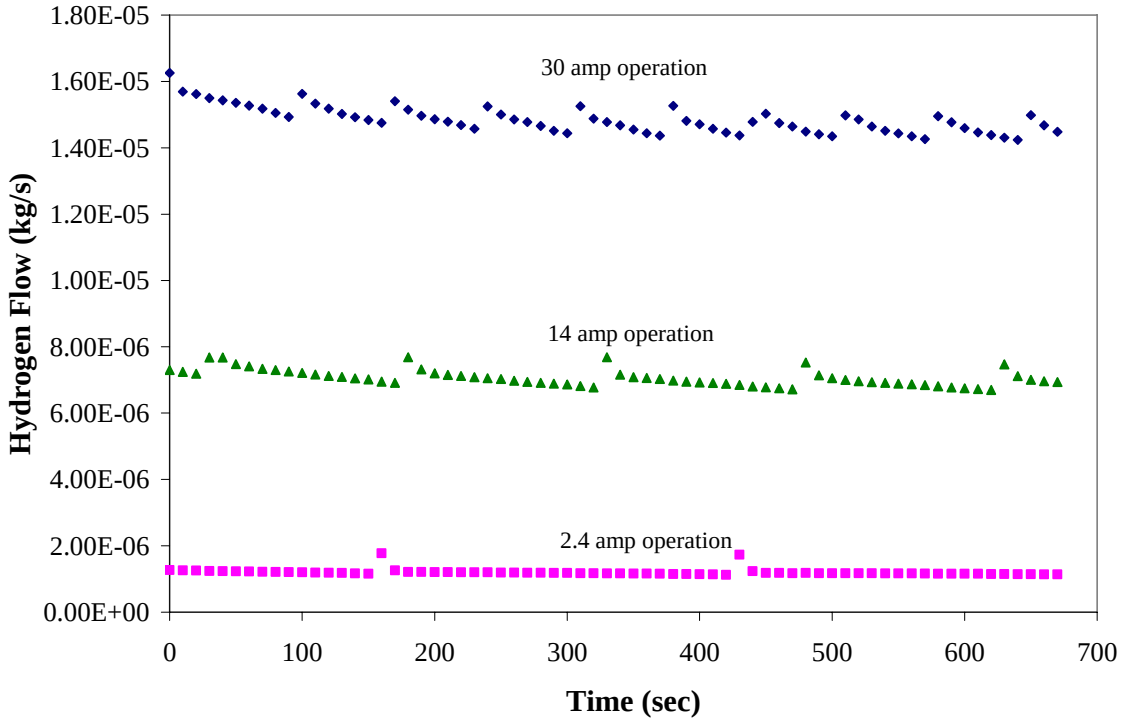

Figure A7.1 Hydrogen mass flow for 11 minutes of operation at 3 different gross currents

A8 – Nexa steady state operation

The Nexa never truly operates at steady state. Even though power to a load may be stable, purge cycles, fluctuations in blower speed, and changes in ambient temperature (due in part to cycling of laboratory ventilation system) occur frequently. Changes in load and blower speed also result in stack temperature changes. Several minutes may pass before the stack temperature becomes stable. The time to equilibrium, however, depends upon the size of the load change, with small load changes resulting in relatively small transient times. Transient operation is not considered in this thesis. Figure A8.1 shows the

average stack temperature after a change in Nexa gross current from 25 Amps to 39.5 Amps and from 39.5 Amps to 28.5 Amps:

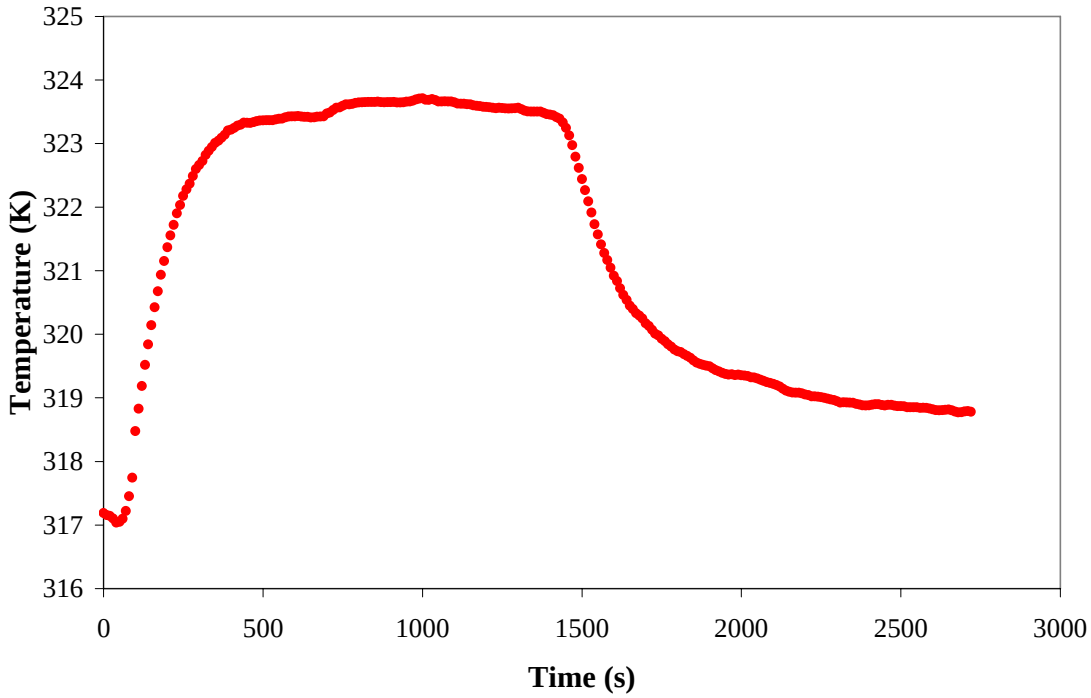

Figure A8.1 Stack temperature at 39.5 and 28.5 amp operation

For the thesis, steady state conditions are assumed once the absolute value of the change in temperature between each data point (i.e. slope of the temperature line) is less than 0.003 for at least 6 adjacent data points (1 minute of operation). Subsequently, the slope of at least 2 minutes of contiguous data, preferably just before a change in load occurs, must have an absolute value of less than 0.003 to be used to find the average values presented in this thesis. Ambient temperature must also adhere to these constraints over the 2 minutes for the Nexa to be considered steady state. Figure A8.2 shows the slope for the above temperatures:

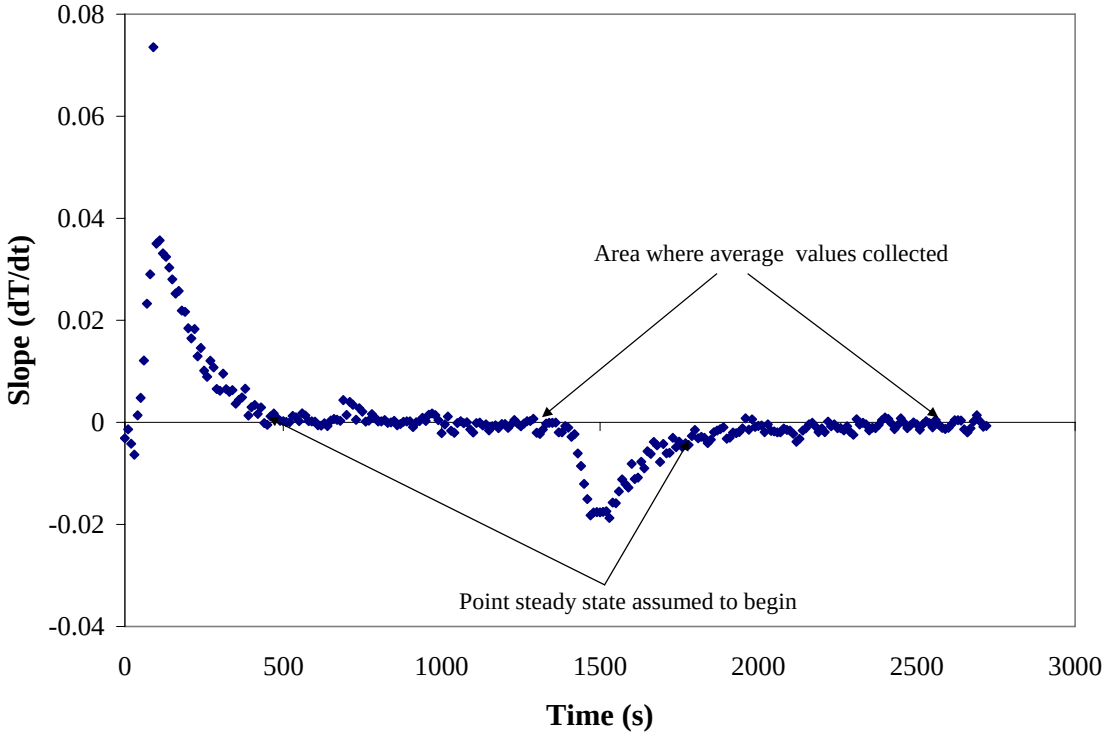

Figure A8.2 Slope ($\Delta T/\Delta t$) for change in stack temperature between each data point

A9 – Coolant mass flow rates

The data presented in this section is for and ambient of $296.55 \leq T_{amb} \leq 298.85$ K. The mass flow of air passing through the Nexa is shown in Figure A9.1. The mass flow is calculated from the velocity measured by the anemometer. For the mass flow calculation, the density of the air is taken at the coolant temperature (i.e. after passing through the Nexa).

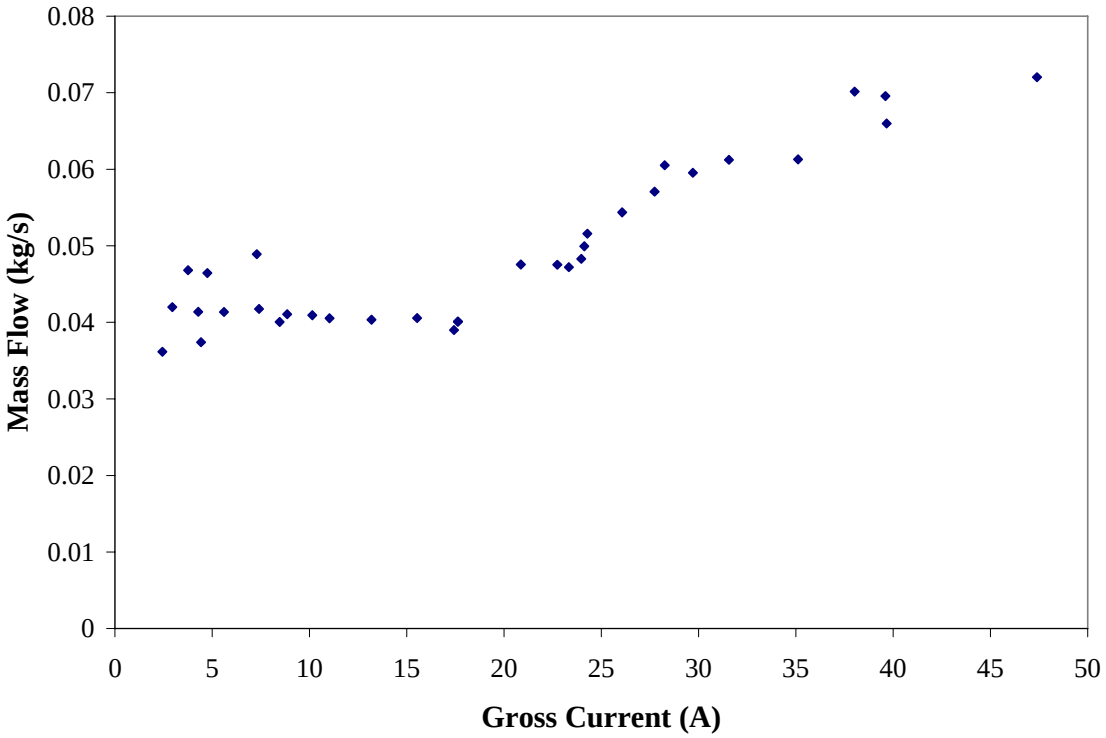

Figure A9.1 Coolant mass flow rate vs. stack current

The coolant mass flow through the Nexa fluctuates around 0.04 $kg \cdot s^{-1}$ up to a gross current of 20 Amps. After 20 Amps, the mass flow increases fairy linearly to the maximum flow rate of 0.07 $kg \cdot s^{-1}$.

The coolant temperature rise is shown in Figure A9.2.

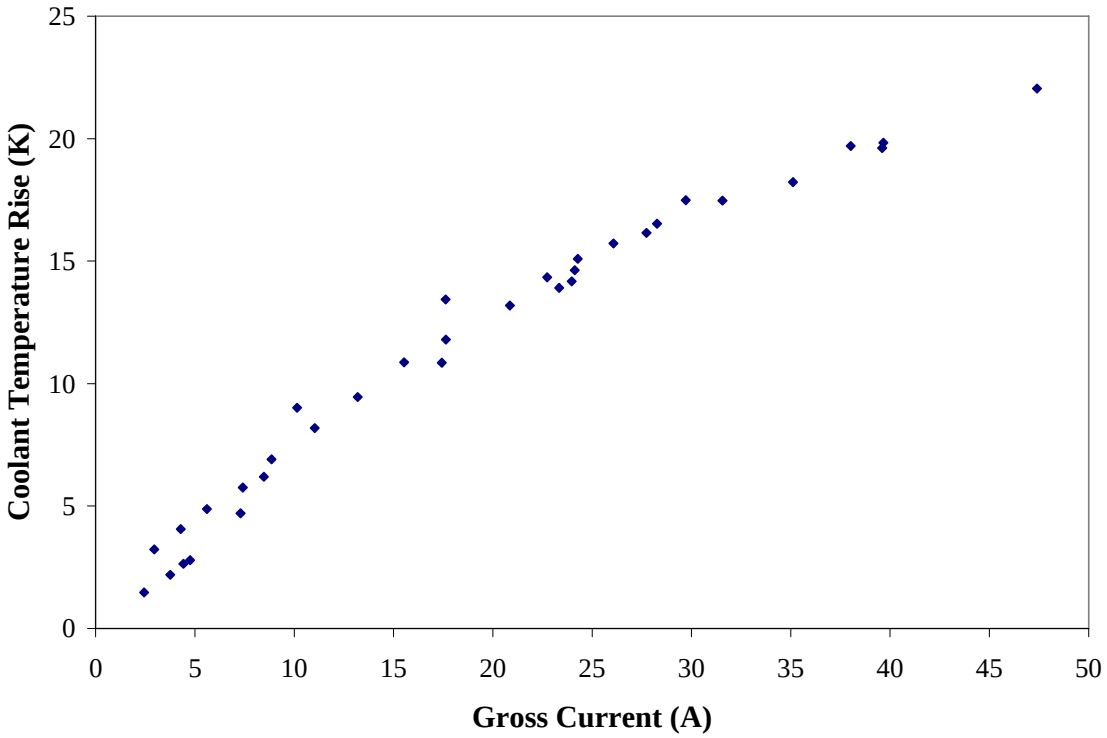

Figure A9.2 Coolant temperature rise vs. gross current

The temperature rise as indicated by Ballard [11] is approximately 17 K. The temperature rise as seen in the experiments was nearly a linear function of current and ranged from 1.5 K to 22.1 K.

A10 – Coastal British Columbia residential heat and power demand

Heat and electrical power consumption by a typical British Columbia residence for a day in the month of January is shown in Figure A10.1. The power data is on an hourly basis.

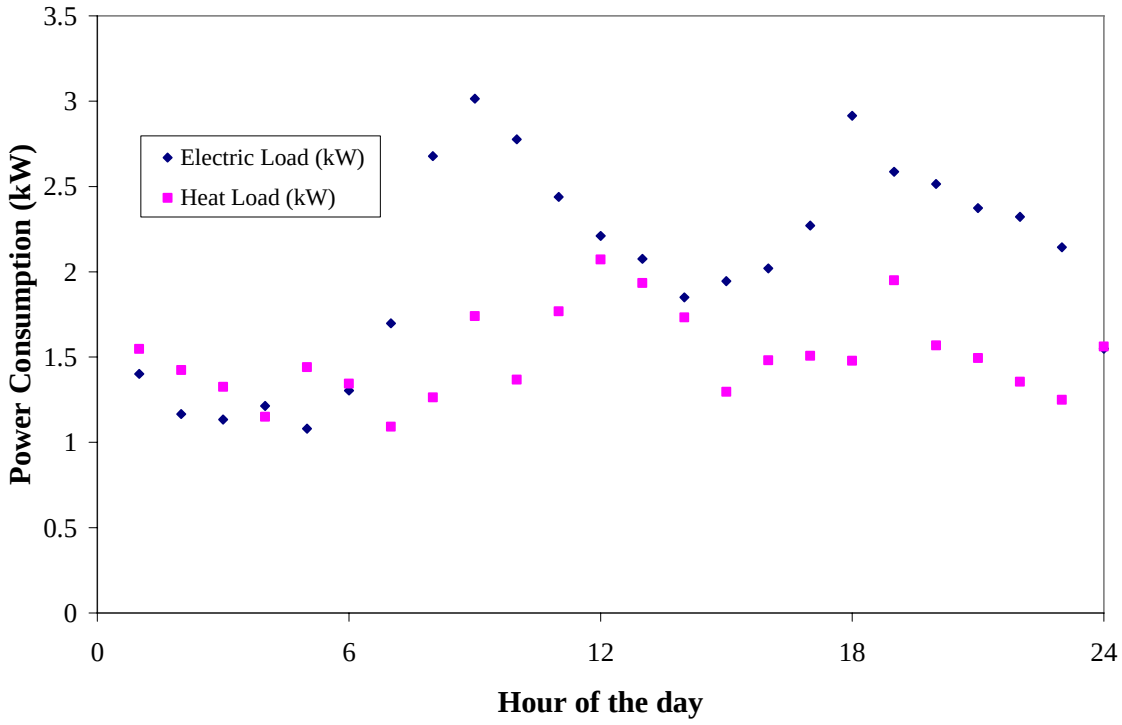

Figure A10.1 Hourly load data for a day in January

Figure A10.1 shows an increase in the electrical load in the morning and evening, which is typical for most days throughout the year. The heat power consumption shows less variability throughout the day than the electrical power consumption. Of the power consumption shown in Figure A10.1, 57% of the total energy consumed is electrical and 43% is heat. On a yearly basis, 66% of the total energy consumed is electrical and 34% is heat.

To determine yearly Nexa heat production, Figure 3.4 needs to be applied to the hourly data. For example, at 0100 hours in Figure A10.1, the residential heat load is approximately 1.55 kW and the electrical load is 1.40 kW. Since the peak electrical load

for the residence is 3.82 kW, four Nexa units would be required (4 units x 1.2 kW = 4.8 kW > 3.82 kW). The 1.4 kW residential electrical load is hence 29.2% full load (1.4/4.8 x 100) assuming all 4 Nexa units operate simultaneously and share the load equally. Looking up 29.2% full load on Figure 3.4 shows that the Nexa fuel cells are operating at an electrical efficiency of approximately 46% and a coolant thermal efficiency of 40%. These values can be used to determine the heat generated by the four fuel cells because 1.4 kW is to 46% as the coolant heat generated is to 40%:

$$\frac{\dot{Q}}{0.40} = \frac{1.4}{0.46}$$

$$\dot{Q} = 1.22 \text{ kW}$$

This is not enough heat to meet the 1.55 kW heat load of the residence. If all of the heat generated can be used, the residence still requires 0.33 kW of supplementary heat (1.55-1.22 = 0.33 kW). However, the temperature of the heat generated by the fuel cells need to be known to determine whether recovery is justified. Again referring to Figure 3.4, at 29.2% full load, the coolant temperature will be approximately 306 K. This is only a temperature rise of 8 K. If the desired temperature rise is 13 K, supplementary heat needs to be supplied to raise the temperature of the coolant before distribution. For the simplified model presented, no heat would be recovered from the fuel cell if a 13 K temperature rise was required.

A11 – Developing laminar flow tabular data

This section presents the tabular data for developing laminar flow as used in the model presented in Chapter 4 [32]. The tables include the *H1* boundary condition mean and local values (Table A11.1) as well as the T boundary condition mean values (Table A11.2).

Table A11.1 *H1* Nusselt numbers for developing laminar flow

	Channel aspect ratio *H1* Mean Nusselt numbers				Channel aspect ratio *H1* Local Nusselt numbers			
$1/x^* = Gz$	$\alpha = 1$	0.5	0.333	0.25	$\alpha = 1$	0.5	0.333	0.25
5	4.60	5.00	5.58	6.06	-	-	-	-
10	5.43	5.77	6.27	6.65	4.18	4.60	5.18	5.66
20	6.60	6.94	7.31	7.58	4.66	5.01	5.50	5.92
30	7.52	7.83	8.13	8.37	5.07	5.40	5.82	6.17
40	8.25	8.54	8.85	9.07	5.47	5.75	6.13	6.43
50	8.90	9.17	9.48	9.70	5.83	6.09	6.44	6.70
60	9.49	9.77	10.07	10.32	6.14	6.42	6.74	7.00
80	10.53	10.73	11.13	11.35	6.80	7.02	7.32	7.55
100	11.43	11.70	12.00	12.23	7.38	7.59	7.86	8.08
120	12.19	12.48	12.78	13.03	7.90	8.11	8.37	8.58
140	12.87	13.15	13.47	13.73	8.38	8.61	8.84	9.05
160	13.50	13.79	14.10	14.48	8.84	9.05	9.38	9.59
180	14.05	14.35	14.70	14.95	9.28	9.47	9.70	9.87
200	14.55	14.88	15.21	15.49	9.69	9.88	10.06	10.24
220	15.03	15.36	15.83	16.02	-	-	-	-

Table A11.2 *T* Mean Nusselt numbers for developing laminar flow

	Channel aspect ratio				
$1/x^* = Gz$	$\alpha = 1$	0.5	0.333…	0.25	1/6
10	3.75	4.20	4.67	5.11	5.72
20	4.39	4.79	5.17	5.56	6.13
30	4.88	5.23	5.60	5.93	6.47
40	5.28	5.61	5.96	6.27	6.78
50	5.63	5.95	6.28	6.61	7.07
60	5.95	6.27	6.60	6.90	7.35
80	6.57	6.88	7.17	7.47	7.90
100	7.10	7.42	7.70	7.98	8.38
120	7.61	7.91	8.18	8.48	8.85
140	8.06	8.37	8.66	8.93	9.28
160	8.50	8.80	9.10	9.36	9.72
180	8.91	9.20	9.50	9.77	10.12
200	9.30	9.60	9.91	10.18	10.51
220	9.70	10.00	10.30	10.58	10.90

A12 – Flow chart for finding stack temperature

The flowchart on the following page (Figure A12.1) is used to find Figures 5.7 and 5.10.

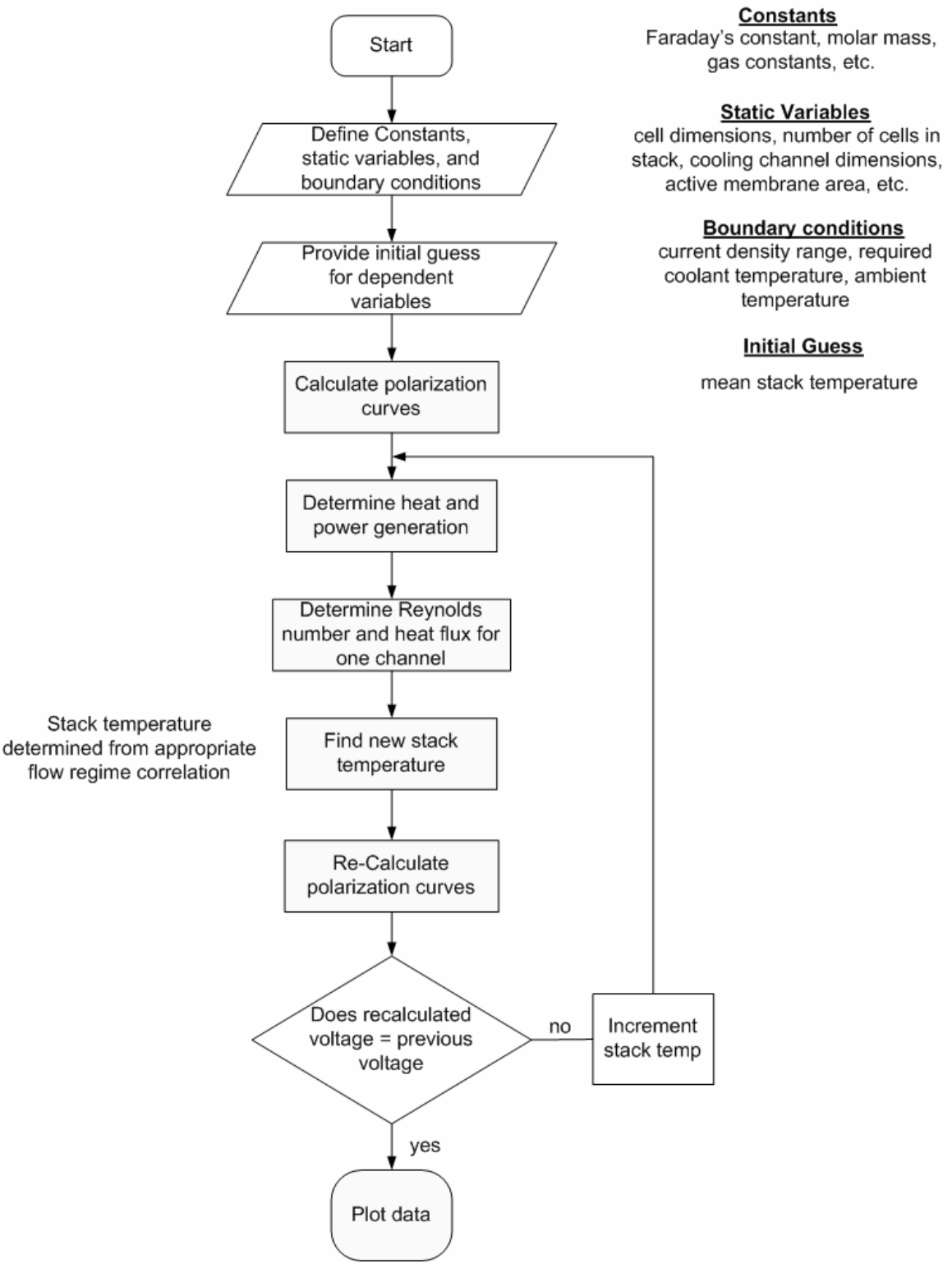

Figure A12.1 Flowchart for convergence of voltage at desired coolant temperature

The stack temperature is initially guessed to be equal to the ambient temperature. The program determines heat and power production for the guessed stack temperature. The flow rate for the desired coolant temperature is then used to determine the Reynolds number for the cooling channels. The coolant heat and the Reynolds number are used to determine the approximate stack temperature necessary to achieve the desired coolant temperature. However, since the voltage is temperature dependent, the voltage needs to be calculated at the newly calculated stack temperature. If the new voltage is not equal to the previous iteration, convergence has not occurred and the stack temperature is incremented and the process repeated.